MICROMACHINED DEVICES FOR IN VITRO BIOMEDICAL APPLICATIONS

by

UDAY SHANKAR TATA

Presented to the Faculty of the Graduate School of
The University of Texas at Arlington in Partial Fulfillment
of the Requirements
for the Degree of

DOCTOR OF PHILOSOPHY

THE UNIVERSITY OF TEXAS AT ARLINGTON
December 2012

ACKNOWLEDGEMENTS

I am grateful to Dr. Jung-Chih Chiao, my advisor and mentor, for his continuous support and belief in my abilities, which motivated me to stretch my limits and achieve this milestone in my research career. His knowledge, commitment and wisdom to collaborate across the departments have provided me the opportunity to work on a multitude of projects. I deeply appreciate his suggestions, guidance, and patience throughout this work. I am also thankful to him for providing financial assistance during the four years of my graduate study.

I am also grateful to Dr. Victor K. Lin for being my committee member and for guiding my research in the past few years. His mentorship has also pushed me to expand the depth and breadth of my knowledge in the area of tissue culture and cancer cell biology. I am thankful to Dr. Samir Iqbal, Dr. Harry F. Tibbals, and Dr. Jonathan Bredow for taking interest in my research and accepted to serve as members of my dissertation committee.

I would also like to extend my appreciation to Dr. Kytai T. Nguyen for giving me access to her research laboratory and also for her guidance

regarding the research work related to “stretch effects on vascular smooth muscle cell proliferation”.

I would like to thank Dr. Smitha M N Rao for her guidance, suggestions and ideas which helped me to overcome major difficulties in the experimental part of this thesis. I would like to appreciate her for constructive criticism and shaping my presentation skills.

I would like to thank my colleagues Akash, Krishna, Kushal, Bandita, Peter Wu, Preethi, Sarah, Nikhil, Stephan, An, Priya and Cristian for their help with the experiments. I would like to thank all the past and current members of iMEMS for their valuable suggestions.

I could not have done any of this without all my supportive, forgiving, generous, and loving friends, who made me feel at home while I am away from home during my 6 years stay in Arlington. In particular, Dr. Aniket Wadajkar and Dr. Hung Cao with whom I unwound at the end of the day over coffee and conversations. I appreciate Aniket’s constant support and inspiration. I am thankful to Sarath Samudrala and Dr. Muthiah Annamalai, who also made UTA a pleasurable experience.

I would like to express my deep gratitude to my father Dr. Kondala Rao and my mother Padmavathi for their love and blessings. I would like to thank my brothers Ganesh, Ramakrishna, Ravi and sister-in-laws Niharika, Manjula, Nikki for their encouragement and support.

October 08, 2012

ABSTRACT

MICROMACHINED DEVICES FOR
IN VITRO BIOMEDICAL
APPLICATIONS

Uday Shankar Tata, PhD

The University of Texas at Arlington, 2012

Supervising Professor: Jung Chih Chiao

Cell migration is a central process in the development and maintenance of tissues. Any deviation in the process can have serious consequences, such as atherosclerosis and cancer metastasis. During cancer metastasis, chemokines produced at secondary sites form chemical gradients and attract the cancer cells from primary sites. One of the primary limitations for the study of cancer cell migration has been the lack of a suitable cost-effective assay for cell migration with easy translatability to clinical situations. To address these issues, a microfluidic device was designed for assaying of cancer cell migration

towards different chemoattractants. The device was created with polydimethylsiloxane (PDMS). The device featured two chambers each with diameter of 5 mm and height of 6 mm. The chambers were designated as cell chamber and attractant chamber and were connected by ten microchannels. Each channel had a width of 20 μm, a length of 1 mm and a height of 10 μm. Using these devices, we obtained cell number, location, migration rate and time taken for cells to migrate in response to chemoattractants. Prostate cancer cells (PC-3), lung metastasized prostate cancer (PC-3 ML), normal prostate cells (PNT1A, PZ-HPV-7) and breast cancer cells (MDA-MB-231) response to different concentrations of Transforming Growth Factor-beta (TGF-β), Vascular Endothelial Growth Factor (VEGF), Epidermal Growth Factor (EGF), and basic Fibroblast Growth Factor (bFGF) was investigated. The effect of chemotherapy drugs like Docetaxel, Doxorubicin, Epirubicin and Gemzar on cell migration was also investigated. The device was also used to test the blood serum of patients with prostate cancer. Prostate and breast cancer preferentially metastasize to a particular set of organs. In order to investigate the preferential organ based metastasis, the effect of different organ extracts from a male rat on lung metastasized prostate cancer cells (PC-3 ML) was studied. To study synergistic effects of chemical and physical gradient on cell migration behavior during cancer metastasis, a tapered microchannels based microfluidic device was designed and fabricated. Width of the channel tapers from 20 μm to 5 μm over transition length of 50 μm. Three phenotype driven migratory behaviors namely,

permeation, retreat and repolarization of PC-3, PNT1A, PC-3 ML and MDA-MB-231 to Epidermal Growth Factor (EGF), was observed. In order to investigate the proliferation driven migration of smooth muscles cells during atherosclerosis, A PDMS based compact 6-well device was developed. This device was used to study the combined effect of cyclic strain and various growth factors on cultured VSMCs. Cell adhesion, alignment, and proliferation under 10% or 20% cyclic strain at 1 Hz were studied using this surface-enhanced PDMS device. The combined effect of cyclic strain and growth factors on VSMC proliferation was also examined. The results demonstrate the utility of these micromachined microfluidic devices as a high throughput, cost effective and real time monitoring platform to study cell migration due to chemical and mechanical factors which is major process involved in diseases like cancer metastasis and atherosclerosis.

TABLE OF CONTENTS

LIST OF ILLUSTRATIONS

LIST OF TABLES

CHAPTER 1

INTRODUCTION

1.1 Introduction

Microfabricated devices have been used in many areas of chemical, biological and medical systems. Several materials were and are used for fabrication of micro bio-analytical devices [1-2]. Common substrates used are silicon, glass and quartz. The devices are fabricated using conventional photolithography techniques. The most issues are the material and process costs and the long time to produce devices. Polymer is well suited as a substrate for bio-application devices due to its high dielectric constant, bio-compatibility, low cost and ease of micro fabrication coupled with the hydrophobic nature and clear optical properties make it promising material for bio-analytical micro devices such as microfluidic devices. On the other hand, new generation of light, flexible, and low cost polymeric sensors are very promising and useful in the field of robotics and wearable and implantable electronics. Some approaches in the design of this type of sensors, to be used in the field of rehabilitation and health monitoring, have already been proposed [3–4].

Applications for the measurement of biological signals such as electrocardiogram, breathing, joint position and movements, ocular pressure,

skin temperature, etc. could be developed through different device implementations.

1.2 Motivation

Cell migration is a central process in the development and maintenance of tissue. Tissue formation during embryonic development, wound healing and immune responses all require the orchestrated movement of cells in particular directions to specific locations. Errors during this process have serious consequences, including mental retardation, vascular disease such as atherosclerosis, tumor formation and cancer metastasis. An understanding of the mechanism by which cells migrate may lead to the development of novel therapeutic strategies.

Metastasis of solid tumors from their primary site to distant sites often renders the cancer incurable. For example, the metastasis of prostate cancer to the bone is associated with a very poor prognosis [5-8]. Metastasis is a complex multi-step process that involves invasive tumor cells entering the blood stream, attaching onto the walls of the blood vessels and invading a secondary organ leading to tumors [9]. This process may be partly determined by chemokines that serve to attract the cancer cells from the primary organ site to specific metastatic sites. The mechanisms and effects of metastasis often span large spatial and temporal scales, which make any experimental and analytical characterization difficult. To address the need for characterizing and screening the metastatic potential of cells, researchers have begun looking for mechanical

markers at the single cell level [10–12]. This is particularly useful since metastasis has been characterized as an inefficient process that eventually works due to successful invasion by very small subpopulations of highly invasive cells.

Similarly cell migration is also an important phenomenon during Atherosclerosis. Atherosclerosis is a disease of the arteries in which fatty material and plaque are deposited on the wall of an artery, resulting in narrowing of the arterial lumen and eventual impairment of blood flow. In extreme cases this may lead to heart attack and sudden death. During this process smooth muscle cells within the arterial wall begin to multiply and move to the surface of the plaque. These cells help in formation of firm fibrous cap over the plaque and give it stability. Later this cap bursts to form a clot stopping the blood flow. The migration and excess proliferation of smooth muscle cells are the results of a number of biochemical factors, including cytokines and growth factors, as well as mechanical stimuli such as compression [13] and cyclic stretch [14] .

1.3 Specific Aims

1. To design and fabricate a chemical gradient generating device to test cell migration.
2. Investigate migration response of different cancer cell migration to chemical factors such as growth factor and patient serum. Also investigate the effect of chemotherapy drugs on cell migration.

3. To investigate response of cancer and healthy cells due to a combination of physical and chemical gradients.
4. Design and fabricate a multi-well array based platform to stretch vascular smooth muscle cells.
5. Investigate the vascular smooth muscle cell migration during atherosclerosis disease due to the growth factors and physiological and pathological strain.

1.4 Dissertation Organization

The Dissertation is organized as follows: In Chapter 2 microfluidic array based chemo-gradient device design and fabrication, gradient formation experimental verification, device characterization for cell migration, prostate cancer cells (PC-3), lung metastasized prostate cancer cells (PC-3ML), healthy prostate cells (PZ-HPV-7 and PNT1A) and breast cancer cells' (MDA-MB-231) migration to various concentrations of different growth factors is presented. Effect of different concentrations of chemotherapy drugs on cell migration is also discussed. This chapter also deals with the effect of patient serum and different rat organ extracts on cell migration. In Chapter 3, spatial gradient device design and fabrication, PC-3, PNT1A, PC-3ML and MDA-MB-231 migration behavior in muscle cell alignment and proliferation, combined effect

of strain and growth factors on vascular smooth muscle cells is explained. Future work is described in Chapter 5. In this chapter, methods to automate the tedious process of data acquisition and processing for the microfluidic devices are explained. Also the future microchannel designs to explore the structural effects on cell migration are discussed.

CHAPTER 2

MICROFABRICATED CHEMICAL GRADIENT DEVICE TO STUDY CELL MIGRATION

2.1 Introduction

In order to assess cell migration in the presence of gradients or chemoattractants, several devices have been proposed. The Boyden chamber or transwell assay [15], under-agarose assay [16], Zigmond chamber [17], Dunn chamber [18], and micropipette assay [19]. The Boyden chamber provides means to measure chemotaxsis in terms of the number of cells that migrate across a barrier, usually a porous membrane between two chambers containing reagents in solution. The disadvantage of this method is that it provides only an end-point measure of number of cells without any information regarding cell migration. In the under-agarose assay, agarose gel with holes punched in it for the cells and chemoattractant on a glass coverslip is used to monitor cell migration. This method provides cell migration information but it cannot be quantified as the path of the cell is not defined and can be random. In the Zigmond and Dunn chambers, cells migrate across two wells separated by a bridge with a gradient between them on glass [20, 21]. There is a cover slip that

encloses the chambers and provides a narrow gap in which the cells need to traverse. The effective volume of the chambers plays a very important role in maintaining a steady gradient across the bridge. Recently optical assays with gradients across microgrooves or patterns in silicon for neutrophils chemotaxsis has been reported [22]. Silicon however is not considered to be biocompatible.

A microflluidic device that uses static fluidic flow was proposed by Campenot [23, 24] in 1977. In this method, a culture dish was coated with collagen. Parallel lines spaced 300 μm apart were scratched in the collagen. Silicone grease was used to seal a three-chamber Teflon attachment to the culture plate. Neurites grown in this set-up grew outwards from one compartment to the remaining two and were aligned parallel to the scratches. A modified Campenot chamber was developed by Ivins et al. that reduced the distance of the parallel grooves from 300 to 150 μm and used a glass coverslip attached to a hemisected Teflon tube. PDMS was used for the attachment and the apparatus with silicone vacuum grease was placed on a tissue culture dish. Provided that the distance between the glass coverslip and the culture plate was narrow enough, neurites extended across the vacuum grease barrier. Irimia et al. have proposed a microfluidic device that allowed observation of cellular chemotaxis and localized treatment of the polarized ends of a cell in a convection free, stationary gradient environment that were separated by an array of channels [25]. A three channel microfluidic chip with stationary linear gradient fabricated by laser etching of a nitrocellulose membrane placed

between a polycarbonate manifold and a Borofloat glass was proposed by Diao et al. [26]. A similar device has been proposed by Shamloo et al. [27]. It consisted of a multicompartment device for neuronal cultures [28] using PDMS and glass or tissue culture dish. The compartments were separated by micron-size grooves across which the growth of neurites was characterized. In order to overcome some of the drawbacks of the previously proposed designs, a new device incorporating the principles of conventional migration assays and other linear stationary gradient generation devices have been designed, fabricated and tested. The continuous flow system device requires a large volume of expensive reagents pumped continuously through the fluidic channels and also there are shear stresses on the cells during the flow of reagents that will affect the cell migration. The most important advantage of the newly proposed device is that a continuous fluid flow is not required to analyze cell migration.

2.2 Materials and Methods

2.2.1 Device Design

The device consists of two chambers named as cell chamber and attractant chamber, both 5 mm in diameter connected with ten micro-channels as shown in Figure 2.1a. Considering that average diameters of epithelium and carcinoma cell is in the range of 30-60 μm and height is in the range of 5-10 μm, the microchannels were designed to have 10 μm height, 20 μm width and 1000 μm length. Successive channels were separated by 20 μm barrier. An

array of 48 such devices (8×6) devices was formed as a single platform to mimic a standard 96-well plate configuration as shown in Figure 2.1 b.

2.2.2 Device Fabrication

The device was fabricated by soft lithography process, which basically started with making of a master mold. The mold then formed the template for soft lithography fabrication of the devices from PDMS. After curing, the devices were peeled, cut, punched, cleaned and prepared for testing.

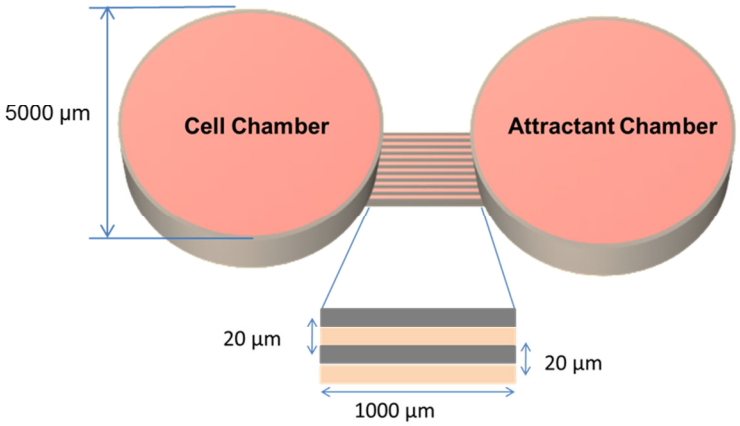

(a)

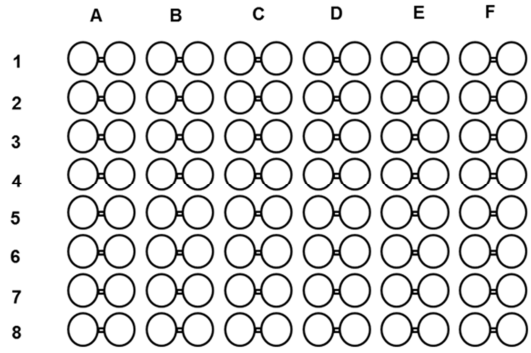

(b)

Figure 2.1 (a) Microfluidic device design for cell migration (b) Array of 48 devices arranged in standard 96 well plate configurations.

2.2.2.1 Silicon Master Mold Fabrication

The substrate of the silicon wafer was cleaned using standard wafer cleaning process and also buffered oxide etch was used to remove native oxide followed by DI water rinse to obtain maximum process reliability. The wafer was dehydrated at 200 °C for 10 minutes on a hot plate to remove any moisture. Dehydration of the wafer helps in adhesion of the photoresist. Approximately 1 ml resist per inch of wafer was used. The process of spinning was done in two steps. During the first step, spin speed was maintained at 500 rpm for 5 seconds. The ramping rate used for this step was 100 rpm/sec. During the second step, speed was maintained at 1200 rpm for 30 seconds to achieve even coating. The ramp rate for this step was at 300 rpm/sec. The spin coated photoresist determines the effective height of the pattern to be formed. The wafer was baked after the resist was spin coated in order to evaporate the solvent and to make the resist film dense. The wafer was then baked for 2 minutes at 65 °C and 5 minutes at 95 °C. The SU-8-5 (Microchem, MA) resist used in the process was optimized to work for near UV (350 – 400 nm) wavelength. The exposure energy used was between 300 mJ/cm^2 – 550 mJ/cm^2. Upon exposure, the negative photoresist cross links leaving the pattern area to be polymerized. The resist was exposed to UV for 14 sec as per the manufacturer's recommendations. A post expose bake was performed for 1 minute at 65 °C and 2 minutes at 95 °C. A 2-minute rinse in the SU-8 developer was used to remove the unexposed areas in the wafer. This process was

followed by rinsing with iso-propyl alcohol (IPA) and nitrogen blow drying. For achieving maximum yield of the photoresist, the device was baked at 150 °C on a hot plate for 90 minutes before using it to fabricate microfluidic devices. Figure 2.2 shows a process flow for fabricating the SU-8 mold on silicon.

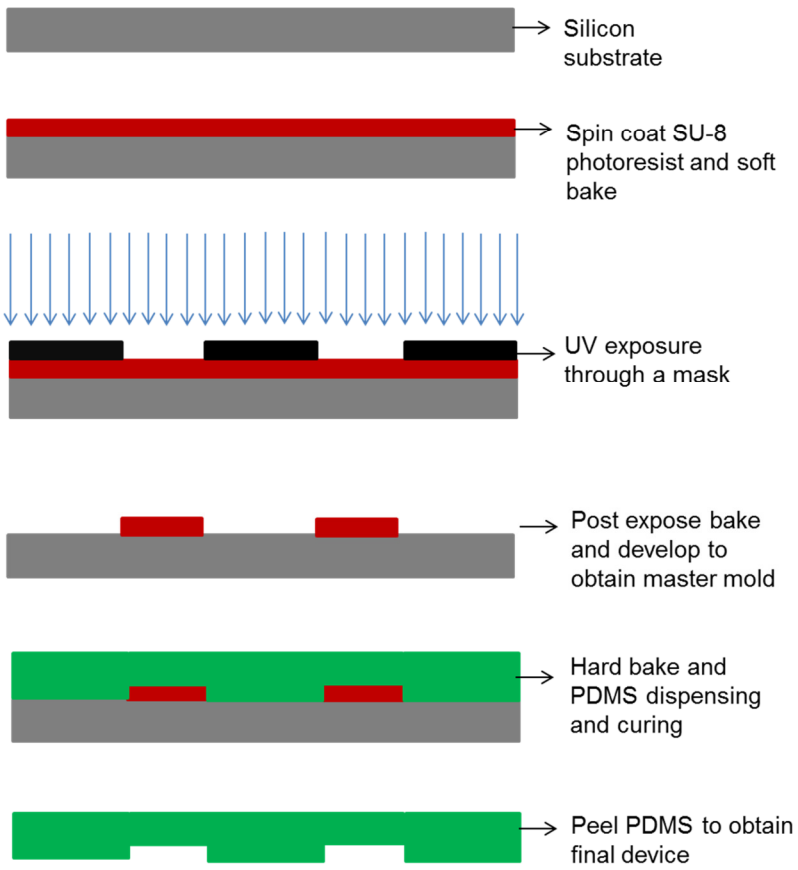

Figure 2.2 Process flow for the fabrication of silicon master mold and PDMS channels/device.

2.2.2.2 PDMS Device Fabrication and Preparation

PDMS (Sylgard® 184, Dow Corning) was polymerized by curing a mixture of 10 parts of PDMS base to 1 part of cross-linker (by weight). Prior to

curing, a controlled quantity of the polymer mixture was poured on the mold placed on a leveled table to ensure the device height was uniformly maintained at 6 mm. The mixture was allowed to set on the SU-8 mold and degassed in a vacuum chamber. The polymer was then cured at 90 ^{0}C for 90 minutes. The cured device was peeled from the mold and diced. Cell and attractant chambers were formed by punching holes using a unicore hole puncher while inspecting the device through an inverted microscope. This process made sure that the holes were punched exactly within the imprinted well boundaries. The PDMS dies were then individually cleaned by DI water and dried using compressed-air. The dust and static cling on the PDMS was removed by taping it using 3M scotch tape. Devices were then soaked in 70% ethanol and dried under UV light inside a biosafety cabinet for sterilization. The sterile devices were mounted on a standard tissue culture dish (100 mm, treated polystyrene, Corning Inc.) by applying pressure on the PDMS with the channel side onto the growth surface of the substratum to form the microfluidic device as shown in Figure 2.3. The device was then primed with growth media by dispensing 50–70 µL in one well and by pulling the liquid through the other well by using a vacuum pump. Priming the device before the experiment eliminates trapped air bubbles and helps in identifying any potential leaks.

2.2.3 Gradient Formation

The gradient generation in the device was characterized by using fluorescence microscopy. Initially the device was primed with RPMI 1640 incomplete media. Media with a volume of 60 µL was added to both chambers.

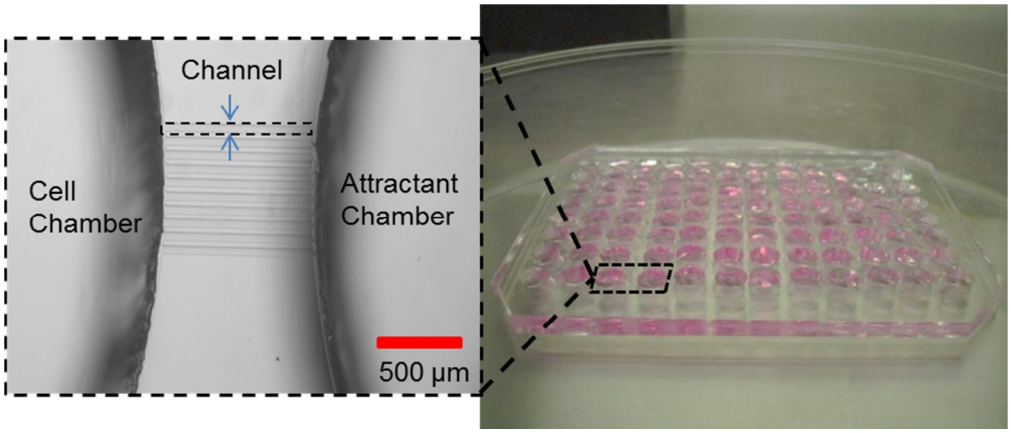

Figure 2.3. PDMS based microfluidic device array placed on a culture dish and primed with the growth media.

Later media in one of the chamber was replaced by media containing 37 µM Fluorescein. Fluorescein is a water soluble fluorescent salt which has excitation at 494 nm and emission at 521 nm. Gradient evolution was monitored with fluorescence time-lapse microscopy at room temperature. Images were acquired every 2 minutes with a CCD camera (CoolSNAP CF, Photometrics, Tucson, AZ) on an inverted microscope (Ti Eclipse, Nikon, Meville, NY). Images were analyzed using NI elements (Nikon, Meville, NY) software. The fluorescence intensity profile across each channel was measured, averaged over 10 channels, background-subtracted, and normalized to the maximum intensity in that frame. Figure 2.4 shows the fluorescein diffusion and gradient

formation at 2, 4, 8, 20, 40,120 and 480 minutes. Initially after the fluorescein dye was introduced into one of the chamber, it rapidly diffused in the first few minutes and reached steady state after 40 minutes. The gradient established was maintained even after 8 hours. Figure 2.5 shows the diffusive gradients profile across the channels at different time points. The results indicated that there was a rapid increase in the diffusion of the Fluorescein from 2 to 20 minutes and a stable gradient was maintained at 40 min, 2 Hrs. and 8 Hrs. The results demonstrate that a stable and steady state gradient can be established with our device. This can be also extended to the situation when the dye was replaced by chemoattractants.

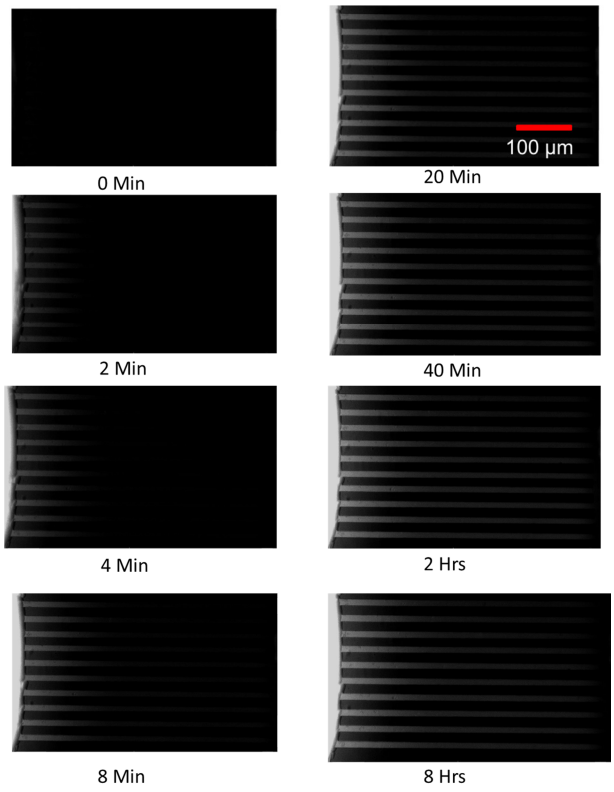

Figure 2.4 Gradient generation in microchannels during different time points.

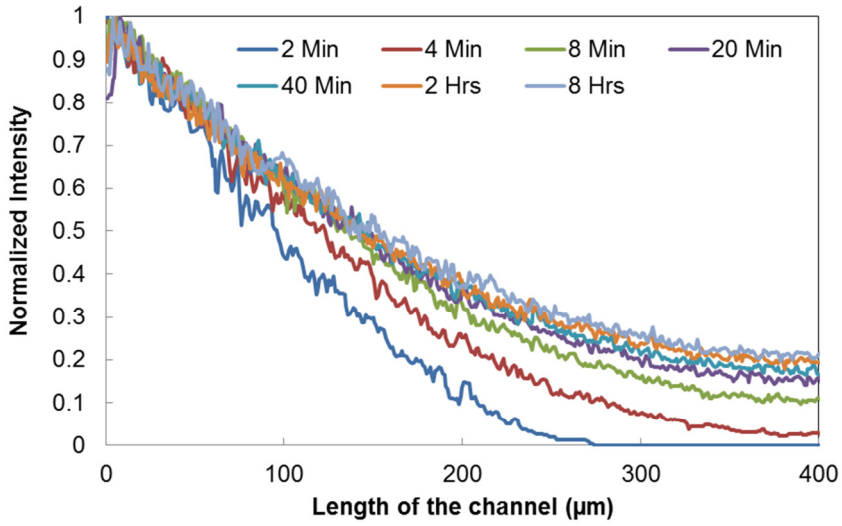

Figure 2.5. Plot of fluorescence intensity across the channel as a function of time. A steady gradient is obtained after 40 min and maintained even after 8 hrs.

2.2.4 Cell Culture

The cell lines used in the experiments were green fluorescent protein (GFP) expressing human prostate cancer line (PC-3), lung-metastasized prostate cancer (PC-3 ML) cells, normal prostate epithelial cell line (PZ-HPV-7) and human breast cancer cells (MDA-MB-231). All cells were cultured and maintained under 5% CO_2 atmosphere at 37 ^{0}C in an incubator.

1. PC-3, PC-3ML and MDA-MB-231 cells were cultured in RPMI 1640 (Lonza) supplemented with 5% fetal bovine serum (FBS) and 100 U/ml penicillin and 100 µg/ml streptomycin.
2. PZ-HPV-7 cells were grown in PrEGM serum-free media (Clonetics), 100 U/ml penicillin and 100 µg/ml streptomycin.

These cells were purchased from American Type Culture Collection (ATCC, Manassas, VA).

2.2.5 Cell Seeding

The priming media present in the reservoirs on the cell side was removed carefully. Immediately, using a pipette, 50-70 µl of the cell suspension was introduced into the cell chamber. The amount of media added to the chambers was decided based on the thickness of the device. The amount was maintained consistent. The two chambers always used equal amounts of media to ensure the gradient formation remained unaffected by difference in volume. The seeded cells were allowed to attach to the substratum and grow for an additional 4-24 hours before the chemoattractant to be tested was introduced on the chemoattractant side of the devices. After 24 hrs, the media from both the wells was removed and 50-70 µl of appropriate growth media was added to the wells on the cell side of the device, Growth media containing the chemoattractant to be tested was added to the wells on the chemoattractant side. In order to minimize the evaporation of the media in the devices, sterilized PBS was added around the PDMS device attached to the culture plate. Precautions were taken to ensure that there was no contamination or cross-contamination. The entire process was carried out inside a tissue culture hood and standard tissue culture equipment and procedures were used.

2.2.6 Image Acquisition and Analysis

Cell responses and movements were assessed by micrographic bright field and fluorescent images taken at designated time intervals using a standard inverted microscope equipped with CCD camera as discussed in section 2.2.3. The images were captured at 40X to show the overall cell distribution in the device and at 100X for cell movement analysis. Due to the limited numbers of cells in each channel and the clear contrast in the phase-contrast pictures, the cells were easily accountable for location as well as their moving distances in the channels. Pictures taken at 24-hour intervals were used to measure the movement of the cells in the channels. The cell positions at the end of each 24-hour period were compared with their previous positions. AxioVision (Carl Zeiss International) was used to analyze the images and determine the positions of the cells. The migration distances for all the leading cells in all the channels of each device were then averaged and compared for different factors. Also total number of cells inside the ten channels was counted manually and averaged over all the devices. Migration distance and cell numbers for individual channels of every device were recorded. Figure 2.6 shows the migration distance calculation using Axiovision software.

2.3 Experiments and Results

2.3.1 Device Characterization Experiment

To demonstrate the measurability of cell migration in the microfluidic device prostate cancer cells (PC-3) were seeded into the cell chamber in media containing 2% FBS at a seeding density of 5000 cells/well. The cells were

evaluated for migration towards a similar concentration of FBS (2%) or higher concentrations of FBS (5% and 10%) introduced in the attractant chamber side in five separate devices for each serum concentration. Migration was evaluated at 24 hour intervals and Figure 2.7 shows the images at the Day 1, 3 and 5.

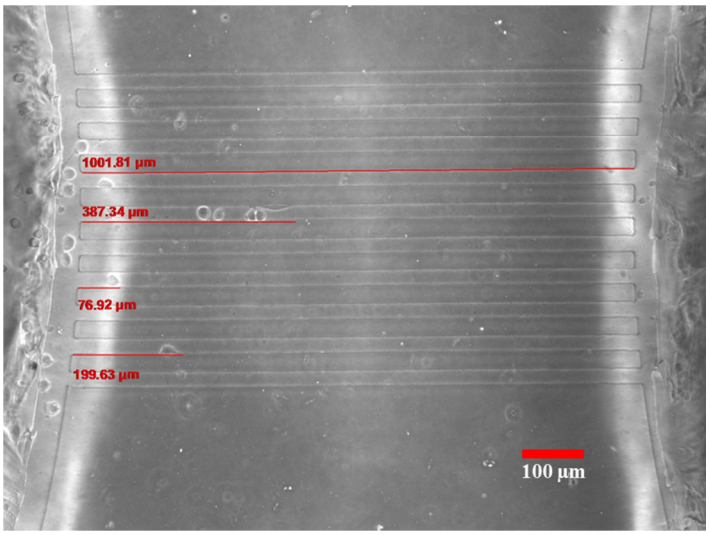

Figure 2.6 Migration distance is calculated by measuring the location of the cell inside the channel with respect to the channel entrance.

Bright-field images were taken. In each image, the left side was designated as the cell chamber and the right side was designated the attractant chamber. Figure 2.8 (a) shows the plot for the average number of cells migrating in the channels towards different concentrations of FBS over a period of 5 days. From day 1 to day 5 the number of cells migrating increased from 2 to 20, 3 to 35 and 3 to 50 at 2%, 5% and 10% FBS respectively. This indicates that there was steady increase in the cells migrating towards attractant from Day 1 to Day 5 for a particular concentration of FBS and also there appeared to

be a concentration-dependent migration of PC-3 cells towards FBS. PC-3 cells entered the migration channels earlier in response to higher FBS concentrations and appeared to migrate in larger numbers and longer distances than in response to lower FBS concentrations. Among the tested concentrations 10% FBS has highest migration potential. The average migration distance per device for a particular FBS concentration and on a particular day was plotted as shown in Figure 2.8 (b).

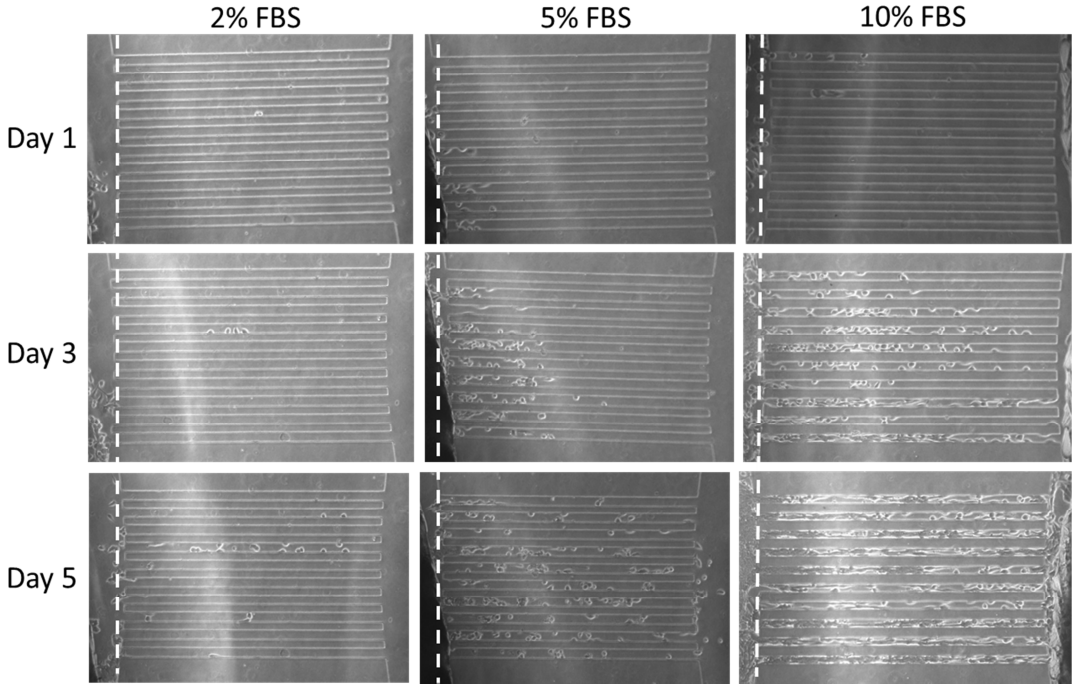

Figure 2.7. PC-3 migration in response to 2%, 5% and 10% FBS. Among the tested FBS concentrations, the highest migration was found to be in 10% FBS. The dashed line indicates the starting edge of the migration channels.

The results suggest that the cells migrated over larger distances for 10%FBS as compared to 5% or 2% FBS. Thus the device potentially mimicked the migration of prostate cancer cells towards a chemokine gradient. These

data indicate the utility of our microfluidic device to evaluate migration in response to concentration gradients, with increased migration towards higher concentrations. This experiment also gives the information on lowest concentration of FBS that can be used in future experiments, so that the cells can survive in the cell wells with sufficient serum and also reducing the effect of migration due to the FBS itself. In all other experiments 2% FBS on cell side and 2% FBS on attractant side acted as control.

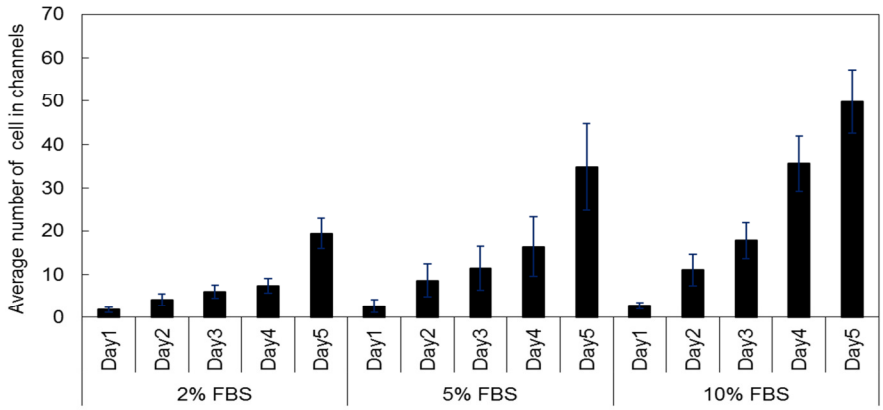

(a)

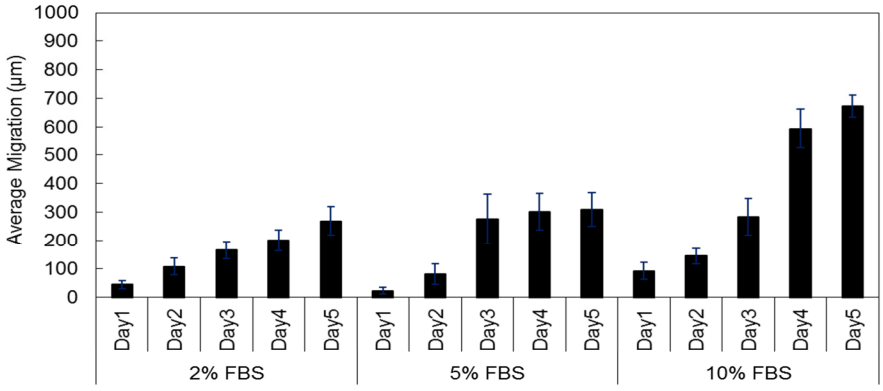

(b)

Figure 2.8 (a) Number of PC-3 cells migrating in the channels in response to different concentrations of FBS. (b) Distance travelled by cells inside the channels on each day, for a period of five days at different concentrations of FBS.

2.3.2 PC-3 Growth Factor Experiments

Migration of the cancer cells may involve chemokines such as growth factors that attract the cancer cell from the primary to secondary sites [29]. Understanding the effects of different growth factors on the prostate cancer metastasis will enable researchers to develop different therapeutic strategies to stop the advance of the cancer from primary to a secondary site.

Experiment Parameters	
Cell Type	PC3
Cell seeding density	5000 cells per well
Media	RPMI 1640
Primed media	2% FBS + RPMI
Control	2% FBS_2% FBS
Experimental condition	2% FBS_2% FBS+ growth factor
N	5
Days of experiment	5 days
Growth factors	VEGF, EGF, bFGF and TGFβ
Concentrations	VEGF: 1, 2.5, 5, 10, 15 and 25 ng/ml EGF: 25, 50, 100 and 125 ng/ml FGF: 0.1, 0.3, 1, 3 and 30 ng/ml TGFβ: 0, 0.1, 0.5, 1, 2.5, 5, 7.5 and 10 ng/ml

Table 2.1 Experimental Parameters used to test the migration of PC-3 cells to different concentrations of growth factors.

The microfluidic array device was used to investigate the effects of four different growth factors on prostate cancer cell migration. Table 2.1 shows the experiment parameters.

2.3.2.1 Effects of TGFβ on PC-3 Cell Migration

Transforming growth factor-beta (TGF β) is a multifunctional regulatory cytokine that is the member of a large family of cytokines controlling many aspects of cellular function, including cellular proliferation, differentiation, migration, apoptosis, adhesion, angiogenesis, immune surveillance, and survival. We used our microfluidic array to evaluate the effect of TGFβ on prostate cancer cell migration. TGFβ at 0.1, 0.5, 1, 2.5, 5, 7.5 and 10 ng/ml was added to the attractant wells, 24 hrs after the cells were seeded in the cell chambers. The concentration ranges were chosen based on literature [30].

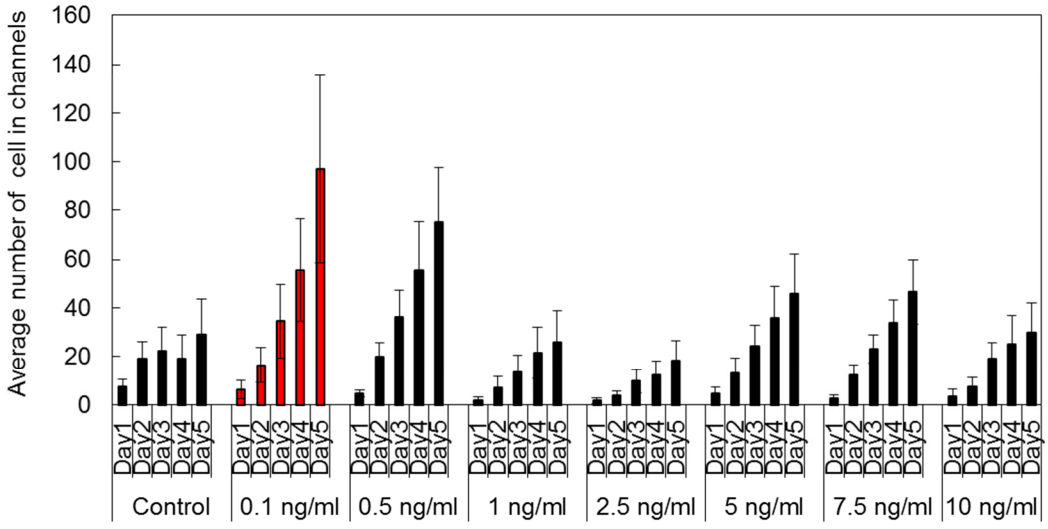

Figure 2.9. Number of PC-3 cells in channels in response to different concentrations of TGFβ.

Pictures were taken every 24 hours for a period of 5 days. The average number of cells that had migrated towards each factor was measured and plotted as shown in Figure 2.9.

The results indicated that from Day 1 to Day 5 there was a steady increase in the migration of cells both in control and at different concentrations of TGFβ. From Day 1 to Day 5, actual number of cells migrating towards the attractant increased from 7 to 29, 6 to 97, 5 to 75, 2 to 26, 2 to 18, 5 to 45, 3 to 47 and 3 to 29 at 0, 0.1, 0.5, 1, 2.5, 5, 7.5 and 10 ng/ml of TGFβ respectively. TGFβ at concentrations 0.1 and 0.5 ng/ml enhanced the migration by 235% and 158% as compared to control. Other concentrations of TGFβ didn't enhance the migration as compared to control. Naturally, TGFβ acts as a growth inhibitor in the case of prostate cancer cells [31]. So when it was used at higher concentrations, the gradient generated by the device produces unfavorable conditions for the cells which could be one of the causes for reduction in migration. The lower concentrations of TGFβ may not provide growth inhibition, so we observe higher migration at low concentration of TGFβ

2.3.2.2 Effects of VEGF on PC-3 Cell Migration

One of the most important growth factors, Vascular endothelial growth factor (VEGF), has been implicated in prostate carcinogenesis and metastasis and identified as a potential target for innovative anticancer therapy. VEGF is

highly expressed by prostate cancer cells [32,33], and this expression correlates with increasing grade, vascularity and tumorogenicity [34,35].

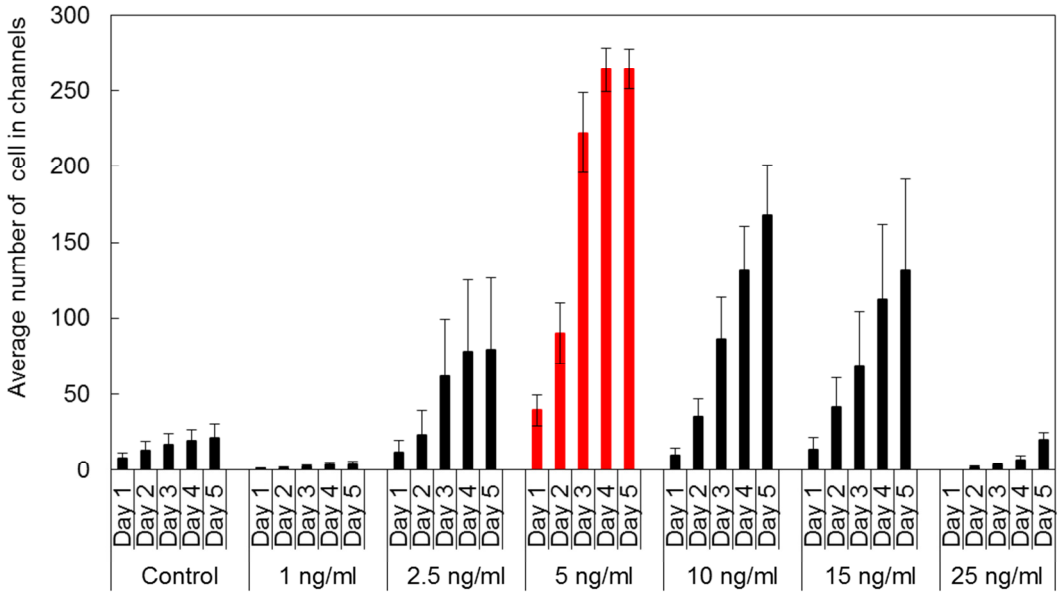

Figure 2.10. Number of PC-3 cells in channels in response to different concentrations of VEGF.

In several animal models, neutralizing anti-VEGF antibodies show encouraging inhibitory effects on solid tumor growth and metastatic dissemination [36, 37]. We used our microfluidic array to evaluate the effect of VEGF on the prostate cancer cell migration. A concentration range was chosen based on the literature [38]. The range of concentration chosen is in such a way that they are in close similarity with that found in the human body. VEGF at 0, 1, 2.5, 5, 10, 15 and 25 ng/ml was added to the attractant wells, 24 hrs after the cells were seeded into the cell chambers. Pictures were taken every 24 hours for a period of 5 days. The average number of cells that were migrating towards

each factor was measured and plotted as shown in Figure 2.10. The results indicated that from Day 1 to Day 5 there was steady increase in the migration of cells both in control and at different concentrations of VEGF. From Day 1 to Day 5, actual number of cells migrating towards the attractant increased from 8 to 20, 1 to 4, 12 to 79, 39 to 264, 10 to 168, 13 to 131 and 0 to 16 at 1, 2.5, 5, 10, 15 and 25ng/ml of VEGF respectively. Concentrations of 2.5, 5, 10, 15 ng/ml enhanced the migration with peak migration at 5ng/ml. However 1 and 25 ng/ml VEGF inhibited the migration as compared to control.

2.3.2.3 Effects of EGF on PC-3 Cell Migration

Elevated level of Epidermal Growth Factors (EGF) receptors has been found in various cancers, which includes breast and prostate cancer [39-42]. However it is also found that EGF has additional effects on these cancer cells' invasion and metastasis characteristics. PC-3, a bone metastasis derived prostate cancer cell line expresses higher level of EGF receptors [40]. We used our microfluidic array to evaluate the effect of EGF on the prostate cancer cell migration. The concentration range is chosen based on the literature [43], where proliferation and migration assay was performed using the same range of concentration. The range of concentrations of EGF used for the experiments was in similar range of concentration that is commonly found in the human body. EGF at 25, 50, 75, 100 and 125 ng/ml was added to the attractant wells, 24 hrs after the cells were seeded in the cell chambers. Pictures were taken every 24 hours for a period of 5 days. The average number of cells that are

migrating towards each factor has been measured and plotted as shown in Figure 2.11. The results indicate that from Day 1 to Day 3 there was a steady increase in the migration of cells both in control and at different concentrations of EGF, whereas it slightly decreased on Day 4 as a large number of cells crossed the channels and entered into the attractant well. From Day 1 to Day 4, actual number of cells migrating towards the attractant increased from 5 to 33, 0 to 14, 28 to 73, 15 to 113, 41 to 136 and 0 to 5 at 0, 25, 50, 75, 100 and 125ng/ml of EGF. The number of cells migrating into the channels increased from 0 to 100ng/ml of EGF with peak migration occurring at 100ng/ml. The migration of cells was significantly inhibited at 125 ng/ml of EGF.

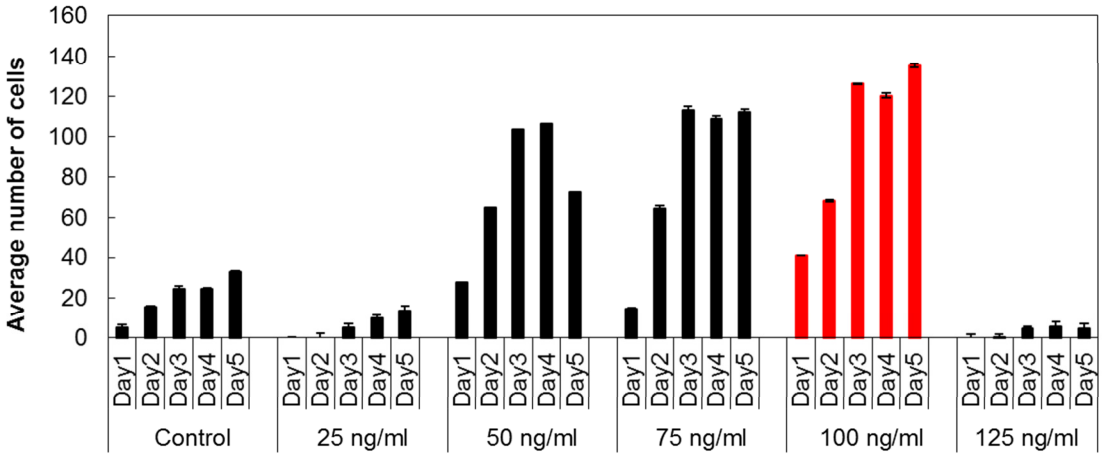

Figure 2.11. Number of PC-3 cells in channels in response to different concentrations of EGF.

2.3.2.4 Effects of bFGF on PC-3 Cell Migration

Fibroblast family growth factors are well known to be essential factors for both normal and abnormal proliferation of prostate cells [44-49]. It was found

that three prostate cancer cell lines, which differed in their dependence on androgens and in their metastatic potential in nude mice [50-53], also differed in their expression of bFGF. We used our microfluidic array to evaluate the effect of bFGF on the prostate cancer cell migration. 24 hrs after the cells were seeded in the cell chambers, bFGF at 0.1, 0.3, 1 and 3 ng/ml was added to the attractant wells. The concentration range was chosen based on the literature [54]. Pictures were taken every 24 hours for a period of 5 days. The average number of cells that were migrating towards each factor was measured and plotted as shown in Figure 2.12. The results indicate that from Day 1 to Day 5, there is steady increase in the migration of cells both in control and at different concentrations of bFGF. From Day 1 to Day 5, actual number of cells migrating towards the attractant increased from 1 to 52, 2 to 37, 9 to 157, 4 to 64 and 2 to 28 at 0, 0.1, 0.3, 1 and 3ng/ml of bFGF. At 0.3 and 1 ng/ml enhanced the cell migration with peak migration at 0.3 ng/ml of bFGF, whereas other concentrations did not enhance the migration significantly.

2.3.2.5 Comparison of Migration Potential of PC-3 for Different Growth Factors

Four growth factors have been tested for their effect on PC-3 cell migration at their respective optimal concentration ranges. The concentration at which there is peak migration is 0.1, 5,100 and 0.3 ng/ml for TGFβ, VEGF, EGF and bFGF respectively. In order to compare the migration potential within these growth factors, Individual growth factor's cell migration was normalized with

respective control cell migration number on Day 5. Figure 2.13 shows the comparison of the PC-3 cells migration potential for all four growth factors on Day 5.

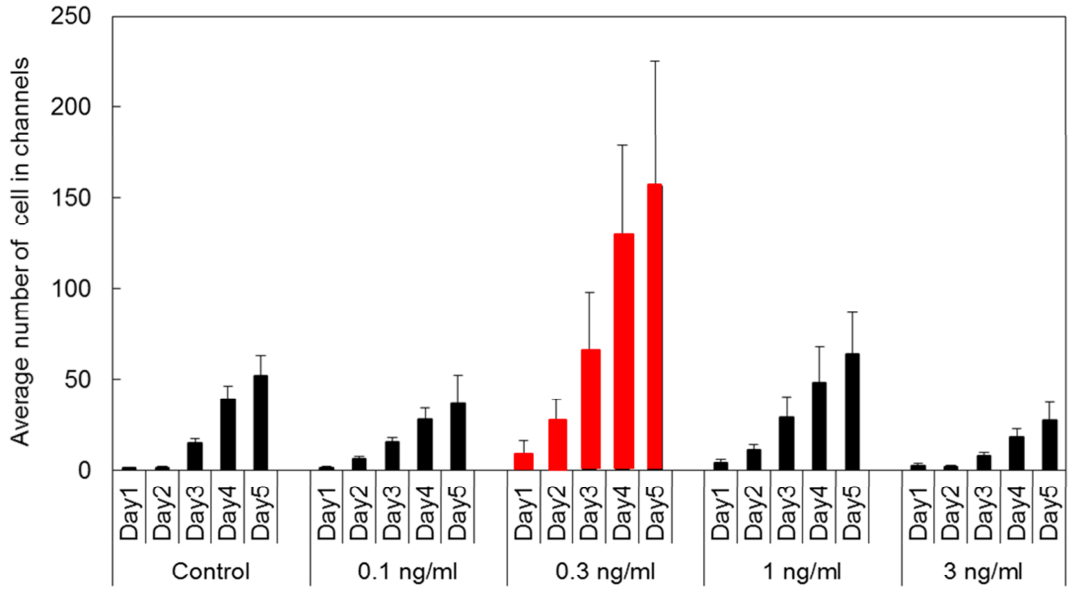

Figure 2.12 Number of PC-3 cells in channels in response to different concentrations bFGF.

The results indicated that highest number of cells had migrated towards VEGF, and was approximately twelve times more than the control. All growth factors enhanced the migration with respect to control. bFGF, TGFβ, EGF and VEGF was the increasing order of the migration potential of PC-3 cells.

2.3.3 PC-3 ML Growth Factor Experiments

The experiment was aimed to find out the effect of different growth factors on migration behavior of lung metastasized prostate cancer (PC-3 ML) cells. This experiment helped us in understanding the behavior of two different

prostate cancer cells with different metastatic ability. The device cleaning, priming and cell seeding protocol was as discussed in section 2.3.2.

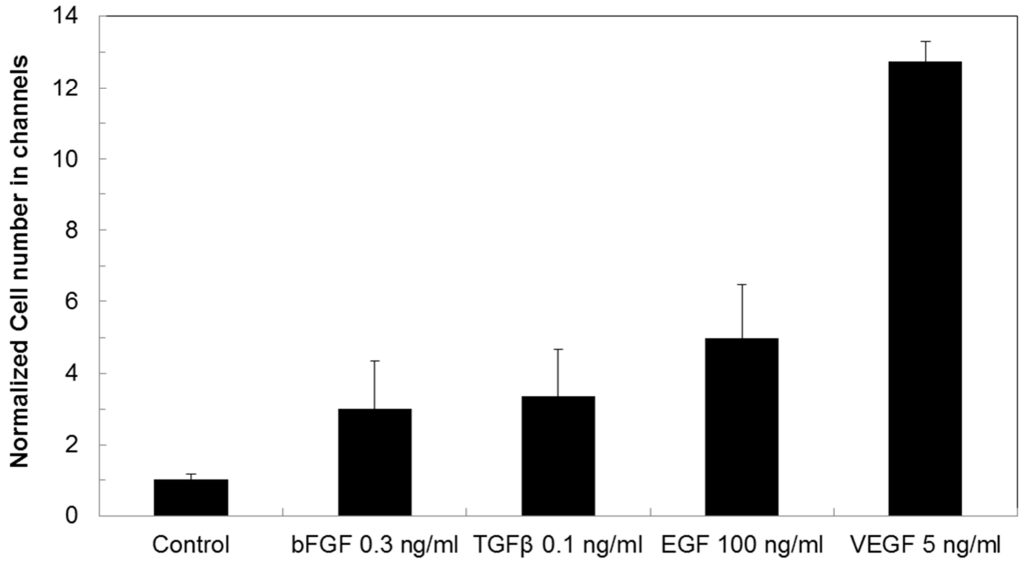

Figure 2.13 Comparison of PC-3 cells migration potential in response to four different growth factors.

The experimental parameters for this experiment are shown in Table A.1 in Appendix A. The average number of cells that were migrating towards TGFβ at 5, 10, 15 ng/ml is shown in Figure A.1 in Appendix A. Though among the tested concentration, peak migration occurred at 5 ng/ml, it didn't enhance migration with respect to control. Rather at 10 and 15 ng/ml concentration the migration was completely inhibited. This could be possibly due to the cell growth inhibition property of TGFβ. The average number of cells that were migrating towards VEGF at 1, 2.5, 5, 10, 15, 25 and 35 ng/ml is shown in Figure A.2. The peak migration occurred at 10ng/ml, but the migration was not significantly enhanced by VEGF as compared to control. The average number

of cells that were migrating towards EGF at 25, 50, 75, 100 and 125 ng/ml is shown in Figure A.3. EGF at 75, 100 and 125 ng/ml significantly increased the migration by 171%, 200% and 157% respectively. Peak migration occurred at EGF 100 ng/ml, while migration decreased at 125 ng/ml. It was due to the fact that the PC-3 ML cells have EGF receptors. The higher concentrations of EGF on the attractant side saturated the receptors and thereby reduced the affinity of the cells to migrate towards it. The average number of cells that were migrating towards bFGF at 0.1, 0.3, 1, 3 and 30 ng/ml is shown in Figure A.4. bFGF at 0.01ng/ml and 3 ng/ml, significantly enhanced the migration by 130% and 150% respectively as compared to control.

2.3.3.1 Comparison of Migration Potential of PC-3 ML for Different Growth Factors

Four growth factors have been tested for their effect on PC-3 ML cell migration at their respective optimal concentration ranges. The concentration at which there is peak migration is 5, 10,100 and 3 ng/ml for TGFβ, VEGF, EGF and bFGF respectively. In order to compare the migration potential within these growth factors, Individual growth factor's cell migration was normalized with respective control cell migration number on Day 5. Figure 2.14 shows the comparison of the PC-3 ML cells migration potential for all four growth factors on Day 5. The results indicates that highest number of cells have migrated towards EGF; approximately two times more than the control. This was closely

followed by bFGF at approximately one and half times the control. TGFβ and VEGF did not enhance the migration of PC-3 ML cells.

2.3.4 MDA-MB-231 Growth Factor Experiments

The experiment aimed to find out the effect of different growth factors on migration behavior of MDA-MB-231 breast cancer cells which has higher metastatic potential to bone. The device cleaning, priming and cell seeding protocol was repeated as discussed in section 2.3.2. The experimental parameters are shown in Table A.2 in Appendix A. The average number of cells that migrated towards TGFβ at 0.01, 0.1, 1, 10 ng/ml is shown in Figure A.5 in Appendix A. The concentrations chosen were based on proliferation data in the literature [55]. Among the tested concentration, peak migration occurred at 0.01 ng/ml, whereas at other concentrations the migration was inhibited by TGFβ. This could be possibly due to the cell growth inhibition property of TGFβ. The average number of cells that migrated towards VEGF at 20, 40, 50, 60 and 100 ng/ml is shown in Figure A.6. The concentrations were extracted from literature which suggested the acceptable concentration range of VEGF used in studies involving proliferation of MDA-MB-231 [56]. The peak migration occurred at 80ng/ml, but the migration was inhibited by VEGF at rest of the concentrations as compared to control. The average number of cells that migrated towards EGF at 1, 5, 10, 50 and 100 ng/ml [57] is shown in Figure A.7. Among the tested concentrations, EGF at 1 ng/ml enhanced the migration. But migration could not be significantly enhanced with respect to control. The average

number of cells that migrated towards bFGF at 1, 10, 30, 50 and 70 ng/ml [58] is shown in Figure A.8. Among the tested concentration bFGF did not enhance the migration as compared to control.

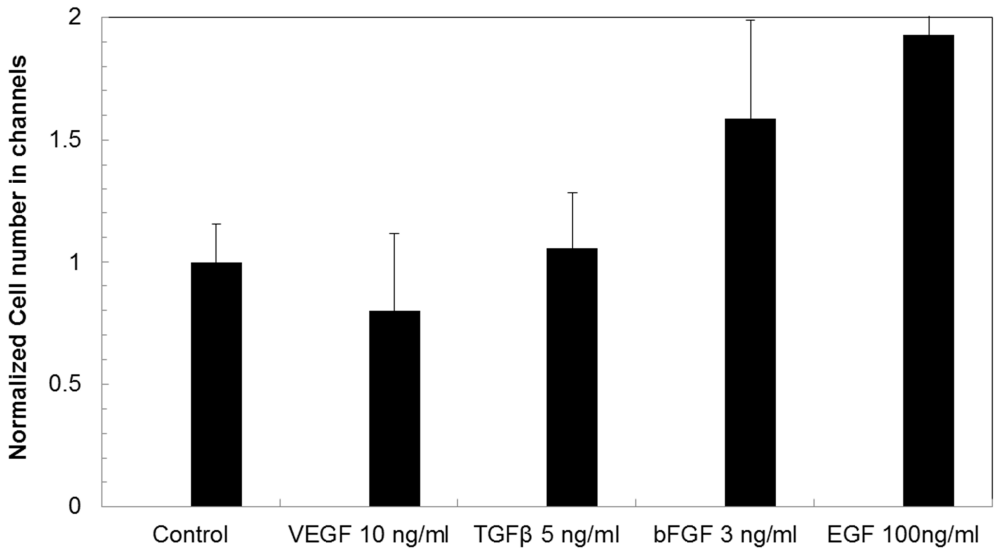

Figure 2.14 Comparison of PC-3ML cells migration potential in response to four different growth factors.

2.3.4.1 Comparison of Migration Potential of MDA-MB-231 for Different Growth Factors

Four growth factors have been tested for their effect on MDA-MB-231 cell migration at their respective optimal concentration ranges. The concentration at which there is peak migration was 0.01, 80, 1 and 1 ng/ml for TGFβ, VEGF, EGF and bFGF respectively. In order to compare the migration potential within these growth factors, Individual growth factor's cell migration was normalized with respect to control cell migration number on Day 5. Figure 2.15 shows the comparison of the MDA-MB-231 cells' migration potential for all

four growth factors on Day 5. The results indicated that highest number of cells had migrated towards VEGF, at 1.5 times more than the control followed by TGFβ and VEGF, at approximately 1.3 and 1.4 times the control. bFGF did not enhance the migration of MDA-MB-231 cells.

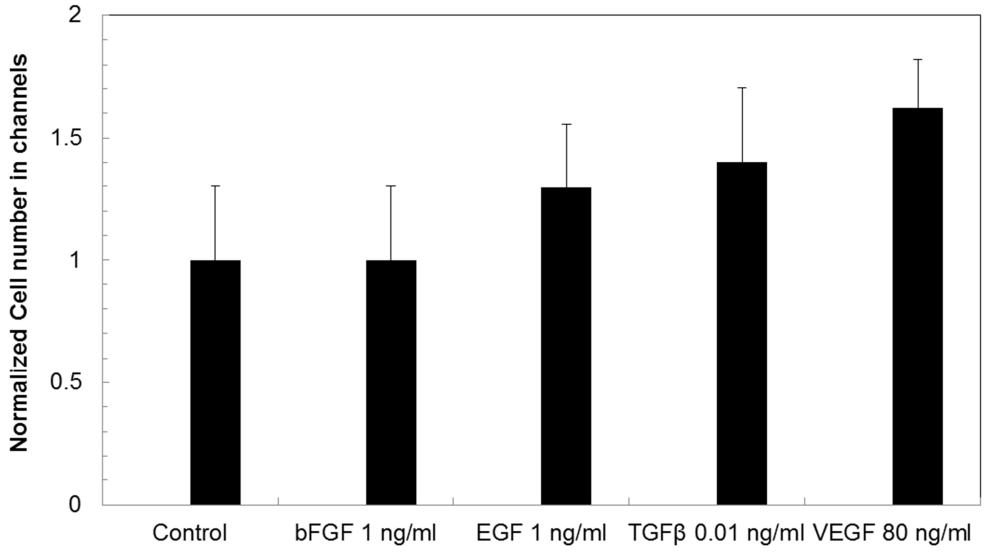

Figure 2.15 Comparison of MDA-MB-231 cells migration potential in response to four different growth factors.

2.3.5 Comparison of Effects of Growth Factors on PC-3, PC-3ML and PZ-HPV-7 Cells Migration Potential

This experiment was aimed to compare the migration behavior of prostate cancer cells (PC-3), lung metastasized prostate cancer cells (PC-3 ML) and nonmalignant prostate cells (PZ-HPV-7) at optimal concentrations of growth factors. Four growth factors such as TGFβ, VEGF, EGF and bFGF were tested at optimal concentrations of 2 ng/ml, 10 ng/ml, 50 ng/ml and 10 ng/ml respectively. PC-3, PC-3ML and PZ-HPV-7 cells were seeded in the cell

chamber at 5000 cells/ well. Twenty-four hours after the cell seeding, growth factors were added into the attractant chamber. Five devices were allocated for each experimental condition (N=5). Pictures were taken every 24 hours for a period of five days. The number of cells migrating through the channels towards the chemoattractant was counted and normalized with respect to percentage of control. Figure 2.16 shows a comparison of cell migration behavior with respect to different growth factors.

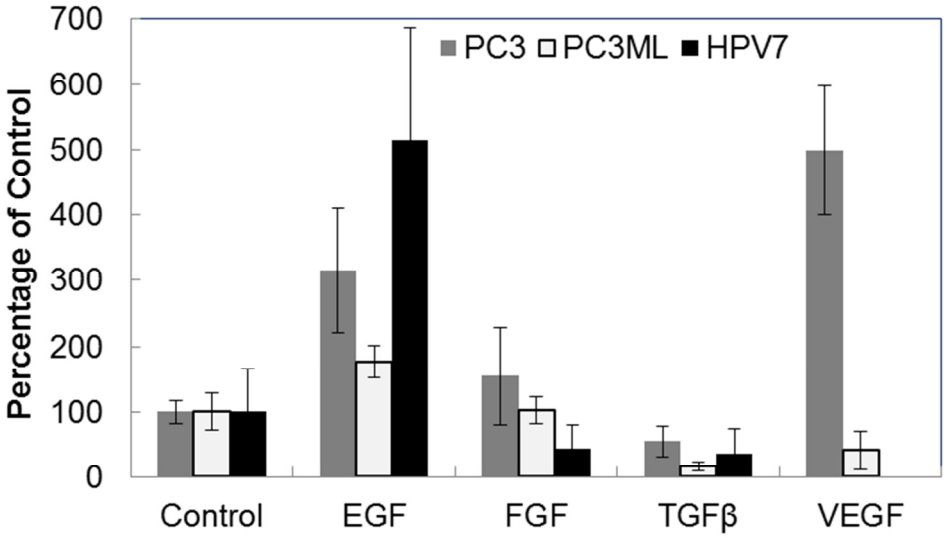

Figure 2.16 Comparison of migration behavior of PC-3, PC-3ML and PZ-HPV-7 cells towards optimal concentrations of growth factors.

Results indicate that EGF enhanced migration in all three cell types with PZ-HPV-7 having highest migration followed by PC-3 and PC-3ML. TGFβ and bFGF did not enhance the migration in all the three cell types. The clear difference in migration pattern among the PC-3, PC-3ML and PZ-HPV-7 cells has been observed in the case of VEGF. Only PC-3 cells' migration was enhanced by VEGF whereas PC-3ML and PZ-HPV-7 cells' migration was

significantly inhibited by VEGF. Literature suggests that the metastatic properties of prostate cancer cells are controlled by VEGF [59]. Also increased levels of VEGF were found in patients with metastatic prostate cancer [59].

2.3.6 Effect of Chemotherapy Drugs on Cell Migration

The ability of chemotherapy to kill cancer cells depends on its ability to halt cell division. Usually, the drugs work by damaging the RNA or DNA that tells the cell how to copy itself in division. If the cells are unable to divide, they die. The faster the cells are dividing, the more likely it is that chemotherapy will kill the cells, causing the tumor to shrink. They also induce cell suicide (self-death or apoptosis).

Chemotherapy drugs that affect cells only when they are dividing are called cell-cycle specific. Chemotherapy drugs that affect cells when they are at rest are called cell-cycle non-specific. The scheduling of chemotherapy is set based on the type of cells, rate at which they divide, and the time at which a given drug is likely to be effective. This is why chemotherapy is typically given in cycles.

Chemotherapy is most effective at killing cells that are rapidly dividing. Unfortunately, chemotherapy does not know the difference between the cancerous cells and the normal cells. The "normal" cells will grow back and be healthy but in the meantime, side effects occur. The "normal" cells most commonly affected by chemotherapy are the blood cells, the cells in the mouth, stomach and bowel, and the hair follicles; resulting in low blood counts, mouth

sores, nausea, diarrhea, and/or hair loss. The low blood counts could also lead to lowered immunity. Different drugs may affect different parts of the body.

Docetaxel (DT) is clinically well established chemotherapy drug. It is cytotoxic or anti-mitotic classification drug, which interferes with the cell division and proliferation. It is commonly marketed under the trade name 'Taxotere'. Docetaxel is administered through a vein (intravenously, IV). It is approved in treatment of breast cancer, non-small cell lung cancer, advanced stomach cancer, head and neck cancer and metastatic prostate cancer.

Doxorubicin (DX) is classified as an antitumor antibiotic. Antitumor antibiotics are made from natural products produced by species of the soil fungus Streptomyces. These drugs act during multiple phases of the cell cycle and are considered cell-cycle specific. Doxorubicin is also administered through a vein. It is approved in the treatment of bladder, breast, head and neck, leukemia (some types), liver, lung, lymphomas, mesothelioma, multiple myeloma, neuroblastoma, ovary, pancreas, prostate, sarcomas, stomach, testis (germ cell), thyroid, uterus.

We used these drugs (Docetaxel and Doxorubicin) to study their effect on PC-3, PC-3ML and breast cancer cell migration. We tested these drugs under two scenarios: 1) When the drug is on attractant side, this mimics the physiological condition of when a drug is injected intravenously, where only a gradient of drug reaches the cancer site and 2) When the drug is on the cell

side, this mimics the physiological condition when a drug is directly targeted to tumor site.

2.3.6.1 Docetaxel (DT) and Doxorubicin (DX) Effect on Migration of PC-3ML Cells

The cytotoxic effects of Docetaxel and Doxorubicin were studied to determine the lethal concentration 50 (LC 50). The LC 50 is defined as the concentration of drug/reagent required to eliminate 50% of the test population. Initially PC-3ML cells were seeded at a density of 5000 cells/ well in 80 µL of a 96 well plate. DT was added to the well plate at a concentration of 1, 5, 10, 50, 100, 250 and 500 nM, 24 hours after the cells were seeded. Each concentration condition of DT was repeated three times. Cell proliferation was assessed by performing MTT assay on the samples. Cells with no drug treatment acted as control. Figure 2.17(a) shows the cell proliferation as a percentage of control under different concentrations of DT. Similar experiment protocol was followed to test the proliferation under effect of Docetaxel at 0.01, 0.04, 0.05, 0.07, 0.1, 0.15, 0.2, 0.4, 0.5, 0.7,1 and 2 µM concentrations. Figure 2.17 (b) shows the cell proliferation as a percentage of control under different concentrations of DX.

Based on MTT assay data, three concentrations corresponding to 95%, 75% and 50% cell viability were chosen. For Docetaxel drug 5, 10, 50 nM (labeled as DT1, DT2, and DT3 respectively) were the concentrations at which cell viability was 95%, 75% and 50% respectively. Similarly for Doxorubicin

drug, corresponding concentrations were 50, 100 and 500 nM (labeled as DX1, DX2 and DX3).

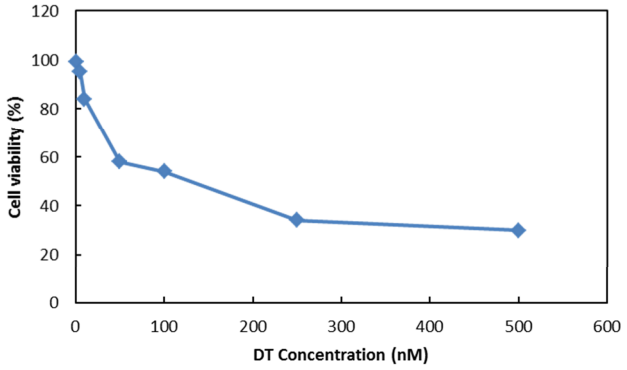

(a)

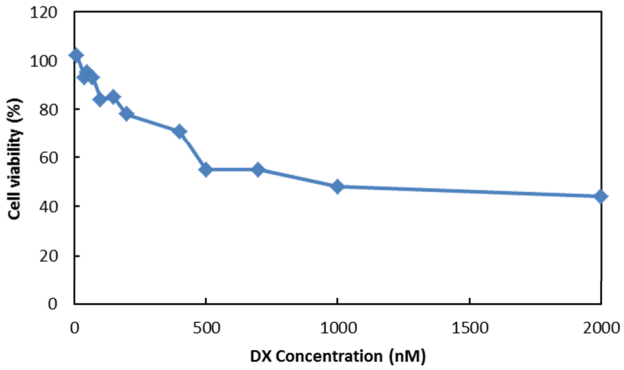

(b)

Figure 2.17 PC-3ML cell viability measured under (a) different concentrations of DT and (b) different concentrations of DX using MTT assay and expressed as percentage of control.

Initially 2% FBS and RPMI were added to cell chamber of the device and primed using a vacuum pump. RPMI1640 with 5% FBS was used as an attractant in the experiment. The condition when no drug was added to either cell or attractant chamber acted as control. The three corresponding concentrations of each drug (DT1, DT2, DT3, DX1, DX2 and DX3) were prepared in both 2% FBS containing RPMI and 5% FBS containing RPMI. Cells in the suspension of 2% FBS, RPMI were seeded in all the devices at a seeding

density of 5000 cells/well and were allowed to attach for 24 hours. In one set of devices the cell side media was replaced by the media (2% FBS, RPMI) containing different concentrations of drugs. This condition is denoted as 'Drug name cell' (for example DT1 cell). In other set of devices the attractant media was replaced by media (5% FBS, RPMI) containing different concentration of drugs. This condition is denoted as 'Drug name attractant' (for example DT1 attractant). The effect of the migration of drugs at various concentrations on cell side alone and attractant side alone was measured using our device. Figure 2.18 shows the average cell number in the channels at different concentrations of DT on cell side and attractant side. The migration of PC-3ML significantly reduced with increase in the concentration of DT on attractant side. On day 5 number of cells that migrated towards attractant containing DT1, DT2 and DT3 tremendously drop down to 40%, 21%, and 24% respectively, with respect to control.

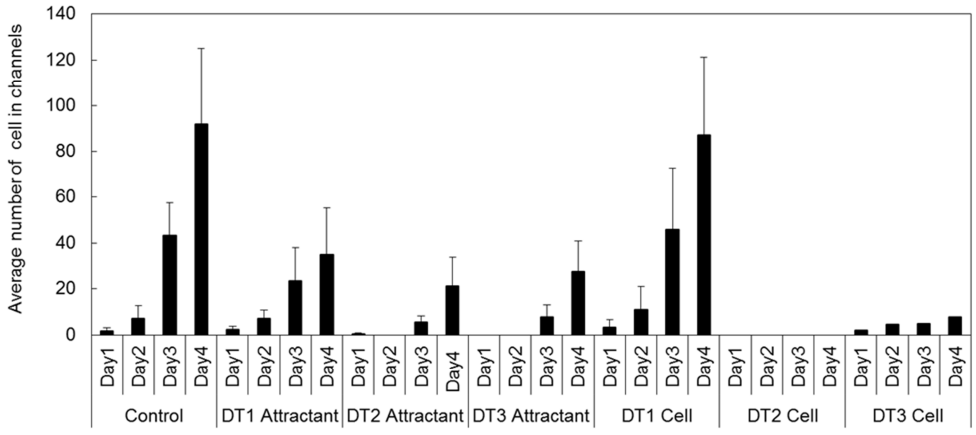

Figure 2.18 Average number of PC-3ML cells migrating to attractant side in microchannels, when Docetaxel at three different concentrations was added to cells side and attractant side individually.

The results imply that, as DT is intravenously injected it reaches varies parts of the body, DT not only eliminated cancer at primary site but it could also help in preventing the migration to secondary site. The migration of cells to attractant also reduced with increase in concentration of drug on the cell side. At lower concentration like DT1 where 95% of cells were alive even after 3 days (from MTT assay data), cell migration occurred similar to that of control. This might be due to the fact that lower concentration of drug didn't affect the cell health and also cells sense an unfavorable or threat condition on cell side and migrated to attractant well, whereas at higher concentration of the DT such as DT2 and DT3, migration was completely stopped due to cell death or unhealthy cells. These results imply that, if drugs are administered locally to the tumor and an optimum dosage of drug is not provided, it might promote the cells to migrate to other potential sites. Figure 2.19 shows the average number of PC-3ML cells in the channels at different concentrations of DX on cell side and attractant side. The migration of PC-3ML also significantly reduced with increase in the concentration of DX on attractant side. On day 5 number of cells that had migrated towards attractant containing DX1, DX2 and DX3 dropped tremendously to 64%, 12%, and 10% respectively, with respect to control. The results imply that, DX not only eliminates cancer at primary site but it could also help in preventing the migration of cancer to secondary site. The migration of cells to attractant also reduced with increase in concentration of drug on the cell side. Unlike DT1, DX1 didn't allow the PC-3 cells to migrate towards the

attractant. Similarly at DX2 and DX3 on cell side reduced the migration significantly. These results imply that, the migration of cancer to secondary site during chemotherapy purely depends on the type of drug, concentration of the drug, method and location of administering drug and also specifically depends on the aggressive nature of the cancer cells.

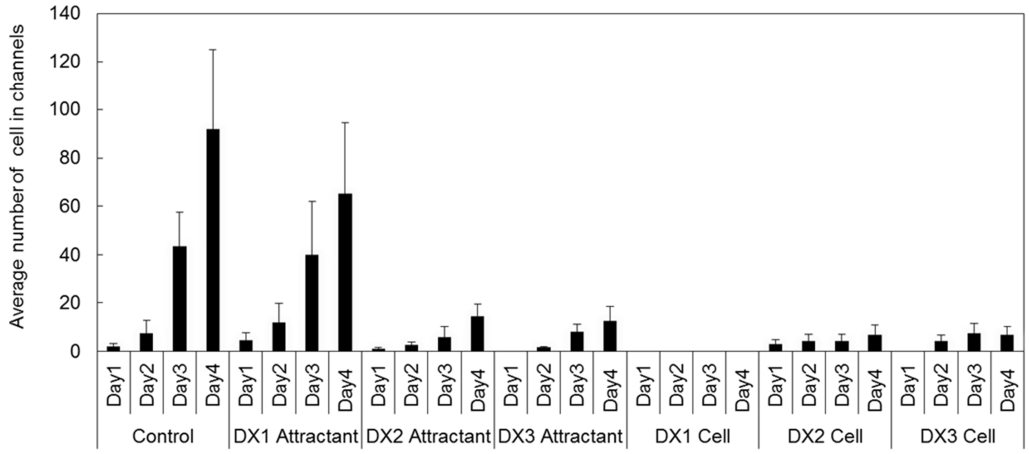

Figure 2.19 Average number of PC-3ML cells migrating to attractant side in microchannels, when Doxorubicin at three different concentrations was added to cells side and attractant side individually.

2.3.6.1.1 Docetaxel (DT) and Doxorubicin (DX) Effect on Migration of PC-3ML Cells when Attractant is EGF 75 ng/ml.

The aim of the experiment was to find out the response of PC-3ML cells under the influence of drugs and a more dominant attractant such as EGF 75ng/ml. Similar procedure as described in section 2.3.6.1 was followed except the attractant was replaced with media containing 2% FBS, EGF 75 ng/ml and RPMI. Figure 2.20 shows the average number of cells that migrated towards EGF 75 ng/ml when DT was added to the cell side and attractant side.

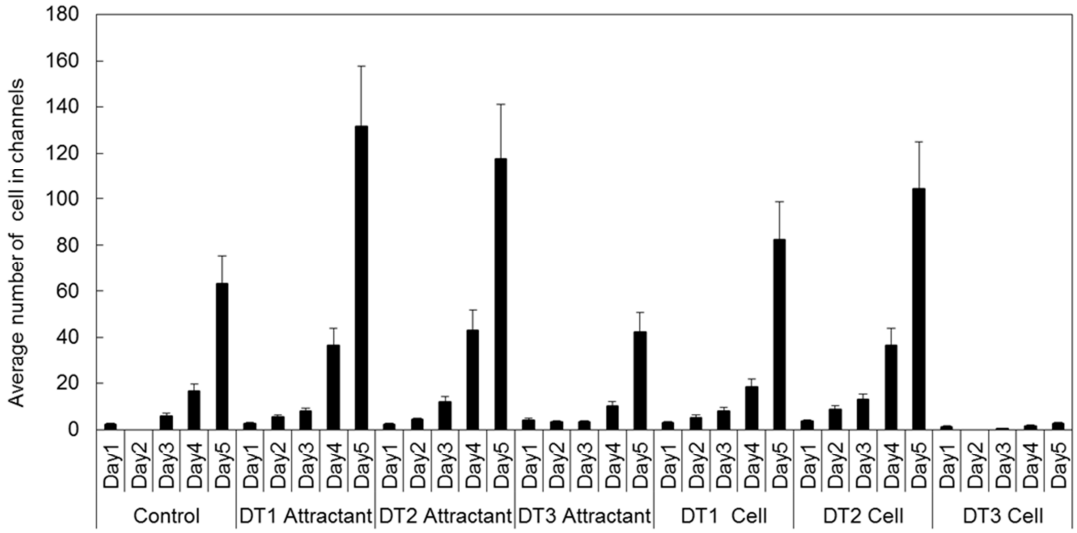

Figure 2.20 Average number of PC-3ML cells migrating to EGF 75 ng/ml in microchannels, when Docetaxel at three different concentrations was added to cell side and attractant side individually.

DT1 and DT2 added to attractant side couldn't stop the PC-3ML cells from migrating. Rather their combination with attractant enhanced the cell migration. However DT3 being the LC 50 concentration could inhibit cell migration by 33% as compared to control. When the drug was added to cell side, DT1, DT2 couldn't stop the cells from migrating to the attractant due the fact that the DT at these concentrations was less effective to eliminate the cells right way and also cells sensed much favorable condition available on the attractant side. However DT3, when added to cell side could significantly stop the cells from migrating by 91%. Results imply that when there is a stronger attractant available at the secondary site and an inappropriate dosage of drug was administered, it could potentially promote the metastasis of cancer.

Figure 2.21 shows the average number of cells that migrated towards EGF 75 ng/ml when DT was added to the cell side and attractant side.Figure 2.21 shows the average number of cells migrating towards EGF 75 ng/ml when DT is added to the cell side and attractant side.

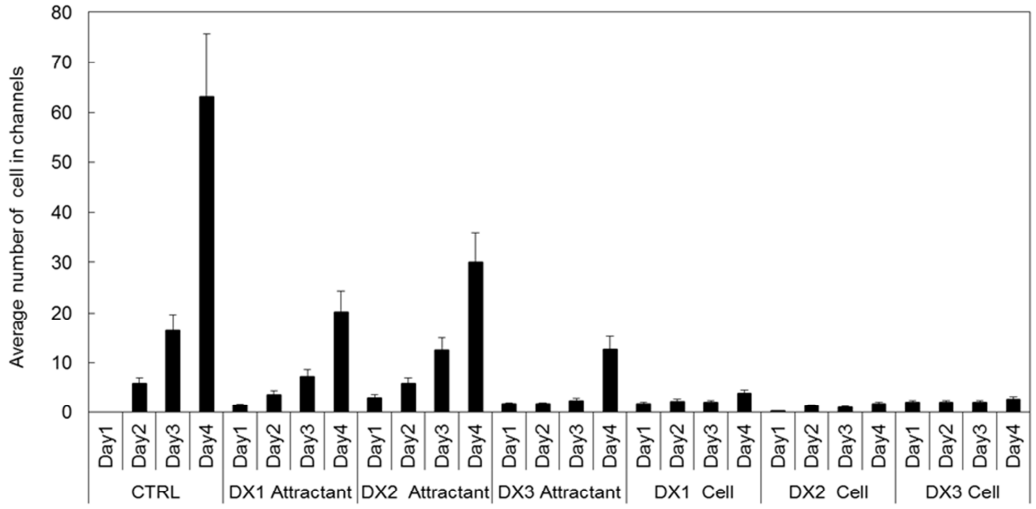

Figure 2.21 Average number of PC-3ML cells migrating to EGF 75 ng/ml in microchannels, when Doxorubicin at three different concentrations was added to cell side and attractant side individually.

All three concentrations of DX on both attractant and cell side significantly inhibited the cells from migrating when the attractant was EGF 75ng/ml. DX1, DX2 and DX3 on attractant side reduced the migration by 66%, 53% and 83% respectively. All concentrations of DX on cell side reduced the migration by approximately 90%. DX is found to be more effective than DT to stop migration irrespective of the attractant used.

2.3.6.2 Docetaxel (DT) and Doxorubicin (DX) Effect on Migration of PC-3 Cells

The experimental procedure was repeated as described in the section 2.3.6.1. The attractant for this experiment was 5% FBS, RPMI. Figure 2.22 shows the average number of PC-3 cells that migrated towards the attractant in the presence of different concentrations of DT added to both attractant and cell side.

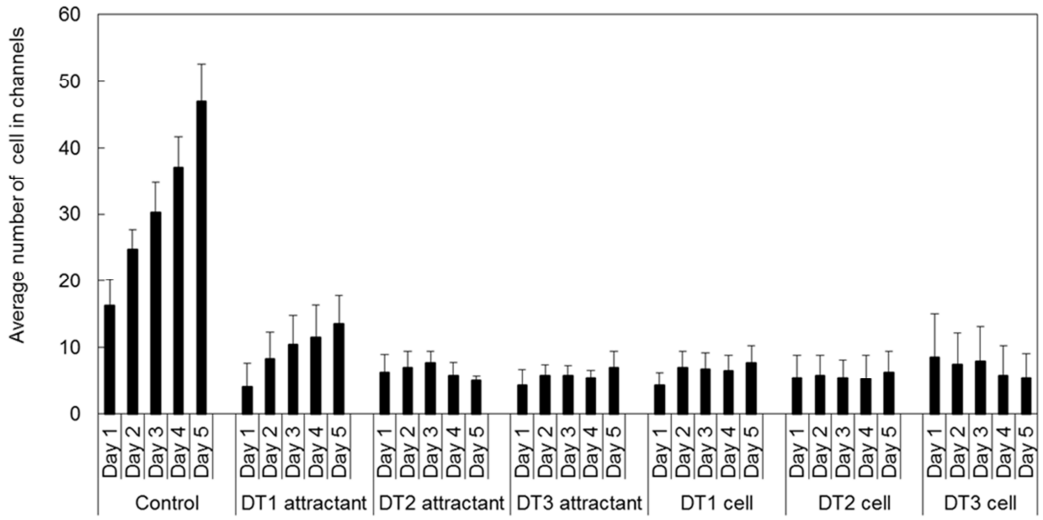

Figure 2.22 Average number of migrating PC-3 cells in microchannels, when Docetaxel at three different concentrations was added to cells side and attractant side individually.

The average number of cells migrating in the presence of DT1, DT2 and DT3 reduced by approximately 64% as compared to control. Migration was significantly reduced by approximately 62%, when all three different concentration of DT was added to cell side. The average number of migrating cells in the channel was constant from Day1 to Day5, when DT was on cell

side. This is due to the fact that as the cells sensed DT a small group of cells migrated in the channel. Even after 5 days these cells didn't move out the channel, blocking the way for other cells to enter the channel. Eventually after 5 days cells died in the channels. Due to this reason we didn't observe a constant increase in the number of migrating cells from Day1 to Day5.

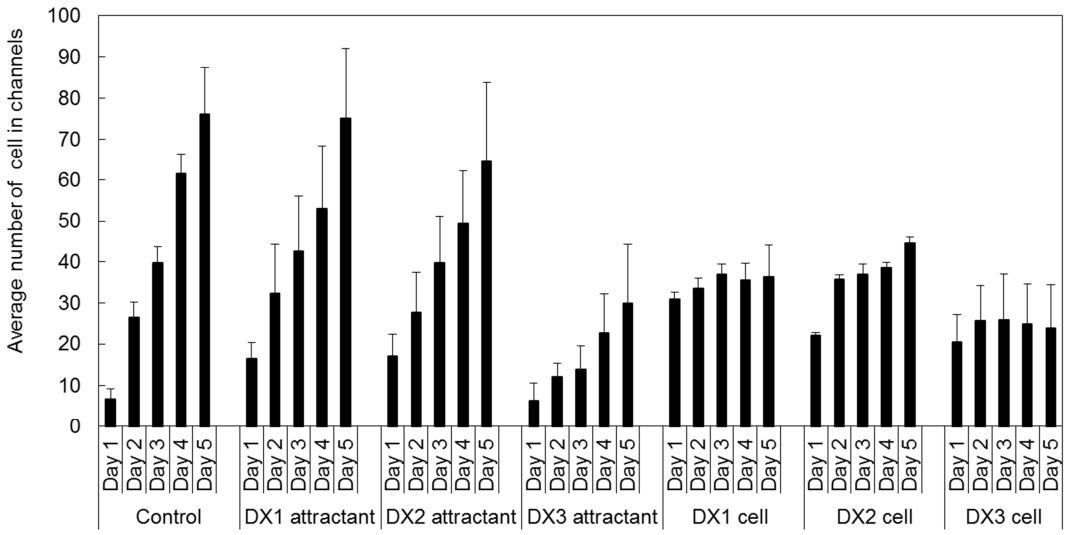

Figure 2.23 Average number of migrating PC-3 cells in microchannels, when Doxorubicin at three different concentrations was added to cells side and attractant side individually.

Figure 2.23 shows the average number of PC-3 cells that migrated towards the attractant in the presence of different concentrations of DX added to both attractant and cell side. DX1 and DX2 on attractant side did not inhibit the PC-3 cell migration significantly as the response was same as control, whereas DX3 on attractant side significantly inhibited the migration by 60%. Similarly DX1, DX2 and DX3 significantly reduced migration by 54%, 44% and 60% respectively. The constant number of cells in the channel from day 1 to

day 5 was due to the same phenomenon as described in the case of DT. Results indicated that compared to DX, DT on both cell and attractant side significantly reduced the PC-3 cell migration.

2.3.6.3 Docetaxel (DT) and Doxorubicin (DX) Effect on Migration of MDA-MB-231 Cells

Based on MTT assay data from literature [60,61], three concentrations corresponding to 95%, 75% and 50% cell viability were chosen. For Docetaxel drug 5, 10, 25 nM (labeled as DT1, DT2, and DT3 respectively) were the concentrations at which cell viability was 95%, 75% and 50% respectively. Similarly for Doxorubicin drug, corresponding concentrations were 20, 1000 and 5000 nM (labeled as DX1, DX2 and DX3). Experimental procedure was followed as described in section 2.3.6.1. Figure 2.24 shows the average number of MDA-MB-231 cells that migrated towards the attractant in the presence of different concentrations of DT added to both attractant and cell side. Results indicated that DT on both cell side and attractant side inhibited the migration by approximately 90–95%. Figure 2.25 shows the average number of MDA-MB-231 cells that migrated towards the attractant in the presence of different concentrations of DX added to both attractant and cell side. Results suggest that DX1 on attractant side did not inhibit the cell migration as compared to control, whereas DX2 and DX3 on attractant side inhibited the migration by 40% and 66% respectively.

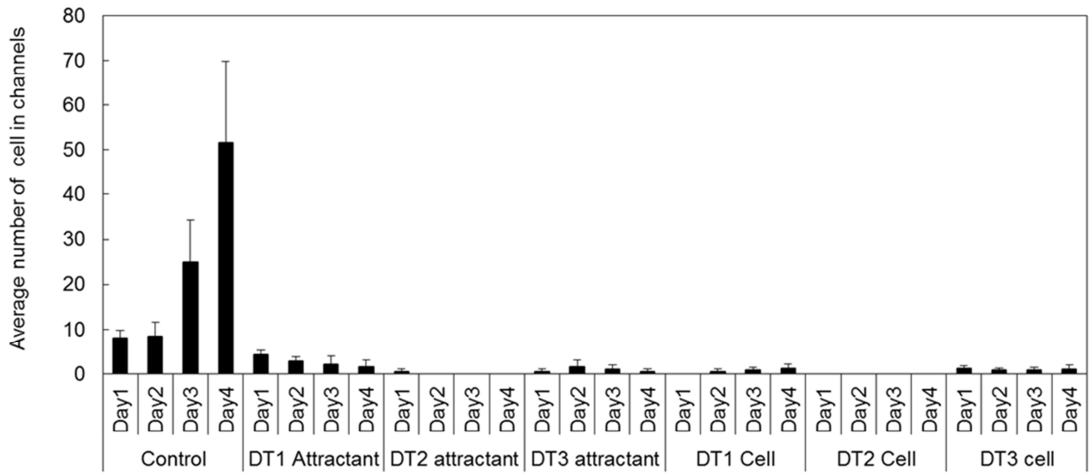

Figure 2.24 Average number of migrating MDA-MB-231 cells in microchannels, when Docetaxel at three different concentrations was added to cells side and attractant side individually.

DX1, DX2 and DX3 on the cell side inhibited the cell migration by 66%, 66% and 90% respectively as compared to control. In MDA-MB-231 drug experiments, as compared to DX, DT was found to be more effective to inhibit cell migration when added to both cell and attractant side.

2.3.6.3.1 Epirubicin and Gemzar Effect on Migration of MDA-MB-231 Cells

Epirubicin is anti-cancer chemotherapy drug which is exclusively used to treat patients with breast cancer. Epirubicin is given by intravenous injection (IV). The syringe needle is placed directly into the tubing of a freely flowing IV solution into a vein or central line and the drug is given over several minutes.

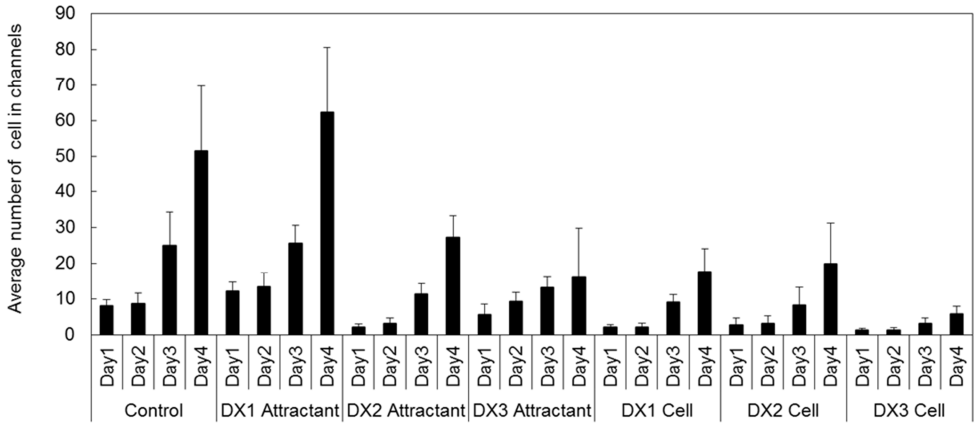

Figure 2.25 Average number of migrating MDA-MB-231 cells in microchannels, when Doxorubicin at three different concentrations was added to cells side and attractant side individually.

Based on MTT assay data from literature [62], three concentrations corresponding to 95%, 75% and 50% cell viability were chosen. For Epirubicin drug, 10, 20 and100 μM (labeled as ER1, ER2, and ER3 respectively) were the concentrations at which cell viability was 95%, 75% and 50% respectively. Figure A.9 in Appendix A shows the average number of MDA-MB-231 cells that migrated towards the attractant in the presence of different concentrations of ER added to both attractant and cell side. Results indicate that ER at all three concentrations on both cell side and attractant side inhibited migration by more than 93%.

Gemzar is anti-cancer chemotherapy drug which is used to treat patients with metastatic breast cancer. Based on MTT assay data from literature [63], three concentrations corresponding to 95%, 75% and 50% cell viability were

chosen. For Gemzar drug, 0.01, 1 and 31 μM (labeled as Gem1, Gem2, and Gem3 respectively) were the concentrations at which cell viability was 95%, 75% and 50% respectively. Figure A.10 in Appendix A shows the average number of MDA-MB-231 cells that migrated towards the attractant in the presence of different concentrations of Gem added to both attractant and cell side. Results indicate that Gem at all three concentrations on both cell side and attractant side inhibited migration by 94–99%.

2.3.7 Effect of PC-3 Cell Migration to Patient Serum and Chemotherapy Drugs

Cancer patient serum may contain the important factors responsible for cancer metastasis. Testing these sera using our device and determining the migration of cells and correlating it to the patient cancer stage would potentially lead to a diagnosis platform which can help in prognosis of cancer metastasis. This would also help in pinpointing the important factors responsible for metastasis. In this study we tested the PC-3 cell migration towards three patient sera. The experiment was setup as a double blind study. We were not privy to the patient medical history or the metastatic condition, if any, of the patients during the time of experimentation. The sera were randomly labeled from 1 through 3. Initially a BCA protein assay was performed to measure the protein concentration of patient sera and FBS. Table 2.2 shows the measured protein concentration for three patient sera and FBS. The total protein concentration for FBS, Patient 1, Patient 2 and Patient 3 were found to be 38, 91.68, 51.11 and 124.19 μg/ml respectively. Initially 2% FBS and RPMI were

added to cell chamber of the device and primed all the channels using a vacuum pump. Cells in a suspension of 2% FBS, RPMI were seeded in all the devices at a seeding density of 5000 cells/well and were allowed to attach for 24 hours. 2% FBS and RPMI used as an attractant acted as control. Patient sera protein concentration were normalized with respect to 2%FBS. In first set of devices, the normalized protein concentrations of three patient sera denoted as PAT1, PAT2 and PAT3 were prepared and added to attractant side. The N number for the experiment was 5. In second set of devices, the cell side media was replaced by the media (2% FBS, RPMI) containing Docetaxel (DT) at 50 nM (LC 50) concentration. In third set of devices, the attractant such as RPMI media containing 2% FBS, PAT1, PAT2 and PAT3 was mixed with DT at 50 nM concentration and added to the attractant well. Figure 2.26 shows the effect of PC-3 cell migration in the presence of patient sera and also in combination with Docetaxel at cell side and attractant side. When the PC-3 cell migration in response to the patient sera was compared to control, PAT2 and PAT3 significantly enhanced the migration by 500% and 300% respectively, whereas PAT1 has similar response to the control. After the experiment and data processing patient status data was verified by the physician. As per the patient status data, PAT2 had terminal prostate cancer. PAT3 had prostate cancer but no signs of metastasis. PAT 1 did not have cancer. Thus migration data was found to be in agreement with the patient status. When drug was mixed with patient serum the migration of PC-3 cells reduced from 500% to 193% in case

of PAT2, from 300% to 160% for PAT3 and from 100% to 66% for PAT1 as compared to control. When the drug was added to cell side, migration of PC-3 cells tremendously reduced in case of PAT2 from 500% to 0%, in PAT3 from 300% to 0% and in PAT1 from 100% to 0% as compared to control.

Patient No	Total Protein concentration (µg/ml)
Patient 1	91.688
Patient 2	51.119
Patient 3	124.192
FBS	38

Table 2.2 Estimated protein concentration of patient sera and FBS using BCA assay.

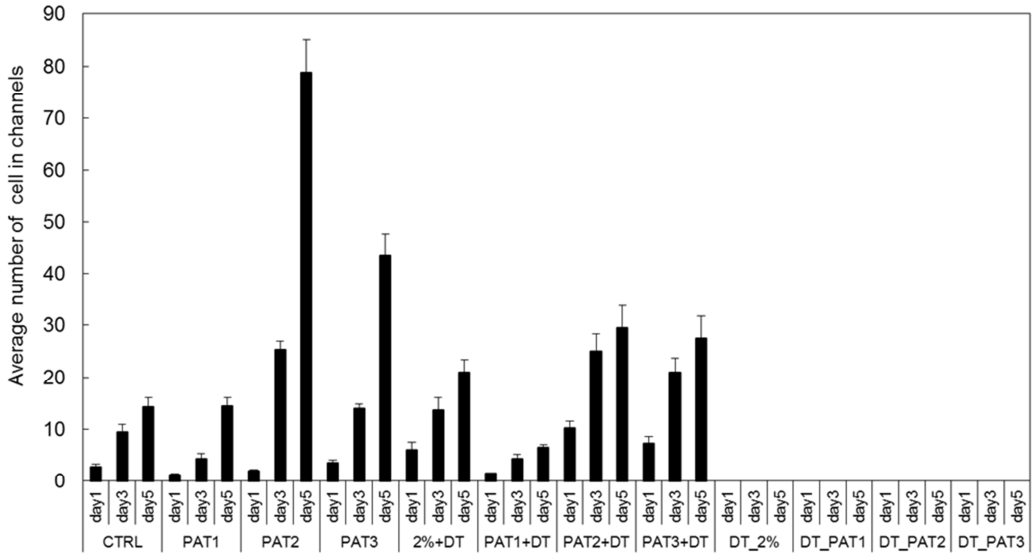

Figure 2.26 Average number of migrating PC-3 cells in microchannels when patient sera used as an attractant and Docetaxel 50 nM used as inhibitor on both cell and attractant side.

2.3.8 Migration of Cancer Cells to Organ Derived Extracts

During metastasis, cancer cells from primary organs migrate to secondary organ. In most cases specific cancers migrate to specific secondary sites. For example, prostate cancer mostly migrates to bone and lung [64]. Also breast cancer is mostly found to migrate to bone [65]. Certain tissues contain unique factors which are chemotactic for metastatic tumor cell lines.

Liver, kidney, prostate, testicles, lung, brain and femur was extracted from a Sprague-Dawley male rat (8 to 10 week old) and washed 3 times in PBS. Tissues were homogenized (1 g tissue per 1 ml buffer) with an Ultra-Turrax homogenizer and extracted for 24 h at 4°C in 0.05 M Trls-HCl (pH 7.4): 0.5 M sodium chloride: 5 mM N-ethylmaleimide: 5 mM EDTA: 1 mM phenylmethylsulfonylfluoride: gentamicin (50 mg/ml). Extracts were centrifuged at 13000 rpm for 30 min in a microcentrifuge, and the supernatant fractions were dialyzed against PBS.

Protein concentration of tissue extract was measured using BCA assay. Figure 2.27 Shows the Protein Concentration of Various Tissue Extracts. Initially 70 µL of media containing 2% FBS and RPMI were added to cell chamber of the device and primed all the channels using vacuum pump. PC-3ML cells in the suspension of 2% FBS, RPMI were seeded in all the devices at a seeding density of 5000 cells/well and were allowed to attach for 24 hours. RPMI with 2% FBS was used as an attractant and acted as the control.

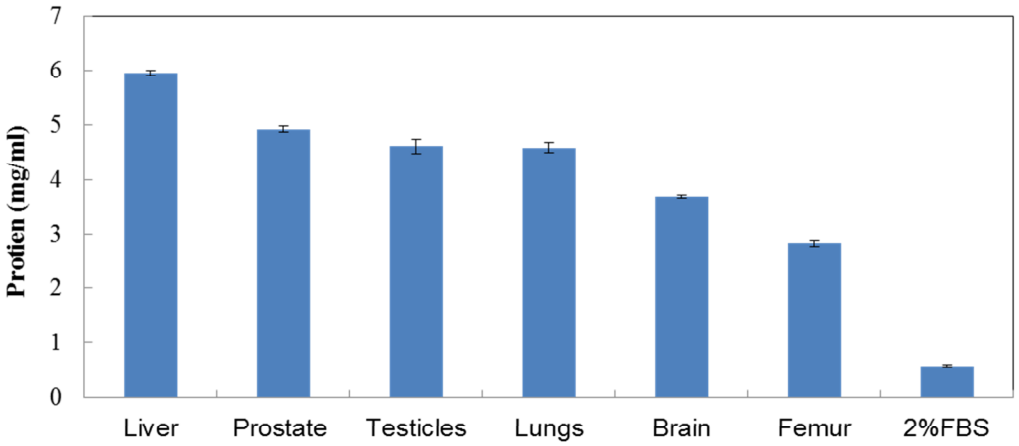

Figure 2.27 Estimated protein concentration of organ extracts and FBS through BCA assay.

Media containing 2% FBS RPMI along with 2, 4 and 8 µg protein equivalent of animal extract was added into attractant chambers. The cell migration was observed for 5 days. Average cell migration on day 5 for all the animal extracts at three concentrations is shown in Figure A.11 in Appendix A. Results indicated that testicle, prostate and brain extracts at 2 to 4 µg enhanced the migration, whereas they significantly inhibited after 8 µg. This could be due to over saturation of factor receptors on cells when the concentration of extract was increased. Lung extract at 2–8 µg enhanced migration. Femur enhanced migration only at 2 µg and liver enhanced migration only at 8 µg.

The peak migration among the tested concentrations for all organ extracts were chosen and plotted as shown in Figure 2.28.

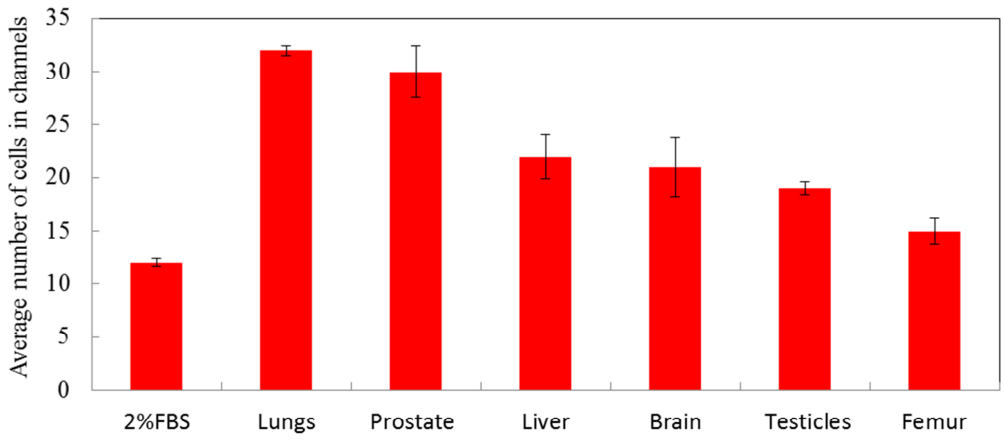

Figure 2.28 Average number of cells migrating towards the various organ extracts.

Results indicated that highest cell migration occurred in the case of lung (32 cells) and prostate (30 cells). Since the PC-3ML cells were initially originated at prostate and later metastasized to lung, cells were more susceptible to the specific factors in lungs and prostate. Other organ extracts such as liver, brain testicles and femur also enhanced the migration. However heart extract didn't enhance the migration, which could be ascribed to the rarity of heart cancer. Enhanced migration in the presence of tissue-specific chemotactic agents may be important in the formation of metastases in specific distant sites. Thus, tissues contain specific factors which can influence the rate and the degree of directed movement, penetration, and proliferation of tumor cells.

2.4 Device Length and Width Optimization Experiments

The microfluidic device's channels were 1000 μm in length, 20 μm in width and 10 μm in height. In order to find out the effect of channel length and channel width on cell migration, we designed devices with channel lengths of 250 and 500 μm and varied the channel width from 5 to 20 μm in steps of 5 μm. These devices were fabricated by a similar procedure as described in section 2.2.2.1. Figure 2.29 shows the fabricated devices with 250 and 500 μm channel length and channel width varied from 5 to 20 μm. Initially devices were primed using 2% FBS, RPMI. PC-3 cells in the suspension of 2% FBS, RPMI were seeded at 5000 cells/well density. 5% FBS, RPMI was added as attractant. Images were taken every 8 hours for 3 days and data was processed using Axiovision 4.7 image processing software. Figure 2.30 shows the average number of cells migrating through 500 μm long channel with channel width varied between 5 to 20 μm. When the average number of cells in the channel after 72 hours was compared, results indicate that number of cells migrated, decreased with decrease in the channel width. As the channel width reduces, it offers a huge resistance for the cells to migrate through the channel. This could have led to less cell migration in the narrow channels. The average number cells migrating through 20, 15, 10 and 5 μm were found to be 72, 45, 27 and 3 respectively.

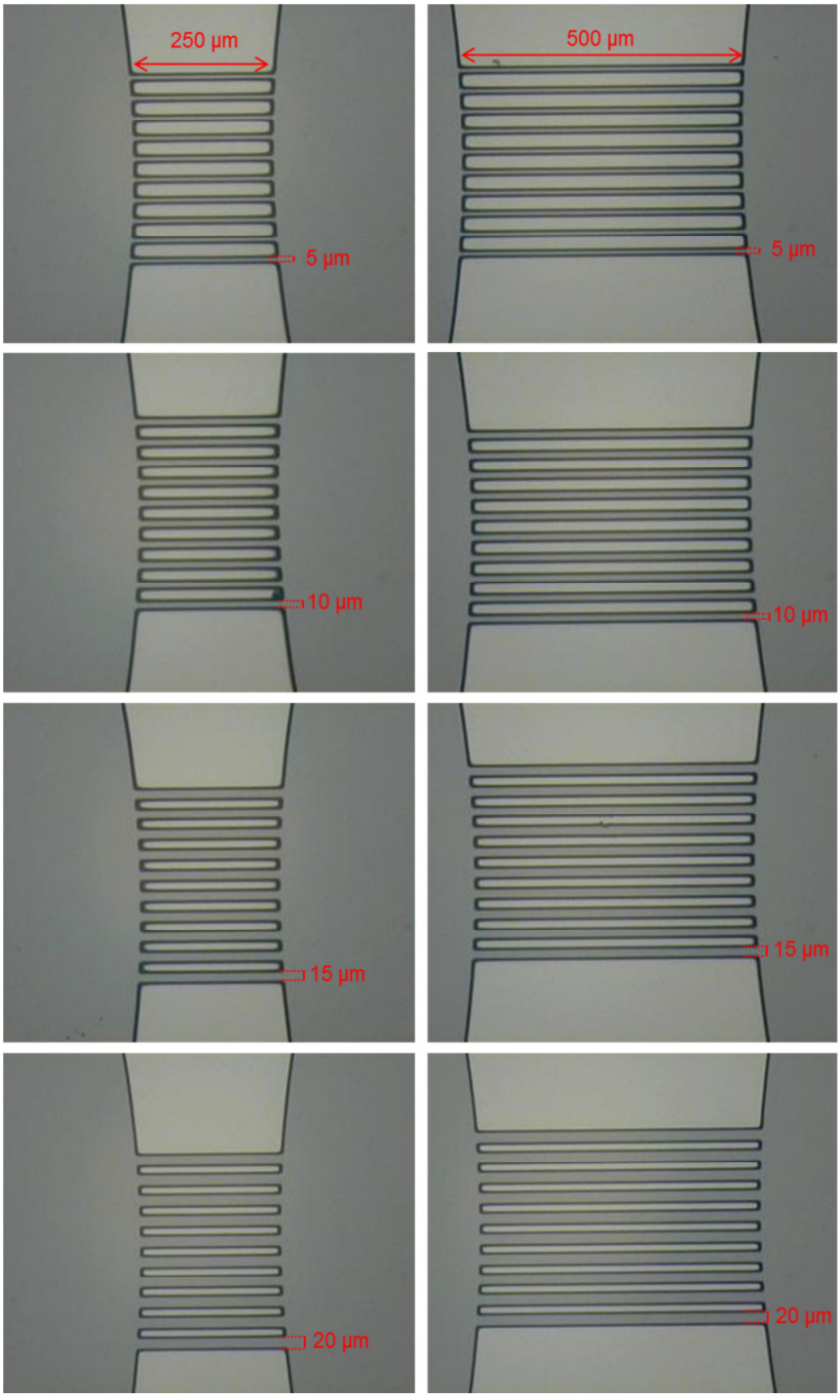

Figure 2.29 Fabricated microfluidic devices with 250 and 500 µm channel length and channel width varied from 5 to 20 µm in steps of 5 µm.

Figure 2.31 shows the average number of cells migrating through 250 μm long channel with channel width varied between 5 to 20 μm. When the average number of cells in the channel after 72 hours was compared, results indicated that number of cells that migrated decreased with decrease in the channel width. The migration trend was similar to the trend observed in the case of channels with 500 μm length. At a particular channel width, when we compare the cell migration number between 250 and 500 μm channel length, there was approximately twice the cell migration observed in 500 μm length channels than 250 μm length channel. This could be due to the fact that the increase in channel length provided more guided space for the cells to migrate. Results from these experiments imply that channel width is critical for cell migration. Lower channel widths can be used to create huge resistance for cells to migrate. So tuning the channel width can help us in finding a more potential attractant responsible for cell invasion as cells will invade through these high resistance paths only when they are strongly stimulated to attractant.

2.5 Conclusion

A microfluidic device made of PDMS on commercially-available standard cell culture substratum with time-lapse measurements of cell migration is presented. The numbers of cells that migrate into guiding microchannels and the cell migration rates appear to be dependent on the chemotaxis effects mediated by factors tested. Cell morphology and behaviors under its migration

process can be observed in real time. The devices present a new tool and method for cell studies.

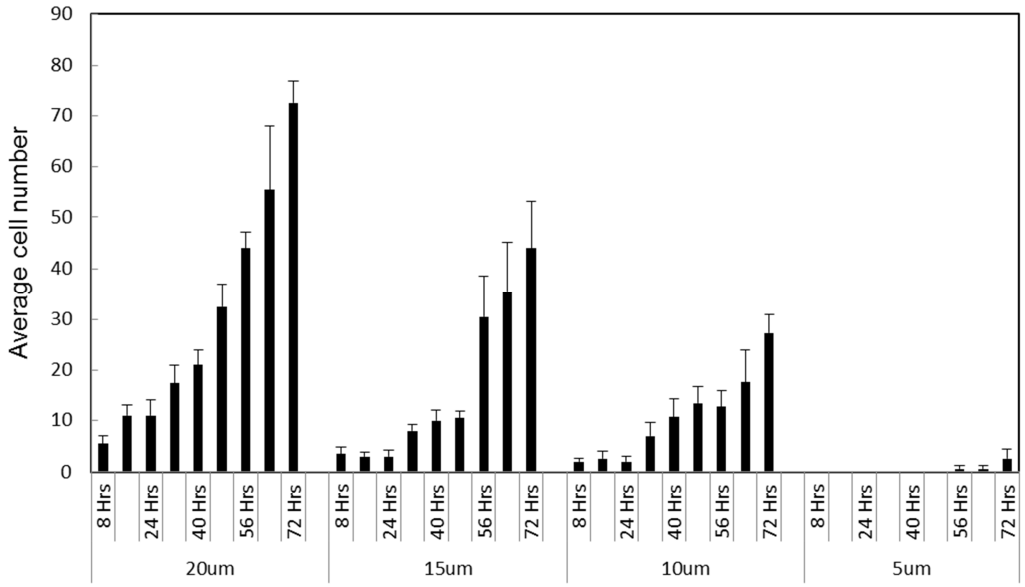

Figure 2.30 The average number of cells migrating through 500 μm long channel with channel width varied between 5 to 20 μm in steps of 5 μm.

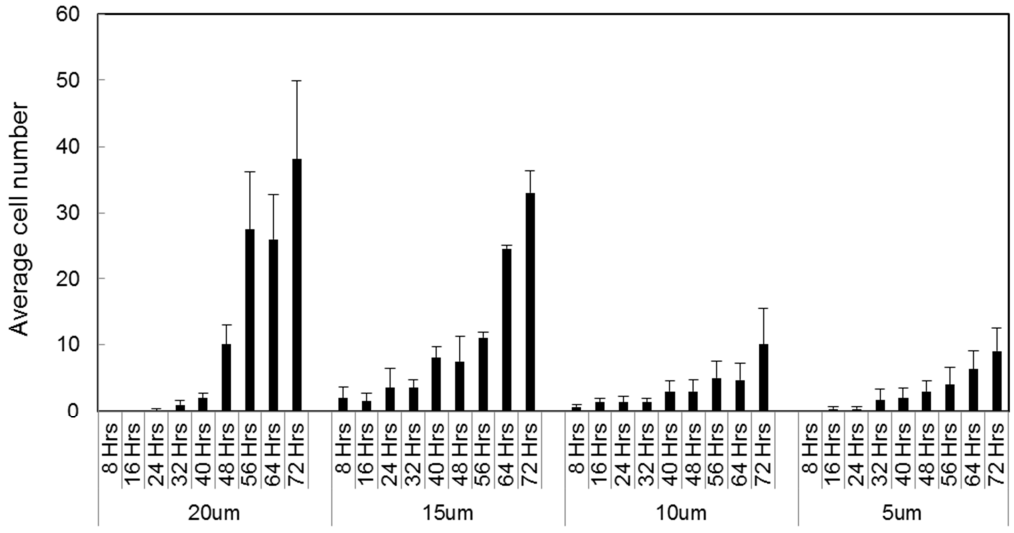

Figure 2.31 The average number of cells migrating through 250 μm long channel with channel width varied between 5 to 20 μm in steps of 5 μm.

CHAPTER 3

MICROFABRICATED PHYSICAL SPATIAL GRADIENT DEVICE FOR CELL MIGRATION

3.1 Introduction

Migration of the cancer cells as an important step in metastasis involves chemokines that establish chemical gradients to attract the cancer cells from the primary to secondary sites. Literature suggests that there are several chemokines found to be at elevated levels in patients with advanced prostate carcinoma. Along with chemical factors researchers also started looking into mechanical markers involved during metastatic process [66-68]. In many cases during metastasis cancer cells subjected to mechanical stress as they have to realign and reconfigure their morphology. Examples include cells passing through the tiny pores of extracellular matrix (ECM) to reach blood vessels, invasion through the tight junctions of the endothelium, migration through the micro blood vessel branches [66-74]. It is important to understand the factors that change the phenotypes of the cells, which in turn promote invasive behavior in cancer cells. Understanding the migration response of the cells when subjecting to a combination of chemical and mechanical gradients,

particularly in the context of squeezing through the tight endothelium pores of the blood vessel at same time subjected to chemokine gradient in blood stream can clarify the phenomenon associated with metastasis.

In numerous recent studies, microfluidic devices of different designs have been used to create controllable and steady concentration gradients of various factors for quantitative evaluation of chemotaxis on cell migration [21-24]. Previous studies from our group reported development of no flow, steady gradient generating microfluidic devices containing straight microchannels with a cross sectional area compared to the cell size for prostate cancer chemotaxis to EGF growth factor [25-26]. The results from those studies indicated that the cells are able to move unidirectionally towards the attractant with in confined paths. The physiological microenvironment is however is non-uniform. Therefore the current studies using uniform channel only provide partial information about cell migration response during the metastasis.

There is a need for a platform which can mimic both physical and chemical gradients that a cell experiences physiologically in vitro.

3.2 Materials and Methods

3.2.1 Device Design

The device consist of two chambers named as cell chamber and attractant chamber, both 5 mm in diameter connected with ten micro-channels as shown in Figure 3.1. Each microchannel was 10 μm in height and 600 μm in

length. The distance between adjacent channels was 20 µm. The channel width initially was 20 µm and it taper down to 5 µm over a transition length of 25, 50, 100, 200, 400 and 600 µm

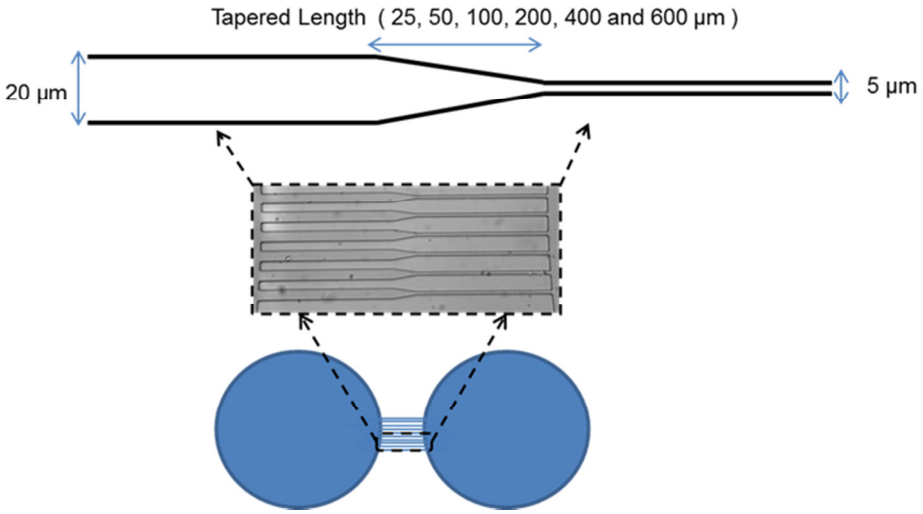

Figure 3.1 Microfluidic devices with tapered channels.

3.2.2 Device Fabrication

The microfluidic devices were fabricated as mentioned in Chapter 2. Briefly, for obtaining master mold, photolithography processes were used. SU-8-5 was spin coated to obtain a thickness of 10 µm. The photoresist was exposed to UV followed by developing and hard baking. PDMS with 10:1 base to curing agent ratio was dispensed on the silicon mold. The PDMS was then cured on the plate and the devices were peeled off the silicon mold. The PDMS based microfluidic devices thus formed were punched open with 5 mm unicore hole punches to form the reservoirs. Devices were cleaned using clear 3M scotch tape to remove PDMS debris followed by sterilization with 70% Ethanol

for 10 minutes. The sterile devices were mounted on a standard tissue culture dish (100 mm, treated polystyrene, Corning Inc.) by applying pressure on the PDMS with the channel side onto the growth surface of the substratum to form the microfluidic device. Figure 3.2 shows the fabricated PDMS microchannels with variable tapered lengths.

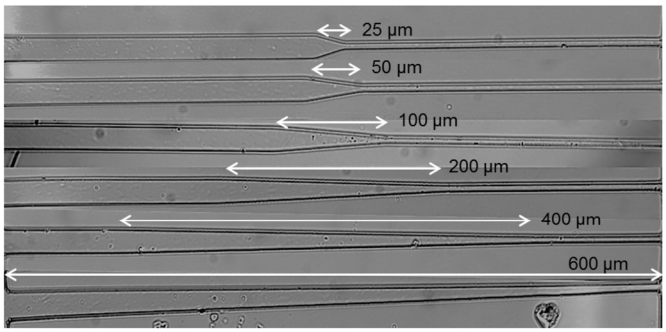

Figure 3.2 PDMS based tapered microchannels with variable tapering distance fabricated by soft lithography process.

3.2.3 Cell Culture and Cell Seeding

The cell lines used for the experiments were PC-3, PC-3ML, PNT1A and MDA-MB-231. Similar cell culturing protocol was followed as explained in the section 2.2.4. Device priming and cell seeding was similar to the protocol as described in section 2.2.5.

3.2.4 Image Acquisition and Cell Migration Analysis

The device in cell culture dish was mounted onto a electric CO_2 stage incubator (Okolab, Italy) as shown in Figure 3.3. The stage incubator basically consists of rectangular metal box with open bottom and a glass cover lid. There is provision to inlet 5% humidified CO_2 gas and also thermocouple controlled

hot air blower to maintain the temperature at 37 ^{0}C. This setup helps in maintaining the standard cell culture environment and also helps in continuously monitoring the cells under inverted microscope. Cell responses and movements were assessed by bright field images taken at designated time intervals using a CCD camera (CoolSNAP cf, Photometrics, Tucson, AZ) on an inverted microscope (Ti Eclipse, Nikon, Meville, NY).The images were captured at 100X for cell movement analysis. Pictures taken at 2 min intervals for a period of 72 hours were used to measure the movement of the cells in the channels. Cells movements were measured using Nikon NIS elements software. T-Test was performed to indicate the statistical significance of the data. Out value of T-Test in indicate as 'P'. The data is statistically significant, if P<0.05.

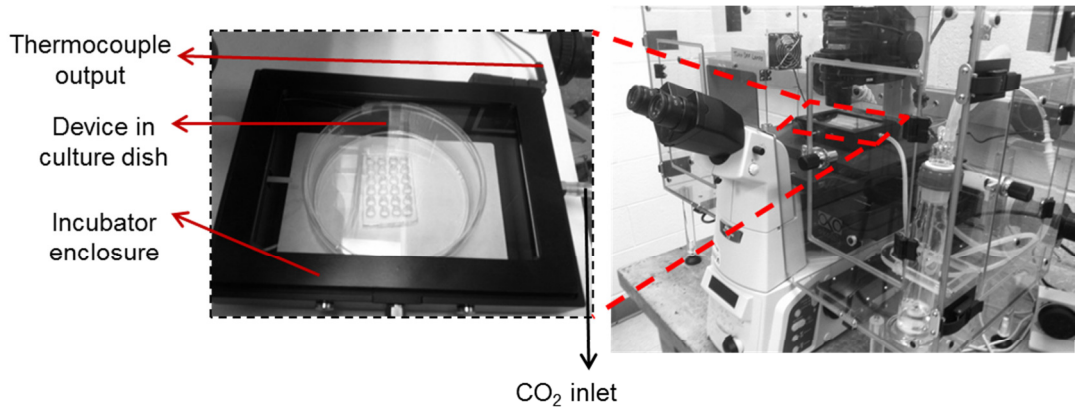

Figure 3.3 Electric CO_2 stage incubator within the inverted microscope for monitoring real time cell migration.

3.3 Experiments and Results

Based on the pilot studies with the six different tapered channel devices, It was found that the device containing tapered channels with 50 μm transition

length has highest migration. Later this particular device was used for all further experiments.

3.3.1 PC-3 Migration through Tapered Channels

3.3.1.1 Cells Seeded at Wider End of the Channels

The device with channels containing 50 μm tapered transition length was primed with media containing 2% FBS. PC-3 Cells were seeded in the well adjacent to wider region of the channels at a density of 5000 cells/well. After cells were seeded, they are allowed to attach to substrate for 24 hours. EGF 75ng/ml was added to the attractant well. Then the devices were monitored under the microscope for 72 hours. Images of the cell migration were captured in time lapsed fashion at rate of 30 frames per hour. Results demonstrated the nontrivial existence of three distinct phenotypes of cells such as 1) Cells which entered the tapered region and pass through the 5 μm narrow channel. These cells were permeating cells. 2) Cells turning around once they reached the tapered region. These cells are repolarizing cells. 3) Cells that re-enter the same or adjacent channels after crossing the complete channel. These cells were retreating cells. Figure 3.4 shows the two distinct cases of response of PC-3 cells from wider to narrow tapering channel. Unlike uniform channels where the cells enter the attractant chamber after crossing the channels, it was observed that large number of cells retreating to the adjacent narrow channels in spite of the presence of chemoattractant. This indicates the phenotype

changes in the cells during their migration towards the tapered channels make them more vulnerable to the spatial gradient than chemo gradient.

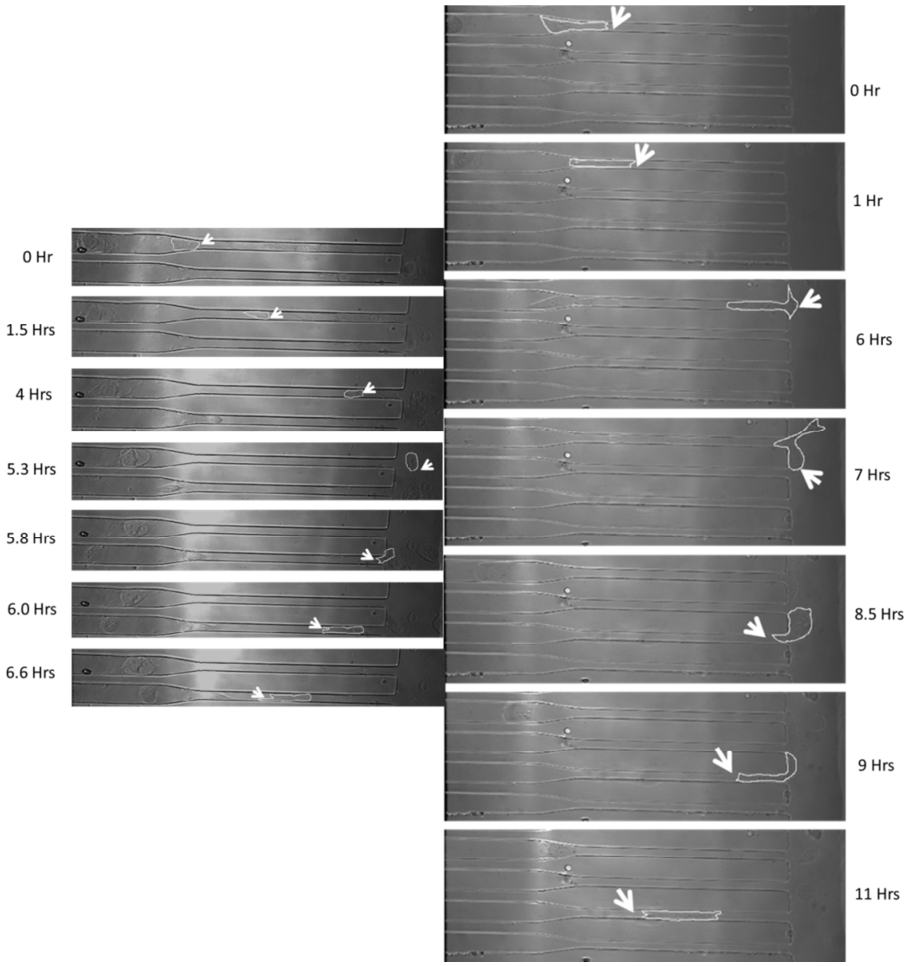

Figure 3.4 Time-lapse montages of PC-3 cells retreating into narrow channels.

3.3.1.2 PC-3 Cells Seeded at Narrow End of the Channels

PC-3 cells were seeded in the well adjacent to narrow region of the channels at a density of 5000 cells/well. After 24 hours of seeding the cells, EGF 75ng/ml is added to the attractant well. Then the devices were monitored under the microscope for 72 hours. Images of the cell migration were captured

in time lapsed fashion at rate of 30 frames per hour. Results indicate that the cells after crossing the tapered region repolarize themselves into narrow region. Figure 3.5 shows a PC-3 cell repolarizing itself to enter the narrow channel. The results from both PC-3 experiments indicate that the cells always tend to enter and stay in the narrow channel region which also indicates the invasive behavior of the cells

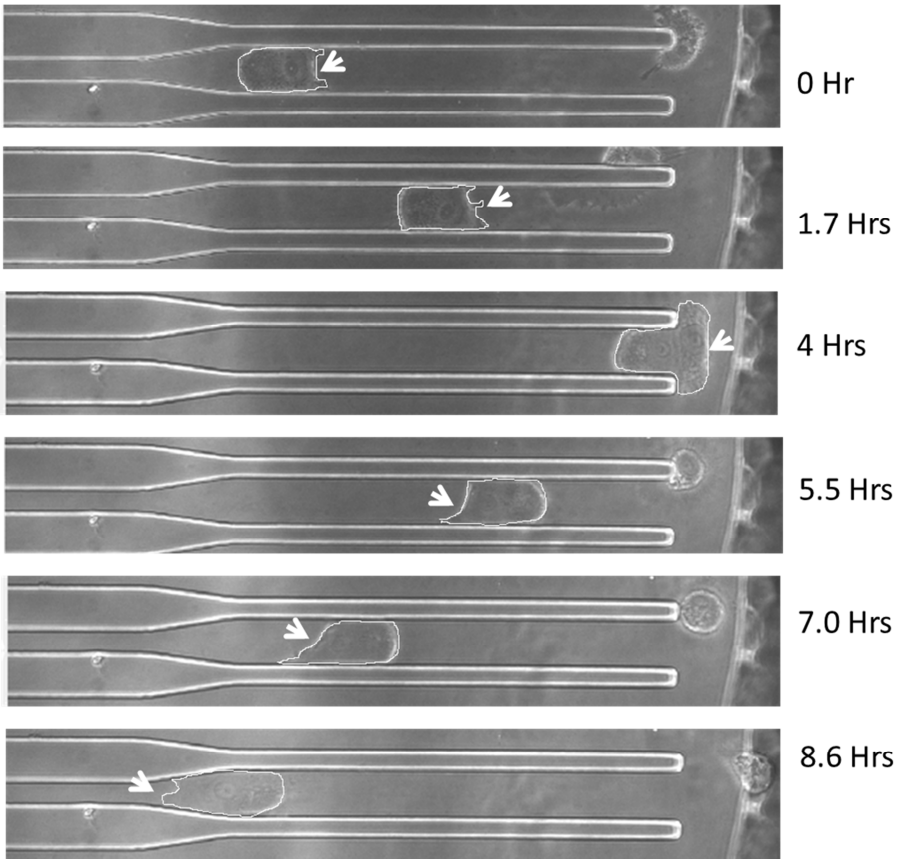

Figure 3.5 Time-lapse montages of PC-3 cells repolarizing into narrow channels.

3.3.2 PNT1A Migration through Tapered Channels

In order to compare the responses of PC-3 cells which are highly metastatic prostate cancer cells with healthy prostate cells, similar experiments were performed using PNT1A cells.

3.3.2.1 PNT1A Cells on Wider End of the Channels

PNT1A cells were seeded in the well adjacent to wider end of the channels. EGF75 ng/ml was added, 24 hours after cell seeding. Images were taken in time lapsed fashion at the rate of 30 frames per hour for a period of 72 hours. Results indicate that PNT1A cells did not exhibit retreating behavior due to the spatial gradient as they enter the taper region and traveled through the narrow channel and cross the channel to enter the attractant well.

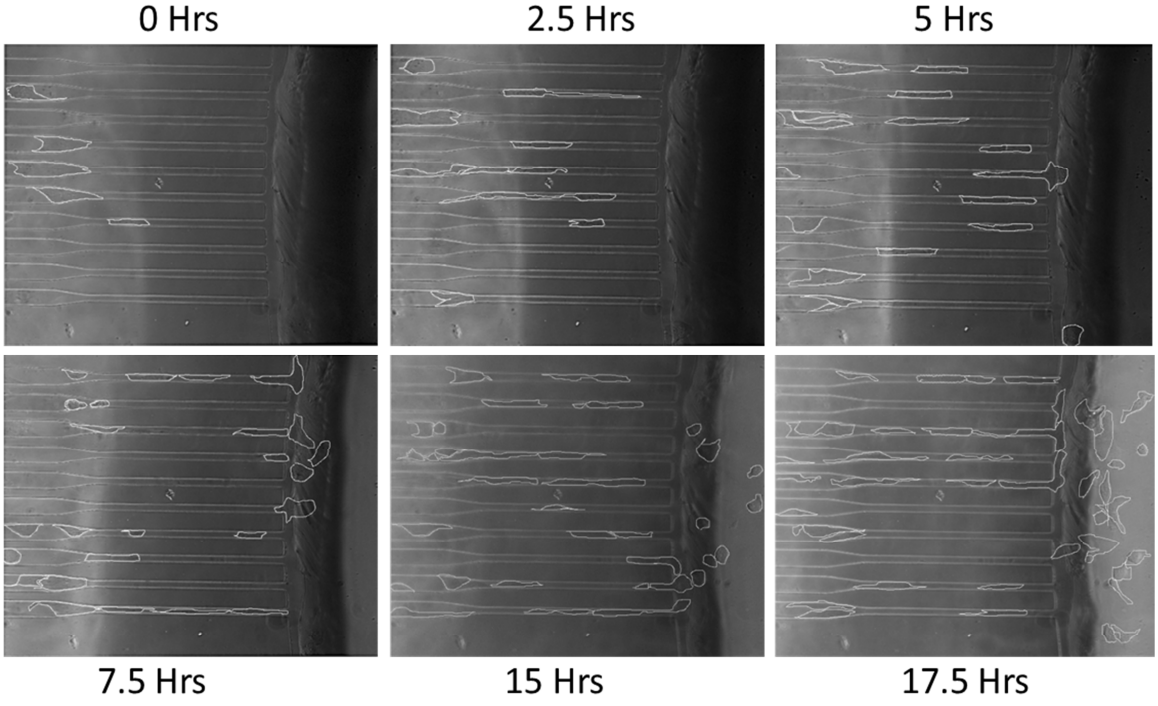

Figure 3.6 Time-lapse montages of PNT1A cells migration from wider to narrow channels and entering the attractant well.

These results implicated that the phenotype of the healthy prostate cells were not affected by the spatial gradients. Figure 3.6 shows the response of PNT1A cells to tapered channels with cells seeded near the wider side of the channel.

3.3.2.2 PNT1A Cells on Narrow End of the Channels

PNT1A cells were seeded in the well adjacent to narrow end of the channels. After 24 hours after the cell seeding EGF75 ng/ml is added. Images were taken in time lapsed fashion at the rate of 30 frames per hour for a period of 72 hours. Results indicate that PNT1A cells were not affected by the spatial gradient as they entered the tapered region and traveled through the wider channel and crossed the channel to enter the attractant well.

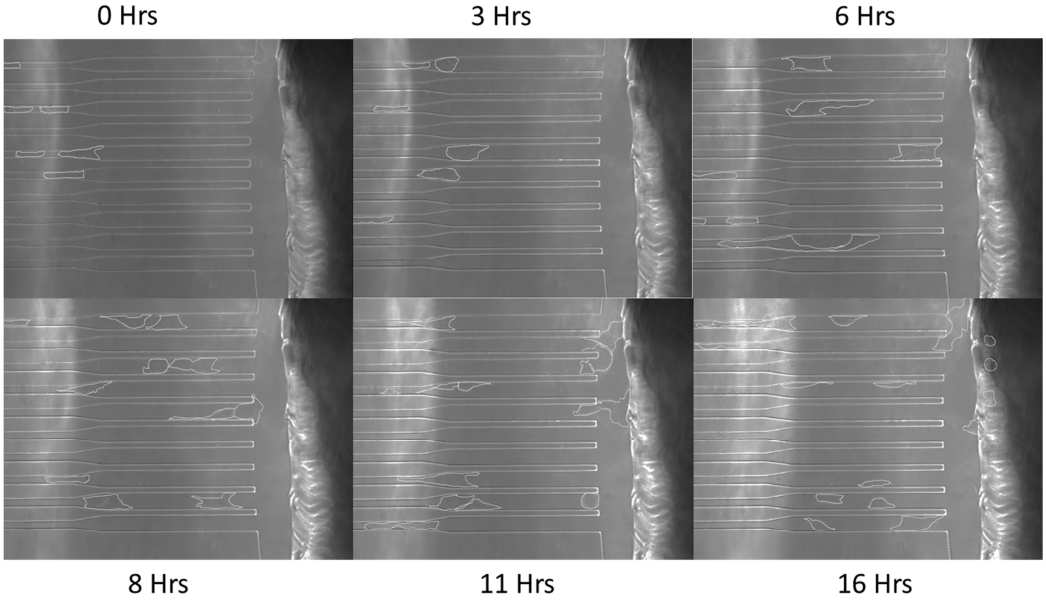

Figure 3.7 Time-lapse montages of PNT1A cells migration from narrow to wider channels and entering the attractant well.

Once again these results implicate that the phenotype of the healthy prostate cells were not affected by the spatial gradients. Figure 3.7 shows the response of PNT1A cells to tapered channels with cells seeded near the narrow side of the channel.

3.3.3 Comparison of Permeation Speeds between PC-3 and PNT1A

The time taken by the each cell, in every single channel of the device to permeate from tapered region to end of the channel was measured. The average migration speed of all the cells in the device was then calculated. 10 cells were considered for both cases of PC-3 migrating from narrow to wider channel and wider to narrow channel. 45 cells were considered in the case of PNT1A migrating from wider to narrow channel. 35 cells were considered in the case of PNT1A migrating from narrow to wider channel.

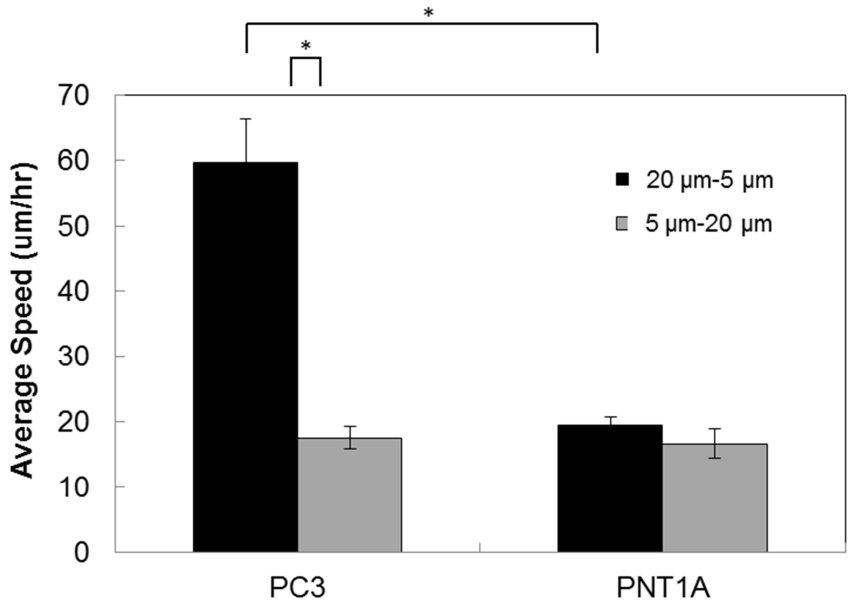

Figure 3.8 Comparison of permeation speeds between PNT1A and PC-3. * indicates the P<0.05

Results indicate that on an average, PC-3 permeating speed was 60 μm/hr and 17 μm/hr while migrating from 20 μm to 5 μm channel and 5 μm to 20 μm channel respectively as shown in Figure 3.8.

The difference in the permeation speed indicates the invasive behavior of PC-3 cells while moving from wider to narrow channels. PNT1A permeation speeds on an average were 19 and 16 μm/hr while permeating from 20 μm to 5 μm channels and 5 μm to 20 μm respectively. The results suggest that PNT1A which is healthy prostate cell, does not exhibit invasive behavior in any spatial gradient condition.

3.3.4 Retreating and Repolarizing Cell Numbers

Probability of cells retreating or repolarizing behavior was calculated as ratio of number of cells showing either retreat or repolarization to the total number of cells that crossed the tapered region of channel.

Figure 3.9 (a) shows the probability of retreating behavior of PC-3 (81%, n=4) is significantly higher ($P<0.05$) than permeating behavior (19%, n=4) while traveling form wider to narrow tapering channel. On the contrary, the probability of permeating behavior (91%, n=10) is significantly higher ($P<0.05$) than retreating behavior (9%, n=10) in the case of PNT1A cells.

Further, in the case of cells traveling form narrow to wider tapering channel, PC-3 cells has higher probability to repolarize (54%, n=6) than to permeate (45%, n=6). On the other hand, PNT1A continue to show significant ($p<0.05$) probability to permeate (99%, n=10) than to repolarize as shown in

Figure 3.9 (b).

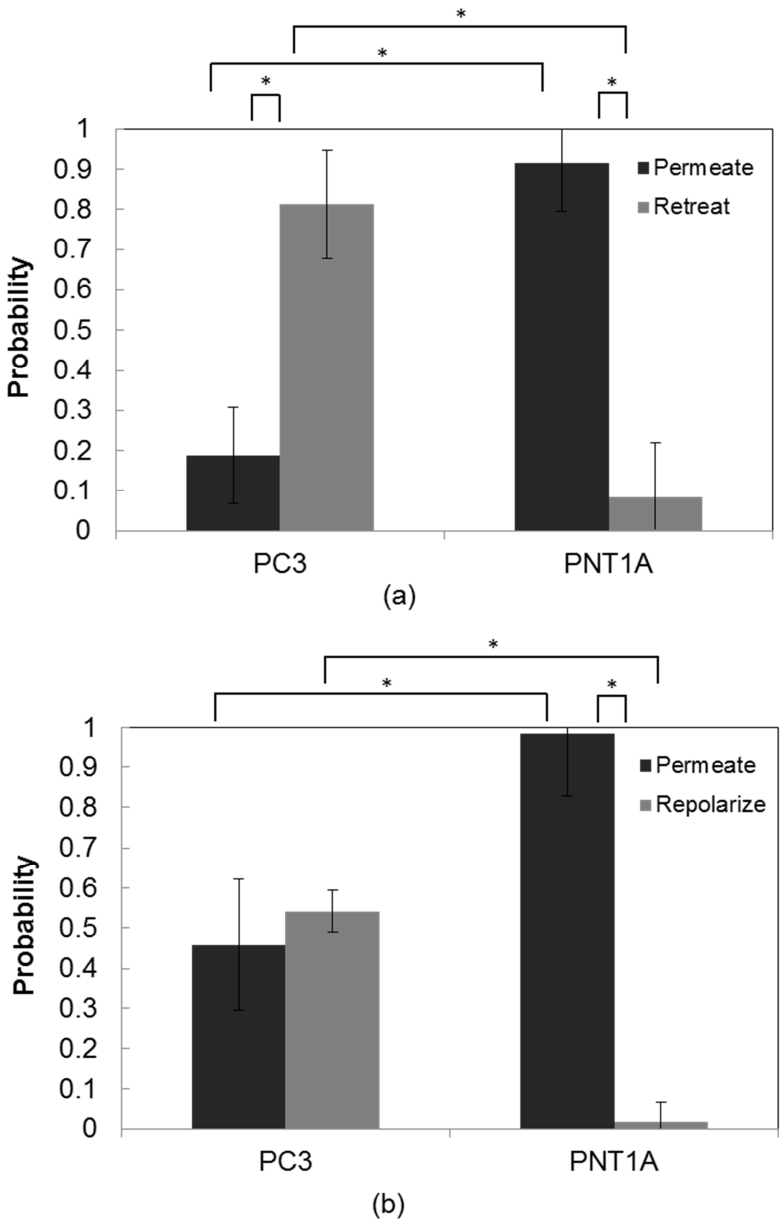

Figure 3.9 Data plots showing the (a) Probability of permeation and retreating behavior of PC-3 and PNT1A cells as they are seeded on the wider end of the tapered channel. (b) Probability of permeation and repolarizing behavior of PC-3 and PNT1A cells as they are seeded on the narrow end of the channel.

3.3.5 PC-3ML Migration through Tapered Channels.

3.3.5.1 PC-3ML Cells on Wider End of the Channels

PC-3ML cells were seeded in the well adjacent to wider end of the channels. EGF75 ng/ml was added, 24 hours after cell seeding. Images were taken in time lapsed fashion at the rate of 30 frames per hour for a period of 72 hours. Results indicate that PC-3ML cells crossed the tapered region and entered the narrow region of the channel. Out 24 cells entered into narrow region, none of them crossed the entire channel to reach the attractant well. They exhibited repolarizing behavior as they moved back and forth in the narrow region. These results implicated that the phenotype of the PC-3 ML

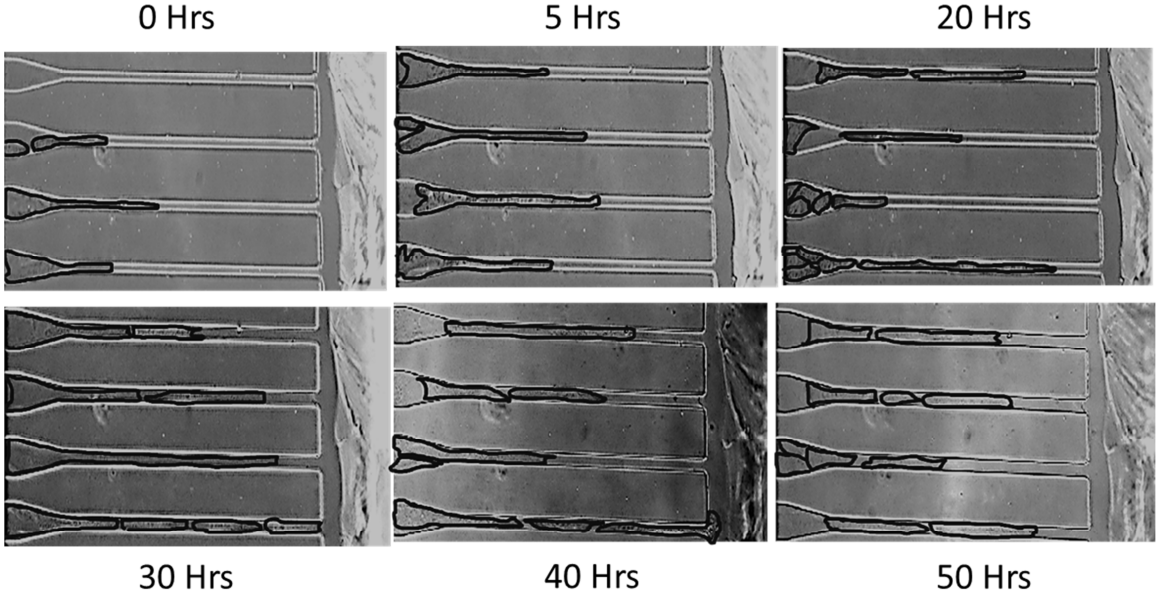

Figure 3.10 Time-lapse montages of PC-3ML cells migration from wider to narrow channels and entering the attractant well.

cells stayed in the narrow channels even after 50 hours after they entered the channels. Figure 3.10 shows the response of PC-3ML cells to tapered channels with cells seeded near the wider side of the channel.

3.3.5.2 PC-3ML Cells on Narrow End of the Channels

PC-3ML cells were seeded in the well adjacent to narrow end of the channels. EGF75 ng/ml was added, 24 hours after cell seeding. Images were taken in time lapsed fashion at the rate of 30 frames per hour for a period of 72 hours. Results indicate that PC-3ML cells did not exhibit retreating behavior due to the spatial gradient as they enter the taper region and traveled through the narrow channel and cross the channel to enter the attractant well. These results implicated that the phenotype of the healthy prostate cells were not affected by the spatial gradients. Figure 3.11 shows the response of PC-3ML cells to tapered channels with cells seeded near the narrow side of the channel

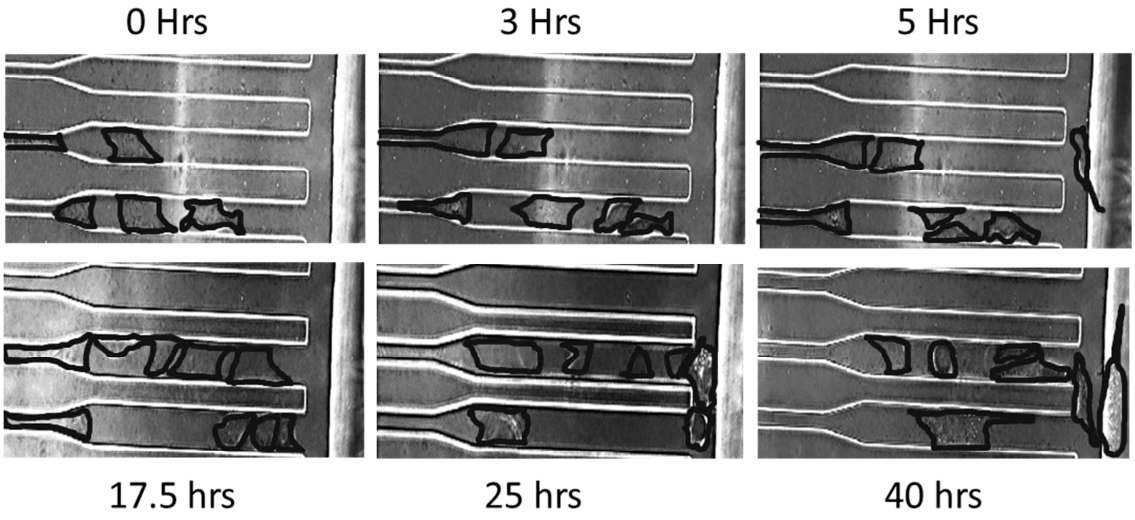

Figure 3.11 Time-lapse montages of PC-3ML cells migration from narrow to wider channels and entering the attractant well.

MDA-MB-231 cells were seeded in the well adjacent to wider end of the channels. EGF75 ng/ml was added, 24 hours after cell seeding. Images were taken in time lapsed fashion at the rate of 30 frames per hour for a period of 72 hours. Results indicate that MDA-MB-231 cells did not exhibit retreating behavior due to the spatial gradient as they enter the taper region and traveled through the narrow channel and cross the channel to enter the attractant well. Once individual cells left the narrow channels, they combined with other crossed cells to form larger clusters. The giant cluster formation impeded the cells to retreat through the successive narrow channels.

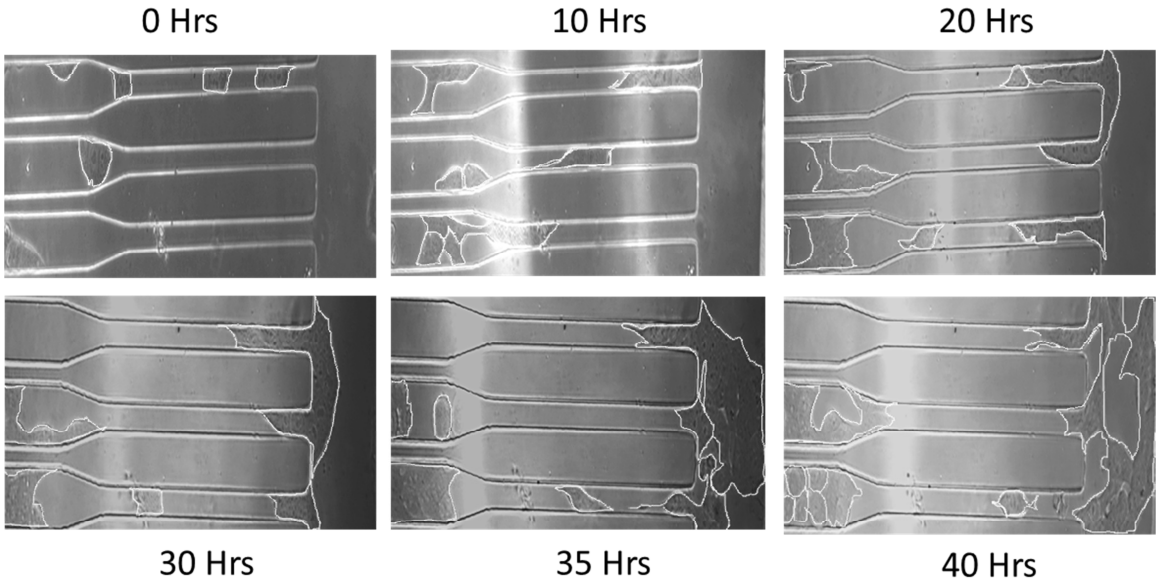

Figure 3.12 Time-lapse montages of MDA-MB-231 migration from wider to narrow channels and entering the attractant well.

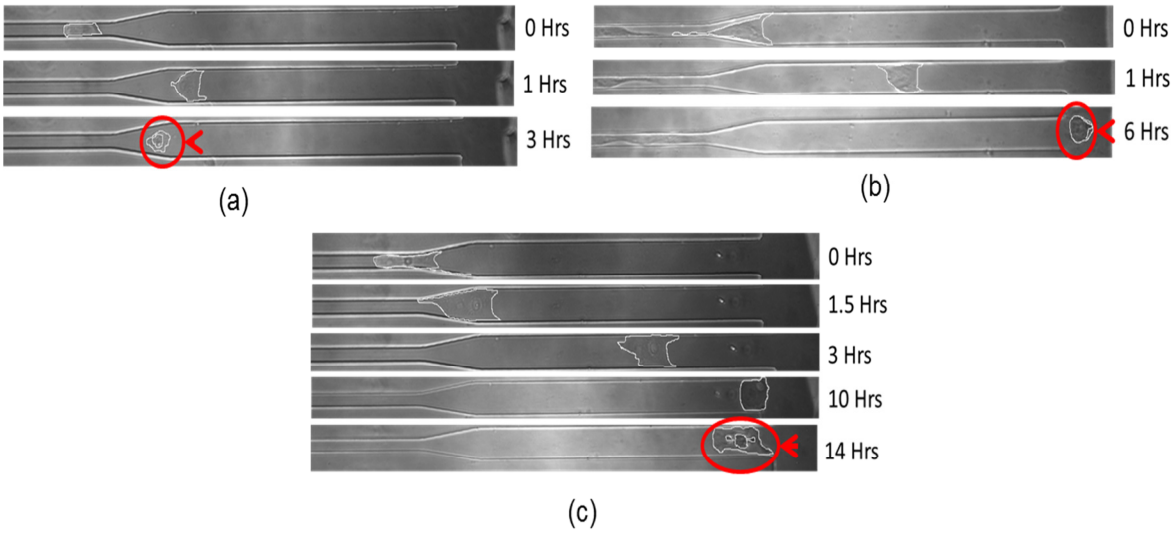

Figure 3.13 Time-lapse montages of MDA-MB-231 cells migration from narrow to wider channels and entering the attractant well.

3.3.6.2 MDA-MB-231 Cells on Narrow End of the Channels

MDA-MB-231 cells were seeded in the well adjacent to narrow end of the channels. EGF75 ng/ml was added, 24 hours after cell seeding. Images were taken in time lapsed fashion at the rate of 30 frames per hour for a period of 72 hours. In this experiment an interesting phenomenon has observed. As MDA-MB-231 cells crossed the narrow channel and tapered region, Cells underwent apoptosis in the wider region of the channel. 7 out of 8 cells exhibited this behavior. The experiment was repeated twice and similar behavior was also observed in the second experiment where 4 out of 5 cells entered underwent apoptosis. Results indicated that MDA-MB-231 cells couldn't withstand the mechanical stress created by the tapered channel which eventually resulted in their apoptosis. Figure 3.13 shows the response of MDA-MB-231 cells to

tapered channels with cells seeded near the narrow side of the channel in three different cases. The circled and arrow indicated cells in the images underwent apoptosis.

3.4 Conclusions

A microfluidic device array with tapered channels was designed, fabricated and tested. Ultimately, our tapered channel assay enables the quantitative analysis of the ability of a cell transition from a region with higher degrees of freedom in movement to a region with lower degrees of freedom. The assay also indicates the difference in the phenotype changes between highly metastatic and healthy prostate cancer cells when they are challenged with spatial gradients.

CHAPTER 4

A WELL ARRAY DEVICE TO STUDY CELL RESPONSES TO CYCLIC STRAIN

4.1 Introduction

Pathological changes of vascular smooth muscle cells (VSMCs) are found in many vascular diseases such as hypertension, atherosclerosis, and arterial stenosis.[75] These changes are the results of a number of biochemical factors, including cytokines and growth factors, as well as mechanical stimuli such as compression [13] and cyclic stretch [14]. The effects of numerous biochemical factors on VSMCs have been extensively studied in the past [76,77]. The effects of cyclic stretch, a major mechanical load, are particularly important to study since all VSMCs are constantly exposed to it under luminal pulsatile pressure loading. Apart from *in vivo* animal studies, three-dimensional (3-D) and two-dimensional (2-D) *in vitro* cell models are often used to study the VSMC responses to cyclic stretch. While 3-D models mimic the *in vivo* environment better and provide the most unique design, the level of stretch experienced by the cells through the 3-D composite matrix, is difficult to control [78]. That keeps the 2-D cell culture model remain to be popular as it provides well-controlled stretching to the cells. Many systems have been developed up to date.

Among them, vacuum-based stretching devices, such as Flexcell^{TM} culture plates, are often used. Using these devices high levels of stretches (> 15 - 20% strain), as often observed in pathological conditions such as hypertension, were found to enhance VSMC proliferation; while physiological magnitude of stretch (< 10% strain) was found to inhibit VSMC proliferation.[13, 24, 79]

However, stretch devices like Flexcell culture plates possess several limitations. First, each plate accommodates only six wells for cell growth due to the design restriction, making it difficult to be used in high throughput screening studies. Due to the size of cell culture wells (35 mm in diameter), large amount of cell culture medium (usually > 2 ml per well) and biochemical factors need to be used, making it cost inefficient. Another limitation of Flexcell culture plates is that it creates non-uniform levels of cyclic strain on the stretch membrane due to vacuum pulls, with higher level of stretch in the center of the well and lower level at the peripheral area.[80, 81] These limitations highlight the need to develop a new mechanical stretch system with less medium consumption and cost efficiency, especially when expensive growth factors or cytokines are used for the study. The stretch studies using these devices helps us understand the synergistic effects of physiological and pathological strain on VSMC cell proliferation.

In the present study, we developed a multi-well stretch device using flexible PDMS membranes with patterned micro-wells (120 μL of medium for

each well). It provided cyclic uniform stretch to all wells. Using this device, we first studied the effect of cyclic stretch on VSMC by examining their mechanical interaction with the substrate, i.e., cell alignment and proliferation. We then studied the combined effect of cyclic stretch and various growth factors on cell growth.

4.2 Materials and Methods

4.2.1 Multi Well Fabrication

The multi-well device was fabricated using two PDMS silicone membranes with different stiffness. The bottom membrane was 1 mm thick, while the top membrane was 4 mm thick with a relatively lower stiffness. For their fabrication, two parts (base and cross-linker) of SYLGARD^{TM} 184 silicone elastomer kit (Dow Corning Inc., MA) were mixed at a pre-defined ratio in a Pyrex glass plate, degassed under vacuum, then allowed to cure for 48 hours at room temperature. By mixing the base and cross-linker at a ratio of 10:1 and 30:1 (w/w), PDMS membranes of different stiffness (Young's modulus 1.2 or 0.2 MPa) were prepared.[82] After curing, both membranes were cut into desired shapes. The overall size of the device was 8 cm (length) x 4 cm (width). The top membrane which forms the well boundaries was punched with a hole-puncher (Harris Uni-Core) to get 1cm diameter holes forming a 6-well pattern, as shown in Figure 4.1. Two membranes were bonded together using plasma treatment method [83].

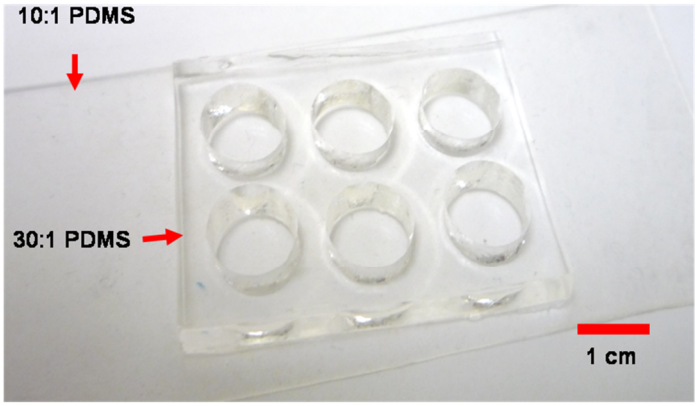

Figure 4.1 Six-well PDMS membrane with 1cm diameter for each well.

4.2.2 Strain Sensor Integration into the Multiwell Array Membrane

Strain sensor integration into the multiwell array membrane was an added advantage over conventional cell stretching devices. Sensor embedded into the membrane helps us in monitoring precise strain that is being applied at any given time. In conventional devices like Flexcell^{TM}, strain sensors are integrated into the cyclic loading device and not the membrane itself. Apart from finding the exact strain on the membrane, these strain sensors when connected to a proper wireless platform can log the strain information into the computer and also can alert us incase these breakage of membrane during the experiment. This is an important feature as it saves experimental time if at all there is membrane breakage during a long period of cell stretching.

4.2.2.1 Design of Carbon Strain Sensor

Some of the important characteristics of the required strain sensor are 1) the strain sensor should be easy to fabricate and cost effective as we integrate them into a disposable membrane (only for 2 – 3 times use). 2) It should have

good sensitivity or guage factor ‘G’ should be at least more than conventional strain gauges (G>2). 3) It should withstand higher strains (ε>10%). Most of conventional strain gauges can withstand maximum strain of 1-2% as they are designed to withstand strain in civil structures. 4) Its performance shouldn’t change with temperature as it will be operated at 37^{o}C. So an amorphous carbon strain sensor was fabricated.

The sensor was designed to have an active sensing element connecting two contact pads. The length and width of the active area are 5 mm and 2.5 mm respectively as shown in Fig 4.2 (a). Initially, a 0.5-μm thick amorphous carbon film was deposited onto a 125-μm thick polyimide film (Kapton, Dupont) by RF magnetron sputtering of a graphite target using a home built sputter plant at 150-W power for a period of 8 hours. The chamber pressure was maintained at 3-5 mTorr and the substrate temperature for the process is less than 200^{o}C. The strain sensors were then obtained by a programmable laser micro-machining system (Oxford Lasers). The laser could produce near vertical wall cuts with a minimum beam spot of 5 μm in diameter. After ultrasonication in acetone for 5 minutes followed by a nitrogen air drying, copper connection wires were attached to the connection pads with silver epoxy. The fabrication processes are illustrated in Figure 4.2 (b). Figure 4.2 (c) shows a photo of the fabricated sensor. The overall dimensions of the entire sensor are 10×4 mm^2.

4.2.2.2 Strain Sensor Testing

The sensor was glued with epoxy on top of an aluminium cantilever at a distance of 2.5 cm from the fixed end as shown in Fig 4.2 (d) for strain characterization. In the free end of the cantilever, loads were applied in discrete steps of 22.5 N up to 113 N. The aluminum cantilever has a nominal Young's modulus of E = 6.9×1010 N/m2 and dimensions of L=40 cm, t=0.63 cm and b=2.54 cm, indicated in Fig. 1(d). The strain follows the formula

$$\varepsilon_x = \frac{6P(L-x)}{Ebt^2} \tag{4.1}$$

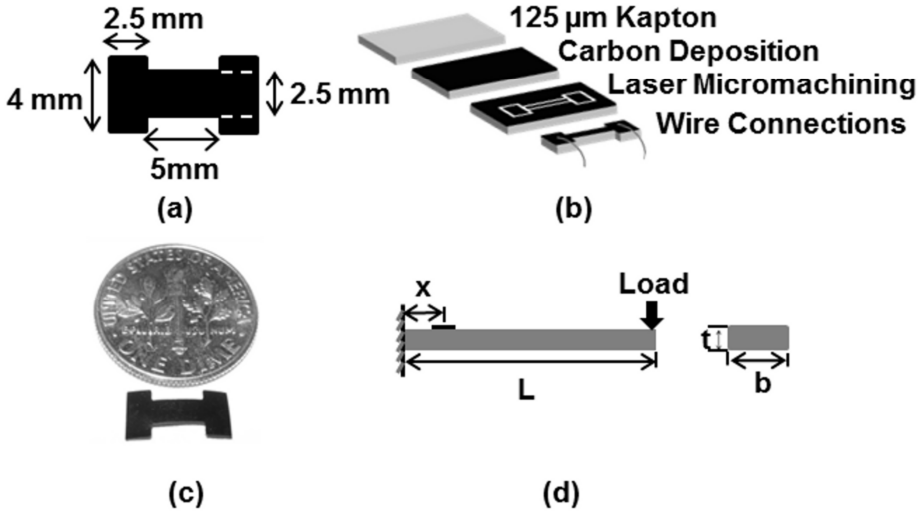

Figure 4.2 (a) The sensor design parameters. (b) The process flow for sensor fabrication. (c) Fabricated sensor compared to a US dime (d) Fabricated sensor mounted onto a cantilever for strain characterization.

Relative changes in resistance with respect to applied strains are shown in Figure 4.3 (a). The slope of the curve indicates a gauge factor, or sensitivity,

of the sensor as 6.34. Ten devices were manufactured and tested in the same method. A range of gauge factors between 6 and 9 were obtained. These numbers are almost thrice as large as the gauge factors of the commonly available metal strain gauges [84]. The variation of gauge factor is likely caused by the carbon thickness variation across the flexible polyimide film surface, microenvironment variations and batch fabrication parameter changes in our custom-made sputter. Measurements were conducted three times for each device. The error bars obtained were less than 1% indicating an excellent repeatability in our sensors. Sensor performance due to thermal effects was investigated by varying ambient temperature. A thermometer was placed on the cantilever to measure the structure temperature at 0, 22, 30, 50, 70, 90 and 110^{o}C while the beam experienced strains. The sensor gauge factors with temperature variations are shown in Fig. 4.3(b). Sensitivity of the sensor was fairly consistent between 22 and 110 ^{o}C with a maximum change of ±5% of the gauge factor. The lower gauge factor at 0 ^{o}C could be due to experimental difficulty since it was very difficult to maintain the ambient, substrate and cantilever temperature all at 0 ^{o}C during the mechanical loading. Sensor was connected in a quarter Wheatstone bridge circuit with a bridge input voltage of 5 V. The output of the bridge circuit was measured at a sampling rate of 30 samples/s. To demonstrate the sensor reversibility, the cantilever was loaded and unloaded to the maximum strain of 0.35% in steps of 0.07% and the result is shown in Fig. 4.3(c). The maximum variation in the output voltage at any

particular strain between the loading and unloading steps was 0.05%. To demonstrate the dynamic response of the sensor, the cantilever was cyclically loaded/unloaded at 30 cycles/minute. The magnitude of the strain increased from 0.07% to 0.35% with 5 loading and 5 unloading for each strain, as shown in Fig. 4.3(d). The response time for the sensor was found to be within 280 ms. The results also indicate the repeatability in the sensor responses.

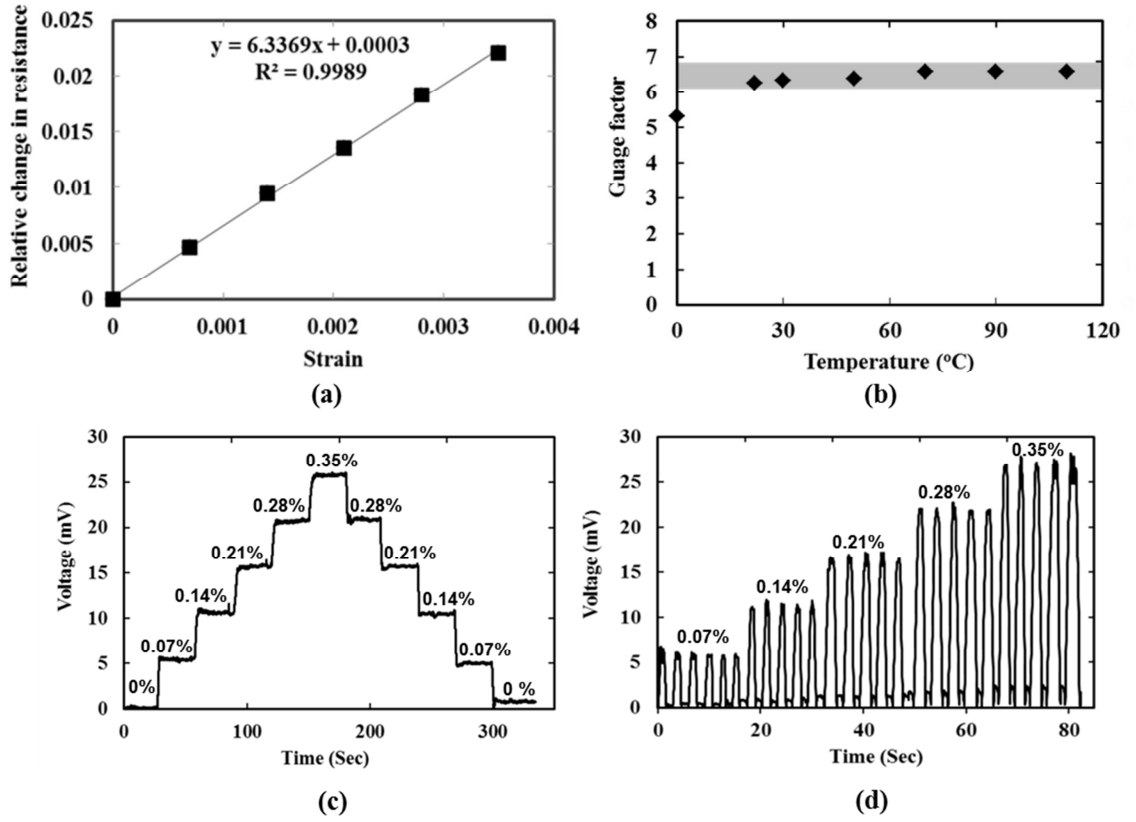

Figure 4.3. (a) Sensitivity, (b) temperature dependence, (c) hysteresis and (d) dynamic responses of the strain sensor.

4.2.2.3 Redesign of Carbon Strain Sensor to Withstand High Strain

The current dumbbell design could withstand 5% strain. At strains higher than 5%, sensor failed due to the formation of cracks in the carbon film. So a meander design of the sensor was designed. So when strain is applied on the sensor, only a partial strain was experienced by the sensor and rest of it is converted to displacement. The sensor had an active sensing element connecting two contact pads of 5 mm × 5 mm. The active sensing element was designed as a shape of a meander line for increasing stretchablity to withstand higher strains. The width and length of the active element were 0.5 mm and 10 mm, respectively, as shown in Figure 4.4 (a). The sensor fabrication is similar to the dumbbell shape sensor as described in section 4.2.2.1. The sensor was embedded into polydimethlysiloxane (PDMS), an elastic biocompatible polymer, in a strip shape. The fabrication processes are illustrated in Figure 4.4 (b) and Figure 4.4 (c) shows a photo of the fabricated sensor.

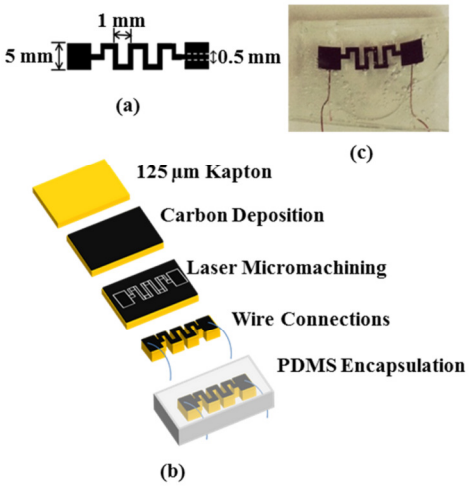

Figure 4.4 (a) The sensor design parameters. (b) The process flow for sensor fabrication. (c) A photo of the fabricated sensor encapsulated in PDMS.

The overall dimensions of the sensor were 20×5×0.125 mm^3. The initial resistances for all fabricated sensors were measured at the zero-strain state with values in the range of 11-13 kΩ. The variations were due to the structure tension during manual handling.

4.2.2.4 Wireless System Design

The wireless system blocks are illustrated in Figure 4.5. The strain sensor integrated the membrane senses the strain and the corresponding signal is fed to an interface circuit. The interface circuit then converts this signal into a format which is suitable to the microprocessor. The microprocessor processes the signals and sends digital data pockets wirelessly to the reader module. The communication between the module near the membrane and the reader is based on two eZ430RF2500 (Texas Instrument) devices. The module has an embedded MSP430 microcontroller, a 10/12-bit ADC, a transceiver chip (CC2500) and a small on-chip antenna. The transceiver operating at the frequency range of 2400–2483.5 MHz supports a sleep mode (400-nA current consumption) with a fast start-up time (240 μs). The wireless communication utilizes SimpliciTI^{TM} which is a standard RF network protocol. The wireless communication range can be up to 35 m in normal situations. In our experiment, the distance was within 5 m.

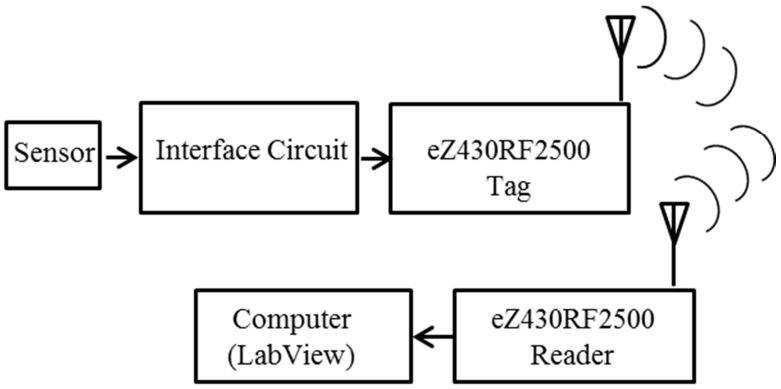

Figure 4.5 Block diagram of the wireless strain sensing system

The strain sensor was connected in a Wheatstone bridge circuit configuration as shown in Figure 4.6. R_G was the gauge resistance, initially 11.29 kΩ. R_1 and R_3 were approximately 11 kΩ. The bridge was balanced using a variable resistor R_2. The output voltage of the bridge V_{BRG0} at the zero strain can be calculated as

$$V_{BRG0} = V\left(\frac{R_G}{R_3 + R_G} - \frac{R_2}{R_1 + R_2}\right) \tag{4.2}$$

The output of the bridge was fed to a differential amplifier. The resistors R_5, R_6, R_7 and R_8 were 11, 11, 110 and 110 kΩ, respectively. The ratio of R_7 to R_5 determined a gain of 10. The output of the differential amplifier V_{DIFF0} at zero strain can be calculated as

$$V_{DIFF0} = V\frac{-R_7}{R_5}\left(\frac{R_G}{R_3 + R_G} - \frac{R_2}{R_1 + R_2}\right) \tag{4.3}$$

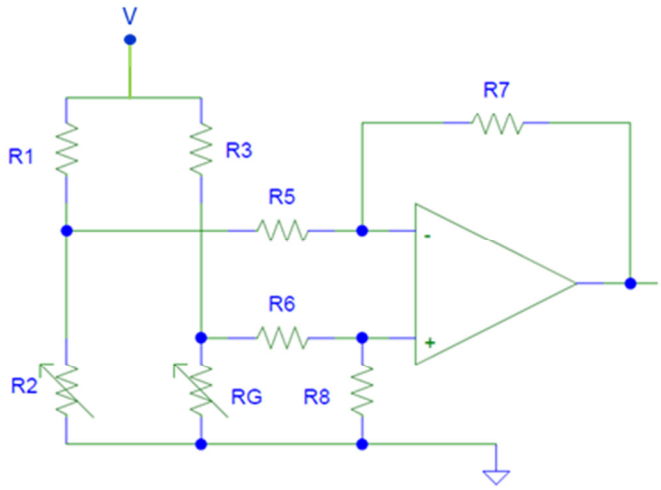

Figure 4.6 Wheatstone bridge and differential amplifier circuit.

4.2.2.5 Meander Strain Sensor Testing

The strain sensors were calibrated with the setup shown in Figure 4.7. The setup consisted of two stages with one fixed and the other one spring loaded for translational motion. Tensile load was applied to the PDMS encapsulated sensor by traversing the translational stage using a lead screw. For each loading, the corresponding strain value was calculated. A CCD camera assembled with a microscopic objective of 10× magnification was used to monitor the deformation of strain sensor under loading. The inset in Figure 4.7 shows the strain sensor deformation under unloaded and loaded conditions. The translational stage was traversed in 20 discrete steps with 200 μm each up to 2 mm. The corresponding strains were in the range of 0–51% in an increment of 2.8% strain. The relative change in resistance as a function of strain is shown in Figure 4.8. The slope of the curve indicated a gauge factor, or sensitivity, of 0.534. The measured gauge factor was relatively small over a large strain range

as it was contributed by both the sensing film and the meander line structure. However, the sensor ability to withstand higher strains was more important than the gauge factor in the proposed applications.

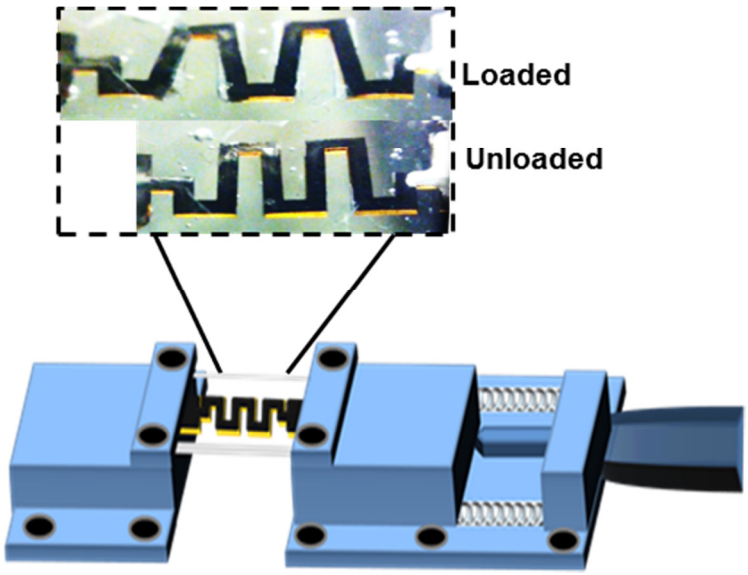

Figure 4.7 Mechanical test setup for the meander strain sensor.

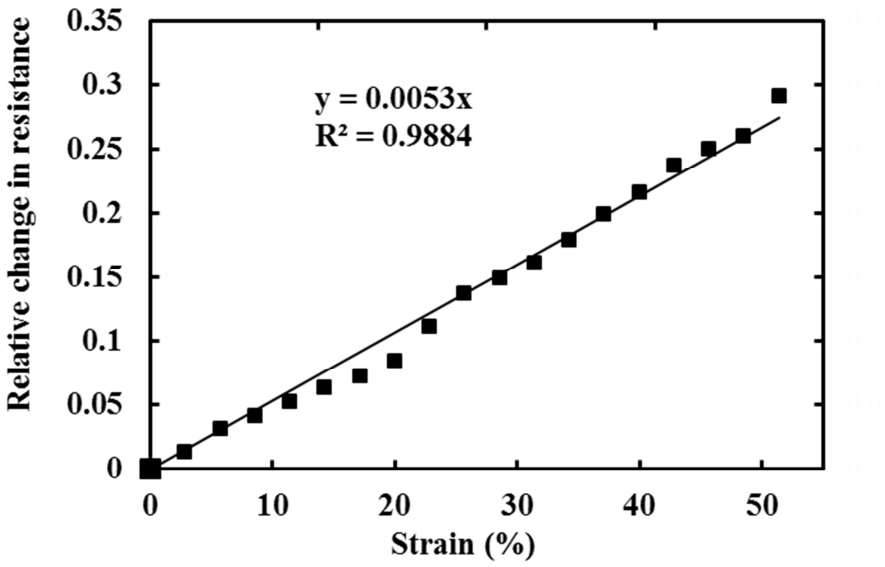

Figure 4.8 Sensitivity of the amorphous carbon strain sensor with a meander line shape.

The strain sensor was interfaced to the wireless module and strains were applied by the mechanical setup. The sensor signals were converted and processed into digital format before wirelessly transmitted to the receiver. After demodulation, output voltage was recorded and displayed in the computer at a sampling rate of 10 samples/s. Figure 4.9 shows the measured results at different strains with an increment of 4% strain. The fluctuation in sensor reading at any particular strain was found to be less than 1.4% which indicated good stability. It should be noted that the fluctuation included all noise and interference sources throughout the wireless communication. Figure 4.9 also shows the calibration relationship between wireless output and applied strain. The sensitivity was found to be 24.15 mV/strain (%).

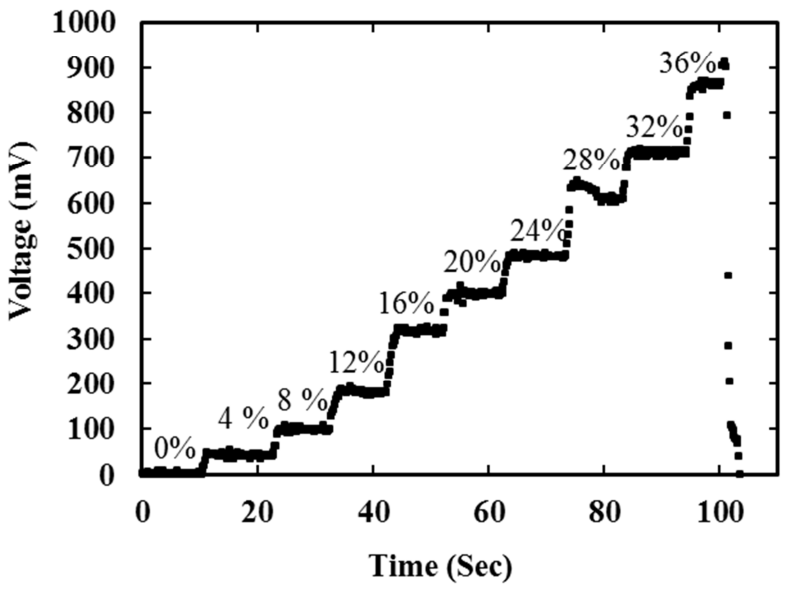

Figure 4.9 Output signals via wireless communication from the sensor to computer for varying strains with an increment of 4% per loading at the sensor.

The bonded PDMS device integrated with strain sensors was shown in figure 4.10 a. The device was mounted to the stretch machine with its two long edges tightly clamped by a pair of aluminum holders. While one holder was fixed, the other was connected to a drive shaft through which the amplitude and frequency of the cyclic stretch delivered to the device could be prescribed. The whole device was sealed inside a closed chamber with filtered vents on its lid to maintain a sterile environment while allowing gas exchange as shown in Figure 4.10 b and c. Membrane is stretched at 10%, 20% strain and at 1 Hz frequency. Data from strain sensor was acquired wirelessly onto the computer as shown in figure 4.10 d.

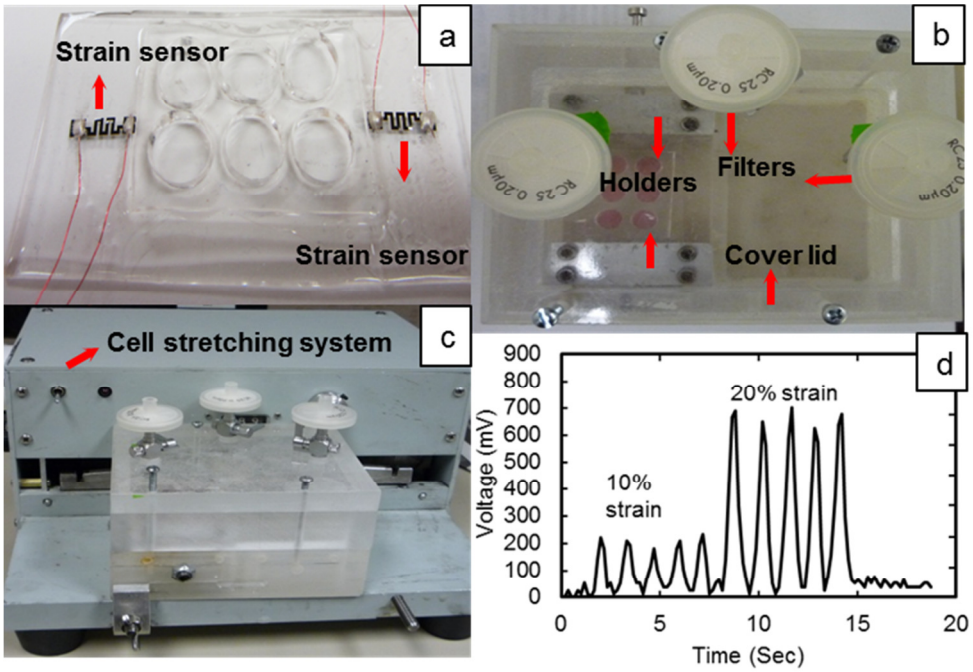

Figure 4.10 (a) The PDMS device mounted to two holders with one of them fixed and the other connected to a drive shaft through which prescribed cyclic stretches are delivered; (b) The PDMS device placed in the chamber that maintains sterile environment and prevents media evaporation; (c) The chamber was finally connected to the stretching module that delivers prescribed loads. (d) Wireless data from strain sensor.

4.2.3 Simulation of Strain Distribution in Multi-Well Device

To assess the strain field at the bottom surface of the wells where cells adhere to, we employed finite element modeling to simulate the transmission of stretch from the stretch mechanism to the wells and examined any nonhomogeneous strains therein due to the presence of the well. Using SolidWorks (SolidWorks, Inc.), we first built a 3D solid model for the PDMS multi-well device and then imported it to ANSYS (version 11, ANSYS, Inc) where we carried out finite element simulation. Either 10% or 20% cyclic stretch was applied simulating the actual load in strain applied to the PDMS multi-well device. We then examined any nonhomogeneous strains at the bottom surface of the microwell where cultured cells adhere to.

4.2.4 Cell Culture

Human Aortic Smooth Muscle Cells (HASMCs, Cascade Biologics Inc., OR) were cultured with Dulbecco's Modified Eagle Medium (DMEM) (Invitrogen Inc., CA) supplemented with 10% Fetal Bovine Serum (FBS, HyClone Inc., UT) and 1 % penicillin–streptomycin in a humidified incubator at 37 ^{o}C. When cultured cells became confluent, they were subcultured or used for experiments. Cells from passage 6 to 8 were used in all experiments.

4.2.5 HASMC Proliferation under Cyclic Strain

To improve the cell adhesion affinity, we pretreated the bottom surface of the wells using a corona discharger (Model: BD-20AC, Electro-Technic

Products Inc.) as described in the previous study [85]. Twenty-four hours after the treatment, the device was rinsed with distilled water then sterilized with 70% alcohol and UV light prior to its use. HASMCs were seeded in the wells of the device at 5000 cells/well in a culture medium of 120 µL. PDMS multi-well device was mounted to the stretching mechanism , 24 hours after the cell seeding as it gives ample time for the cells to adhere to the surface.

Either 10% or 20% of cyclic strain was delivered to the cultured cells at 1 Hz frequency by the stretching mechanism to mimic physiological or pathological strain levels at resting state as described by previous studies.[79, 86, 87] The applied steady state cyclic strain is shown in Figure 4.11,

$$\varepsilon = 0.05\cos(2\pi ft + 1) \text{ for 10\% peak strain and} \quad (4.4)$$

$$\varepsilon = 0.10\cos(2\pi ft + 1) \text{ for 20\% peak strain} \quad (4.5)$$

Where *f* is the frequency in Hz and *t* is the time in seconds. The entire assembly, consisted of mounted multi-well device and the stretch mechanism, was kept inside an incubator with 5% CO_2 at 37 °C throughout the experiment. The cells grown on the same multi-well device but cultured at static condition were used as the control. After 6, 24, or 72 hours of stretch loading, the cells inside the wells were lysed with 1% Triton X-100 and the total amount of cell DNA was analyzed using PicoGreen DNA assays (Invitrogen Inc., OR), following the manufacturer's instructions. The total amount of cell DNA was normalized with respect to the data from static control group at the same time points.

4.2.6 HASMC Alignment under Cyclic Stretch

The alignment of HASMCs in relation to the direction of the applied cyclic strain of 10% or 20% for 24 or 72 hours were measured from images taken by a digital camera (Axiocam MRC) mounted to an inverted microscope (Zeiss Axiovert 40CFL, Germany) at 10X magnification. For each cell, we first established a line parallel to the long axis of the cell that passes through the center of its nucleus. The cell alignment was measured as the angle between this line and the direction of the applied cyclic strain using ImageJ software (NIH). An angle of 0° signifies perfect alignment of the cell to the direction of the applied strain; while an angle of 90° means the cell alignment was perpendicular to the direction of the applied strain. At each cyclic strain level and time duration of exposure, we measured the angle of cell alignment from 400 randomly picked cells and summarized these results in terms of the percentage of cells in every 10 degrees from 0° to 90°.

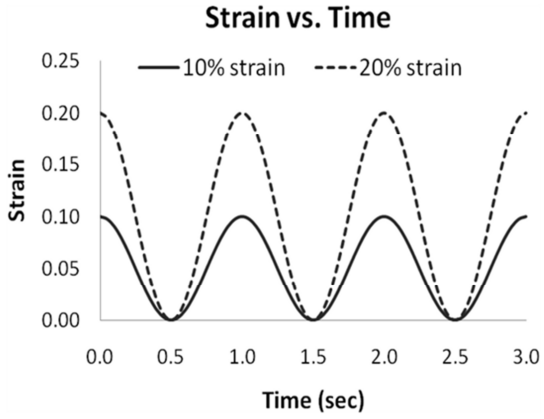

Figure 4.11 The cyclic strain applied to the multi-well device at steady state versus time.

4.2.7 HASMC Proliferation under Combined Effects of Cyclic Stretch and Growth Factors

HASMCs were treated with DMEM supplemented with 2% FBS for 24 hours before one of the growth factors, Transforming Growth Factor-beta (TGF-β, Invitrogen), Vascular Endothelial Growth Factor (VEGF, Thermo Scientific), Epidermal Growth Factor (EGF, Invitrogen), or Fibroblast Growth Factor (FGF, Invitrogen), was added to the culture medium. The used concentration of these growth factors was 10 ng/mL, similar to that of previous studies [79, 87,88]. After the addition of growth factors to the medium, the multi-well device was kept in static cell culture condition or subjected to either 10% or 20% of cyclic strain for 72 hours. Cells under static condition and not treated with growth factors were used as the control. The amount of cell DNA was measured for each of the groups as described earlier and normalized with respect to its corresponding static control sample without any growth factor.

4.2.8 Statistical Analysis

Data were presented as mean ± standard error. One-way ANOVA at a significance level of $p < 0.05$ was performed using StatView 5.0 software (SAS Institute).

4.3 Results

4.3.1 Simulation of Strain Distribution in the Multi-well Device

Due to symmetry, we plotted results of principal strains in vectors on a quarter of the multi-well device, which display its geometry in unloaded and loaded states Figure 4.12a). Since the depth of the well (4 mm) is relatively small in comparison with its diameter and the bottom layer of the device is relatively stiff in comparison with the upper layer (cylindrical walls), the strains at the bottom surface of the well are relatively uniform except peripheral regions right next to the cylindrical wall. The zoom in view shows uniform principal tensile strains in red and principal compressive strain in green along the lateral direction throughout most of the well bottom surface (Figure 4.12b). Using this approach, we were able to translate the strain which the stretch machine delivered to the multi-well device to the actual strains the cultured cells sense at the bottom surface of the wells.

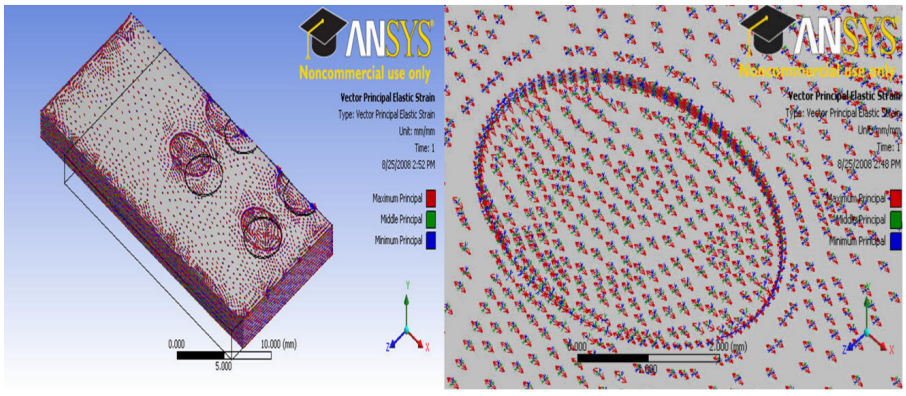

Figure 4.12 Simulation of strain distribution in the multi-well array device. (a) Regional differences in principal strains in a membrane with wells, when the membrane is under 20% strain. (b) Zoom in view of the principal strain distributions at the bottom of a well and in its immediate vicinity.

4.3.2 HASMC Proliferation under Cyclic Strain

Exposure to 10% or 20% cyclic strain at 1 Hz for 6 hours did not seem to affect the total amount of HASMCs compared with those under static condition, as shown in Figure 4.13. After 24 hours of exposure to 10% cyclic strain at 1 Hz, we found that cell proliferation was inhibited compared with the static control group. A significantly inhibitory effect on HASMC proliferation was found when the cells were exposed to 10% cyclic strain for 72 hours ($p<0.05$). On the other hand, the growth of HASMCs exposed to 20% cyclic strain for 72 hours was not inhibited significantly and it maintained a similar level as the static control.

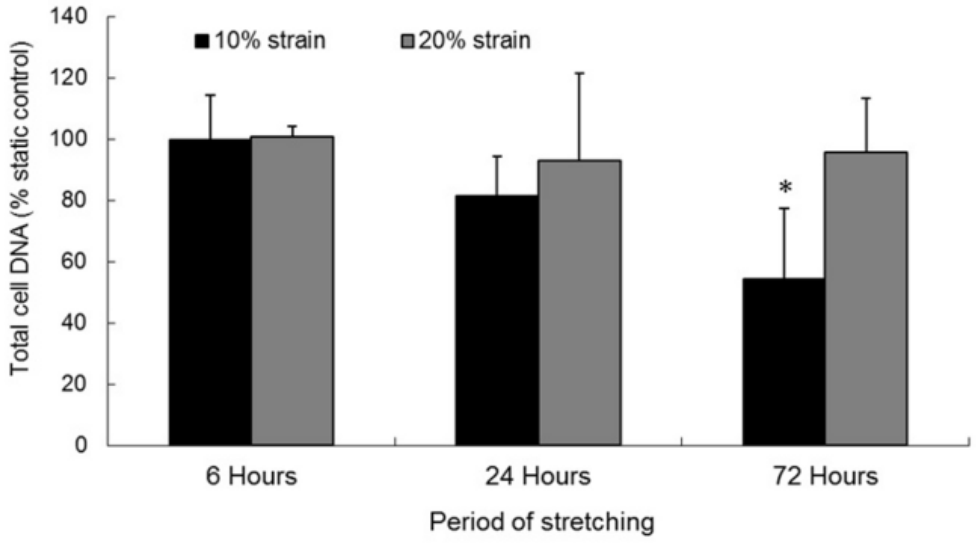

Figure 4.13 Effects of cyclic strain (10% or 20% at 1 Hz) on HASMC proliferation. N=4, *: $p < 0.05$.

4.3.3 HASMC Alignment under Cyclic Strain

At the static condition, all HASMCs were randomly oriented as they adhered to the bottom surface of the wells and there were no preferred

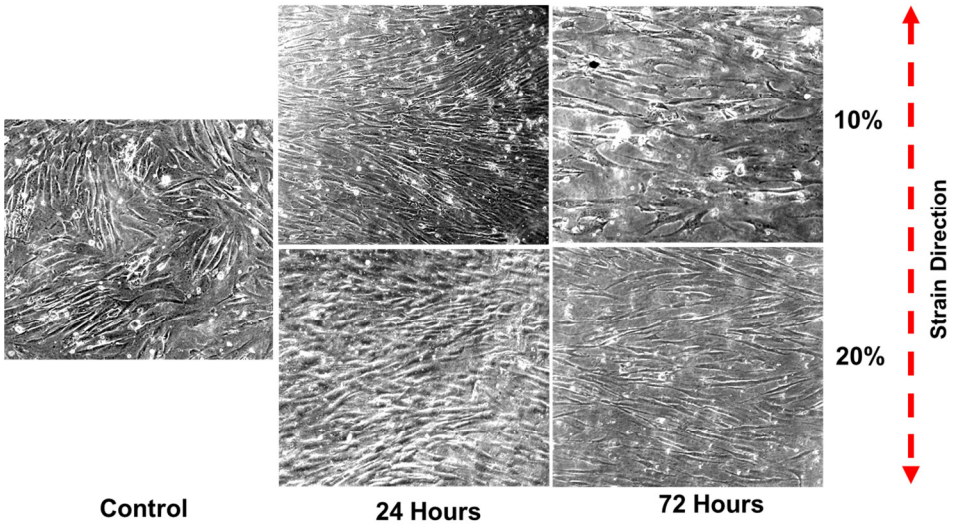

a

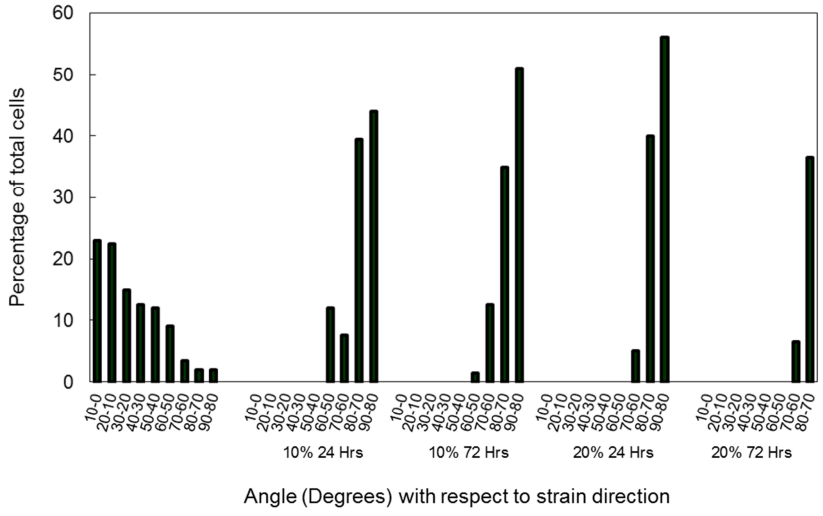

b

Figure 4.14 Cell re-alignment after exposure to cyclic stretch. (a) Microscopic images showing HASMC's re-alignment in relation to the direction of cyclic stretch after 24 and 72 hours. (b) Histogram showing the angular distribution of cell alignment at 24 and 72 hours for both 10% and 20% stretch cases.

directions in cell alignment. After 24 hours exposure to either 10% or 20% cyclic strain at 1 Hz, the majority of HASMCs realigned themselves at the direction perpendicular from that of the applied strain (Figure 4.14 a). This re-alignment appears to persist after 72 hours of exposure. Histograms of cell alignment angles clearly showed increasing percentage toward 90° for both 10% and 20% cyclic strains at 1 Hz at increasing time duration of exposure. It further showed higher percentage towards 90° with 20% strain level; indicating 20% strain induced more pronounced cell re-alignment than 10% strain as shown in Figure 4.14 b.

4.3.4 Mitogenic Effects of Growth Factors on HASMC Proliferation under Cyclic Strain

When applied at static conditions, all growth factors caused significantly greater cell proliferation than the control group (without addition of any growth factor), as shown in Figure 4.15. However, the mitogenic effects of these growth factors were greatly inhibited when treated HASMCs were exposed to either 10% or 20% cyclic strain. At 10% cyclic strain, cells treated with TGF-β, EGF, or FGF failed to induce cell proliferation compared to those without growth factor treatment, whereas VEGF increased cell proliferation by approximately 30%. When the cells were exposed to 20% strain, the inhibitory effects of the cyclic strain appeared to be less significant. EGF, FGF, and TGF-β all caused significantly higher cell proliferation than the control group when cells were

exposed to 20% strain only. However, this cell proliferation induction was lower compared to that of static conditions.

4.4 Discussion

Blood vessels, particularly arteries, are constantly exposed to mechanical strain due to the pulsatile blood flow; therefore, mechanical loads on the VSMCs are often pivotal, affecting their growth and functioning in both normal and diseased status [77]. Under physiological or pathological conditions, the magnitude of cyclic strain could vary significantly and pose varying effects on the VSMCs [89]. In the present study, we developed a system, consisted of a 6-well PDMS device mounted to a stretch mechanism that delivered programmable cyclic strain and frequency for the study of combined effects of mechanical stretch and different growth factors on cultured cells. PDMS does not have good affinity to living cells. With corona treatment and fibronectin surface coating, cell adhesion can be significantly improved [85].

Our results confirmed the strong adhesion of the HASMC to the surface-enhanced PDMS as the cells did not detach after 6-hours exposure to 10% or 20% cyclic strain. Consistent with other previous studies [79].

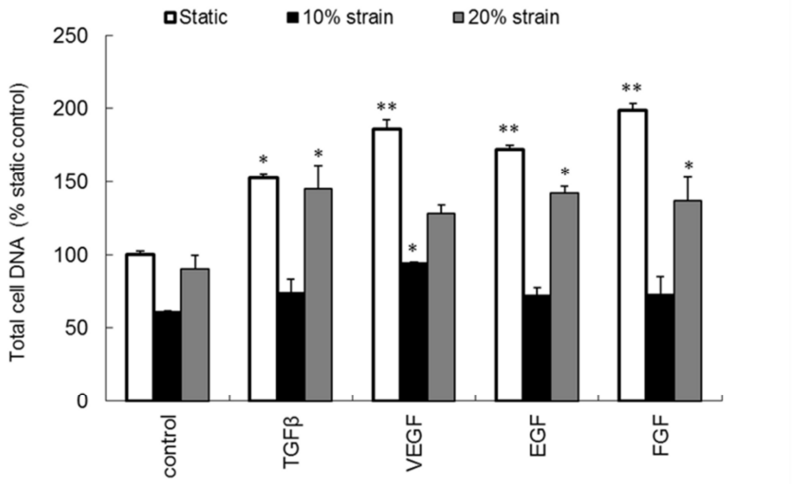

Figure 4.15 Effects of growth factors (TGF-β, VEGF, EGF, and FGF) on HASMC proliferation under cyclic stretch (10% or 20% at 1 Hz). N=4, *: $p < 0.05$ **: $p < 0.01$ vs. the same control group without addition of any growth factors.

We found that HASMC proliferation at 10% cyclic strain was much slower than that under static condition (Figure 4.13). This finding is in accordance with the phenomenon that VSMCs are quiescent in proliferation under physiological conditions [79]. However we found that when cells were exposed to 20% strain their proliferation was at a similar level as that under static condition. This finding is different from some of the earlier studies reporting that high pathological-level strain enhances VSMC proliferation.[90, 91] While there are a number of possibilities that could contribute to this discrepancy, the major difference between our multi-well device to previous vacuum-based stretch device, such as Flexcell plate, is that the strain provided

by our device is uniform throughout the membrane, while it is less uniform from those vacuum-based devices.

Besides affecting cell proliferation, cyclic stretch has also been found to cause cell re-alignment. Using this device, we observed that VSMCs align themselves at 90° from the direction of loading strain. Under each stretching condition, more than 80% of the cells were found to realign at 70° to 90° with respect to the direction of the applied cyclic strain, while under static conditions cell alignment were found to be random (Figures 4.14 a,b). Our results are consistent with previous studies that dynamic cyclic strain influences VSMC alignment [92]. In addition to mechanical stimuli, VSMCs are constantly exposed to cytokines and growth factors *in vivo*. Although a number of studies have been conducted to study the effects of biological factors on VSMC, the majority of the *in vitro* studies were performed with cells maintained under static condition, different from the cyclic strain loadings these cells normally undergo. Therefore, it is meaningful to study the combined effect of biochemical factors and cyclic strain. In this study, we examined the HASMC proliferation when they were exposed to TGF-β, VEGF, EGF, or bFGF under the 10% or 20% cyclic strain. We found that the mitogenic effects of these growth factors under cyclic strain, particularly under 10% strain, were significantly inhibited compared to that when they were applied under static conditions, suggesting that cyclic strain might interfere with the interaction of the growth factor to the cells. This interference and the involved mechanisms may play an important role in VSMC

responses and will be further investigated in future studies. A few studies have investigated effects of cyclic stretch and growth factors and/or cytokines. For example, the mitogenic effect of platelet-derived growth factor (PDGF) was found to be inhibited under 10% cyclic strain.[79] Another examples is that the combination of endothelin and 18% cyclic strain caused higher rate of rat VSMC apoptosis which did not occur when exposed individually to either stimuli.[81] Yet our study is the first to investigate the combined effects of stretch at different levels and various growth factors in a systematic way.

A major advantage of this multi-well device is its small growth medium requirement (120 μL of media per well) compared to other vacuum-based devices, thus making its use more economical for high throughput applications. Although this prototype was developed with 6 wells, similar devices with larger numbers of wells can easily be fabricated. Overall, this simple and novel multi-well device could be used as an alternative, if not a replacement, for the classic Flexcell plate for studying cell responses under both mechanical stretch and biochemical factors.

4.5 Conclusion

In the present study, we reported our development of a novel PDMS-based stretchable 6-well prototype device and its use in the study of cellular responses to combined mechanical stretch and biochemical factors. This device requires only small growth medium for cell culture than other devices. It can easily be modified for more economical and high throughput applications.

CHAPTER 5

FUTURE WORK

5.1 Automation of Data Acquisition and Processing

In the chapter 2 a microfluidic device was used to study the effect of cell migration by chemical and physical factors. The data collection and data processing for the experiments with this device was performed manually. There were approximately 5000 pictures taken corresponding to data presented in this dissertation. The number of channels in which cells and their migration distances were manually counted was 50000, as every device consisted 10 channels. Each channel's data processing was repeated twice to avoid the bias, which will make count of the total number of channels processed to 100000. So manual data processing of the images is a tedious job and also can be influenced by individual bias. Thus there is need for automation of the cell counting and data processing. Cell counting can be done by image processing and pattern recognition techniques. Cell morphology completely varies, when it is inside and outside the microfluidic channel. Cell morphology also depends on cell type. Some cells tend to stay in clusters and colonies even inside the microchannel. These issues often complicate the process of training the image

processing algorithms. Also image processing tools does not eliminate the tedious job of image acquisition of the array of devices. One of the efficient methods would be to integrate a real time monitoring system to detect and monitor cell movement on to the same microfluidic chip itself.

5.1.1 Impedance Based Cell Motility Monitoring

Electrical Impedance spectroscopy (EIS) is a well-established method used for various science and technology applications. The EIS technique, combined with microfluidics, micromachining and MEMS techniques, demonstrated that it can be a very useful and valuable tool in biochips for easy and fast characterization of bio-samples. EIS also has been used to detect cell properties such as dead vs. live cells and cancer vs. non-cancerous cells [93]. Although many studies investigated the cell detection in a cell suspension [94], there were no studies related to live cell movement detection.

5.1.1.1 Device Design

The structure of the device is shown in figure 5.1, consists of a 5 pairs of metal electrodes integrated into a single channel microfluidic device with a length of 1000 μm and width of 20 μm. These metals electrodes are provided with contact pads, which can be probed to measure the impedance changes. The inset of the Figure 5.1 shows the three types of electrodes that are integrated into the microfluidic channel: 1) planar electrodes 2) parallel electrodes 3) interdigitated electrodes. The distance between the planar electrodes, parallel electrodes and interdigitated electrode inside the

microfluidic channel was designed to be 5 µm. As the cells pass through this active sensing area (electrode pair separation) of the electrodes, the impedance changes between the electrode and hence detects the cell motility.

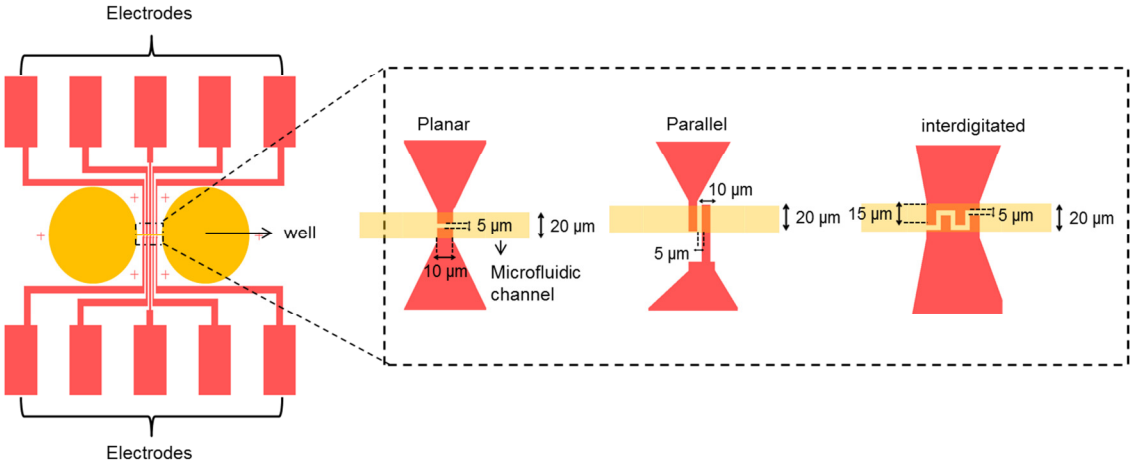

Figure 5.1 Schematic representations of microfluidic chip for impedance based cell motility detection.

5.1.1.2 Device Fabrication

Intially 1500 A^0 of gold was deposited on the surface of the glass slide using e-beam evaporation. A layer of hexamethyldisiliazane (HMDS) was spin coated onto the glass substrate at 2000 rpm for 30 sec in order to provide adhesion between the photoresist and gold layer of the substrate. S1813 positive photoresist was spin coated with the same speed and time recipe as mentioned above. After the spin coating procedure is done the glass samples were baked at 100^0C for one minute. The samples were exposed to UV light for 8 sec through the clear field mask to transfer the required pattern. The samples were developed in MF319 developer for 25 sec. Thus photoresist masks only

the electrodes pattern. The unmasked region of gold is etched using a gold etchant solution for 30 sec. The photoresist masking layer is stripped using acetone. The glass substrate with electrodes was spin coated with SU-8 photo resist at a spin coating speed of 1200 rpm for 30 sec. The spin coated photoresist determines the effective height of the pattern to be formed. The glass slide with electrodes was baked after the resist is spin coated in order to evaporate the solvent and to make the resist film dense. The wafer was then baked for 2 minutes at 65 °C and 5 minutes at 95 °C. Upon UV exposure, the negative photoresist cross links leaving the pattern area to be polymerized. The resist was exposed for 14 sec as per the manufacturer's recommendations. A post expose bake was performed for 1 minute at 65 °C and 2 minutes at 95 °C.

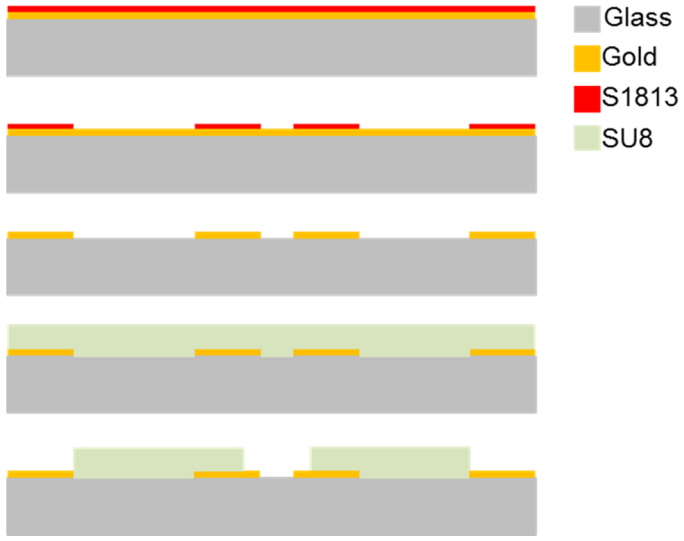

Figure 5.2 Process flow for the fabrication of microfluidic device for impedance based cell motility detection.

SU-8 developer was used to remove the unexposed areas in the wafer for 2 minutes. This process was followed by rinsing with IPA and nitrogen blow

drying. The fabrication process flow is shown in figure 5.2 and fabricated devices are shown in figure 5.3.

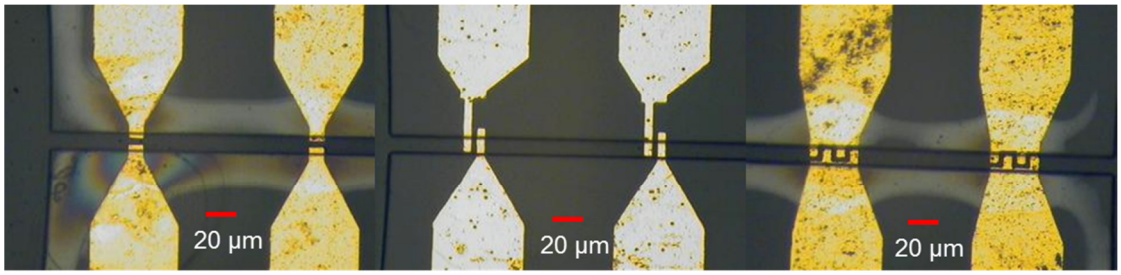

Figure 5.3 Fabricated micro gold electrodes integrated inside a microfluidic channel.

5.1.1.3 Device Characterization

The device consisting of parallel electrode was subjected to liquid drop test. The electrical impedance measurement using a precision impedance analyzer (4294A, Agilent Technology, Inc., CA) was carried out at an operating voltage of 500 mV and over a frequency range of 20 kHz – 1MHz. The frequency was swept in steps of 20 kHz from 20-100 kHz and steps of 200 kHz from 200 kHz to 1MHz. The impedance between bare electrodes in air and 1X PBS was measured. PBS impedance was tremendously reduced as compared to air. As PBS consists of ions, it reduced the resistance between the electrodes and resulted in total decrease in impedance as shown in Figure 5.4 a. Later 200 µl PBS consisting of 100000 PC-3 were added onto the device. Impedance was recorded once cells settled onto to the electrodes after 30 min. Impedance between the electrodes tremendously increased by 30-40% with respect to PBS, when cells exactly aligned in the gap between the parallel

electrodes. Cell membrane is made of lipid bilayer, which acts as a dielectric layer and prevents the electric field lines to pass through it. As a result the impedance between electrodes increases as compared to PBS as shown in Figure 5.4 b.

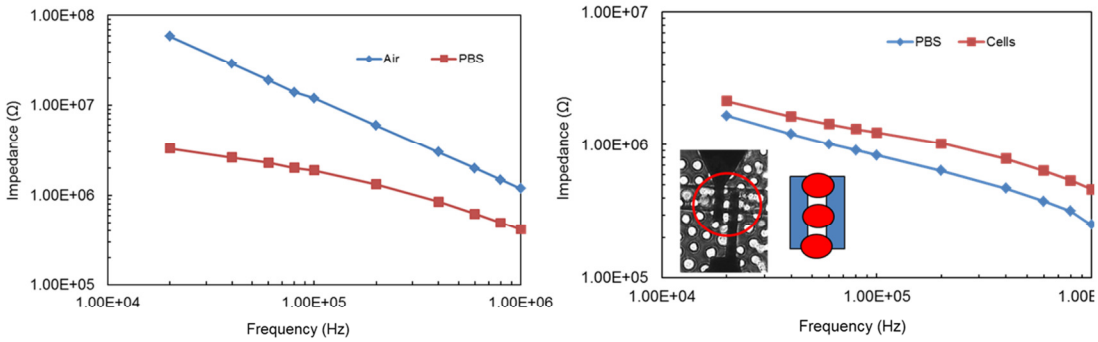

Figure 5.4 Impedance characteristics of planar electrodes, when the sensing area is covered with (a) air, PBS and (b) cells

5.1.1.4 Live Cell Motility Monitoring

The current device was modified to fit the experiments for live cell motility monitoring as shown in figure 5.5 a. A PDMS device consisting of two chambers of 5 mm in diameter and 6 mm in height connected with single microchannel was fabricated using soft lithography process. The PDMS device was manually aligned onto the electrode sensing area as shown in figure 5.5 b. Wire connections to contact pads were made using silver epoxy. The entire device was placed in a petri dish to maintain sterile environment as shown in figure 5.5 c.

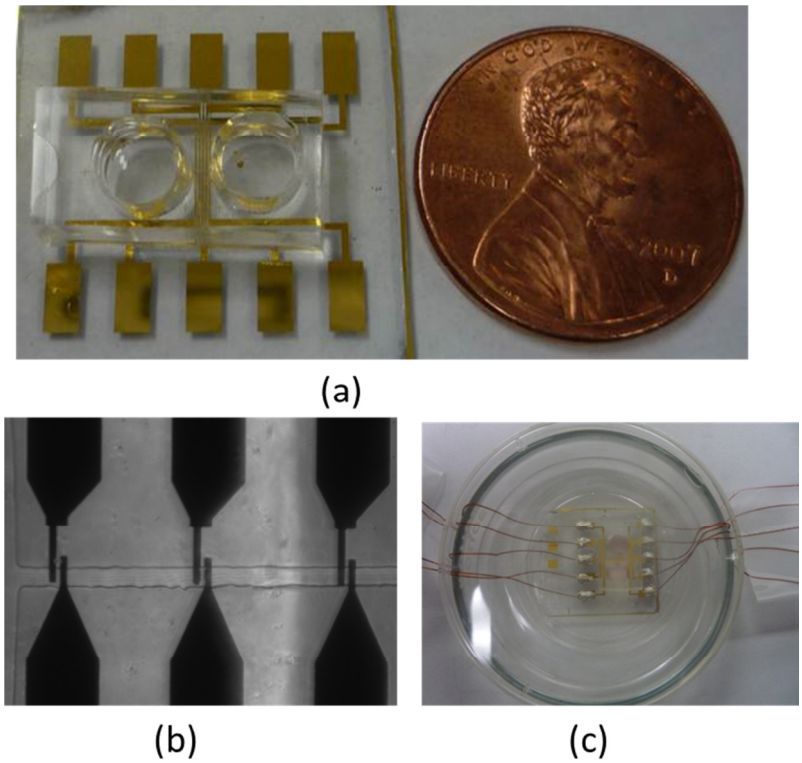

Figure 5.5 (a) live cell motility detection device area consisting metal electrode and PDMS microfluidic device, (b) microchannel manually aligned onto metal electrodes, (c) wire connections made using silver epoxy and device placed in petri dish.

The microfluidic channel is primed with RPMI media containing 2% FBS. PC-3 cells were seeded at 5000 cells/well density into cell chamber. EGF 75ng/ml was added in the attractant well, 24 hours after the cells were attached in attractant well. The electrodes wire connections are connected to Pinnacle 8102 potentiostat. Voltage of 500 mv was applied and the current across the electrodes was measured. Data was recorded at rate of 3 samples/ min. The device was kept in an incubator integrated with microscope. Time lapse imaging was performed where images were acquired after every 2 min.

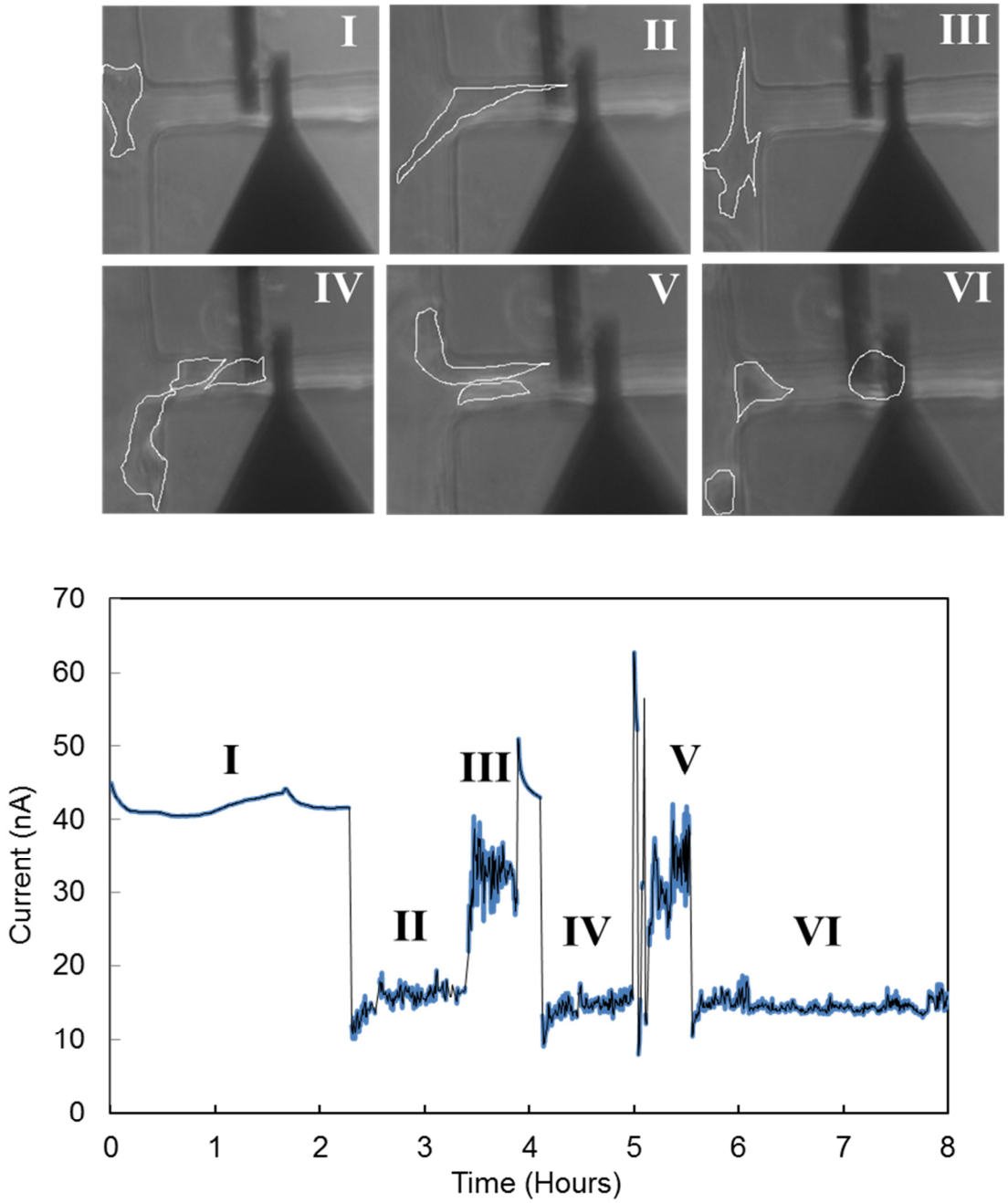

Figure 5.6 Time lapses images of the cell migration over sensing electrode and corresponding correlation to the potentiostat data recorded from the device.

This procedure was similar to the time-lapse acquisition procedure described in chapter 3. Figure 5.6 shows the time lapse images and corresponding potentiostat data. Since media was conductive, when cells did not enter the sensing region, there was constant current of approximately 40 nA recorded across the electrodes. However, when the cell entered the sensing region, the current dropped down to 15 nA. This is due to current blocking nature of the cell membrane. Incidents I, III and V represents the condition, when the cell was not in between the electrodes. Similarly Incidents II, IV and VI represent the condition, when the cell entered the sensing region.

Thus, these experiments suggest the feasibility of cell motility detection. In future other electrode systems will also be evaluated and a sensitive electrode system can be used. This device can be further improved by integrating with microcontroller and other embedded systems to automatically detect and record migration rate and the number of cells migrated through the channels.

5.2 Study of Cell Migration in Curved and Zigzag Channels

In chapter 2 and chapter 3 cell migration response in uniform and tapered channels has been studied. Physiologically, when the cancer cells migrate through the blood vessel or extracellular matrix, the pores and channels through which they migrate are not uniform. Statistics indicate that prostate and breast cancer mostly tends to metastasize to bone and lung. Apart from chemical factors, the structure of tissue of secondary organ might also attract the cancer cells and promote growth. For this reason, different curved and

zigzag were designed and fabricated. Fabricated curved microchannel devices are shown in figure 5.7. The device fabrication was done using a similar soft photolithography process as described in chapter 2. In curved channel design the length and width of the channel was kept same as uniform microchannels.

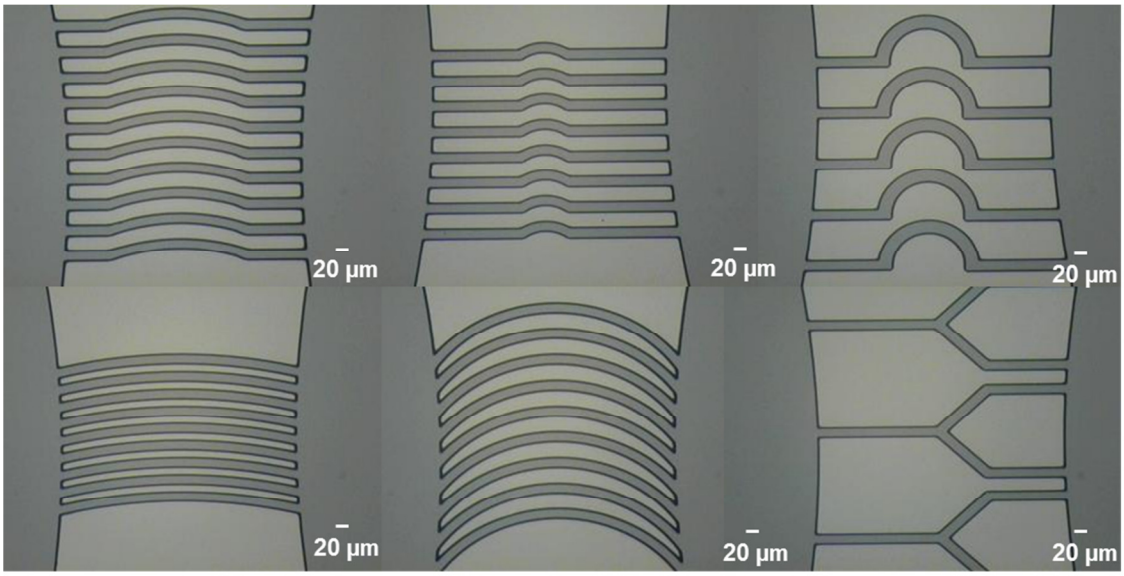

Figure 5.7 Fabricated curved microfluidic channels.

The curved channel devices were tested for cell migration by seeding 5000 PC-3 cells in cell well and EGF 75ng/ml was used as attractant. PC-3 cells migrated through different kind of curved channels after 5 days. The images of cells in the curved channels are shown in Figure 5.8. The affinity of cells to a particular structure due to the phenotype changes could be further investigated with series of time lapse imaging experiments.

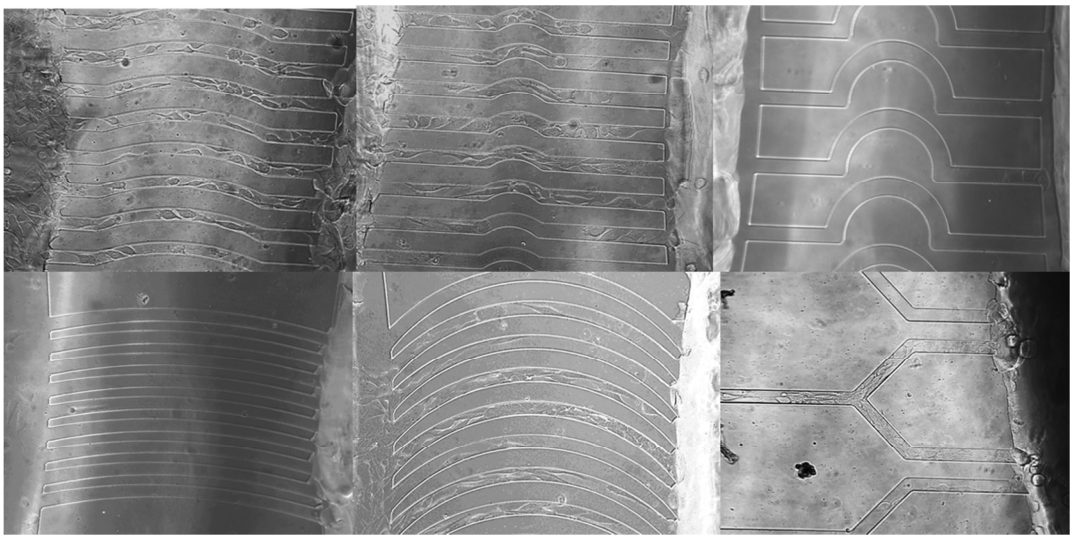

Figure 5.8 Cell migrations in curved channels.

A zigzag microfluidic channel device was designed and fabricated as shown in figure 5.9 a. The channel was designed to have period widening and narrowing of channel width from 20 μm to 5 μm. The pattern was repeated after every 50 μm to cover entire 1000 μm channel length. The device was tested by seeding PC-3 cells in cell well and EGF 75ng/ml was added to attractant well. A similar time-lapse microscopy was performed as described in Chapter 3. Results indicated that the cells entered and crossed the entire zigzag channel and reentered the adjacent channel with same zigzag patterns as shown in figure 5.9 b. The periodic patterns in the channel could have induced a memory in the cells as they tend to migrate through similar spatial patterns.

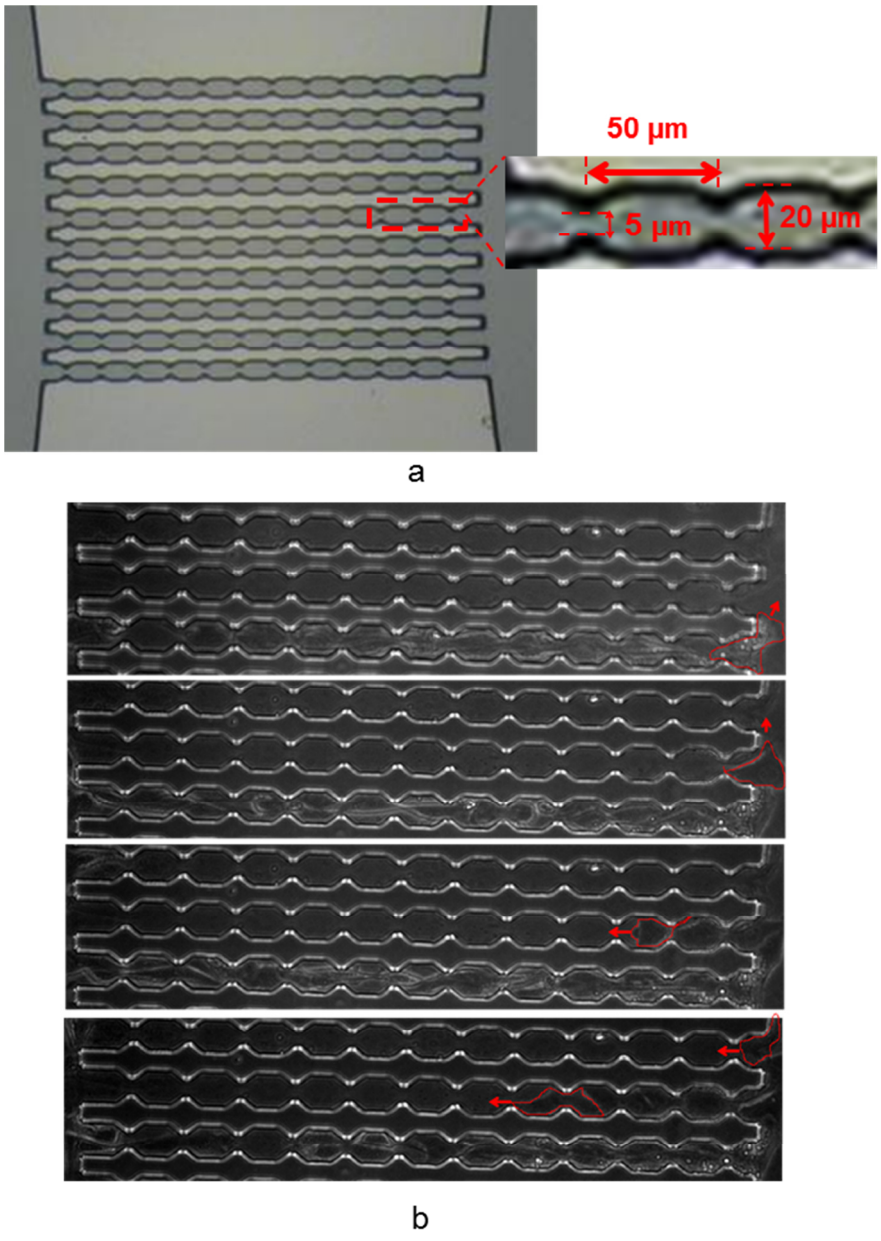

Figure 5.9 (a) Fabricated zigzag channel (b) cell migrations in zigzag channels.

In future more microchannel designs can be investigated to find out structure based affinity of cell migration. By performing immunohistochemistry on the cells that have migrated through these channels, we can understand the

exact phenotype changes in the cells, which might uncover more interesting facts about the cancer metastasis.

APPENDIX A

SUPPLEMENTAL DATA FOR EXPERIMENTS WITH CHEMICAL GRADIENT DEVICE

Experiment Parameters	
Cell Type	PC3ML
Cell seeding density	5000 cells per well
Media	RPMI 1640
Primed media	2% FBS + RPMI
Control	2% FBS_2% FBS
Experimental condition	2% FBS_2% FBS+ growth factor
N	5
Days of experiment	5 days
Growth factors	VEGF, EGF, bFGF and TGFβ
Concentrations	VEGF: 1, 2.5, 5, 10, 15, 25 and 35 ng/ml EGF: 25, 50, 100 and 125 ng/ml FGF: 0.1, 0.3, 1, 3 and 30 ng/ml TGFβ: 5, 10, 15 ng/ml

Table A.1 Experimental parameters used to test the migration of PC-3ML cells to different concentrations of growth factors.

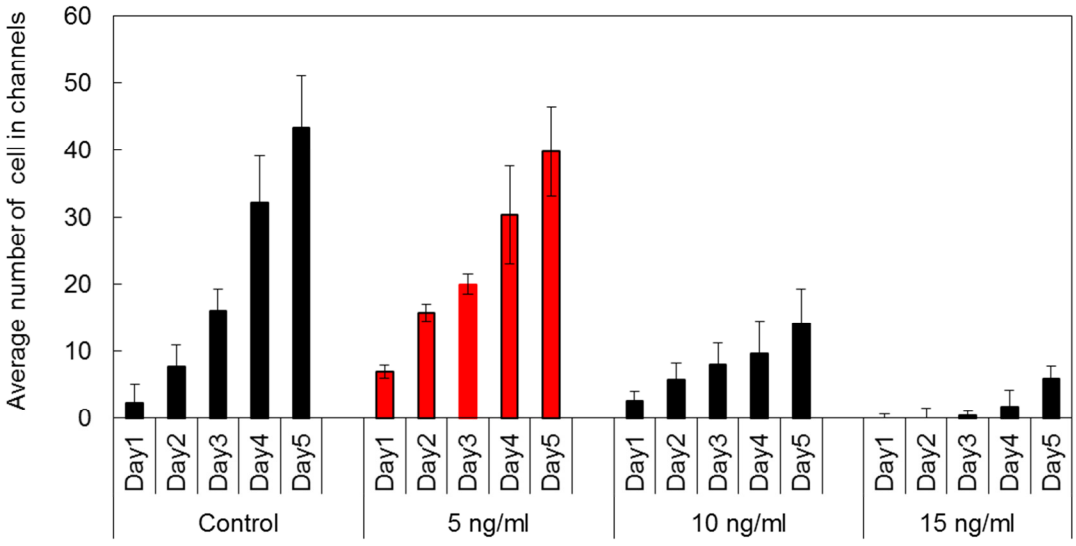

Figure A.1 Number of PC-3ML cells in channels in response to different concentrations of TGFβ.

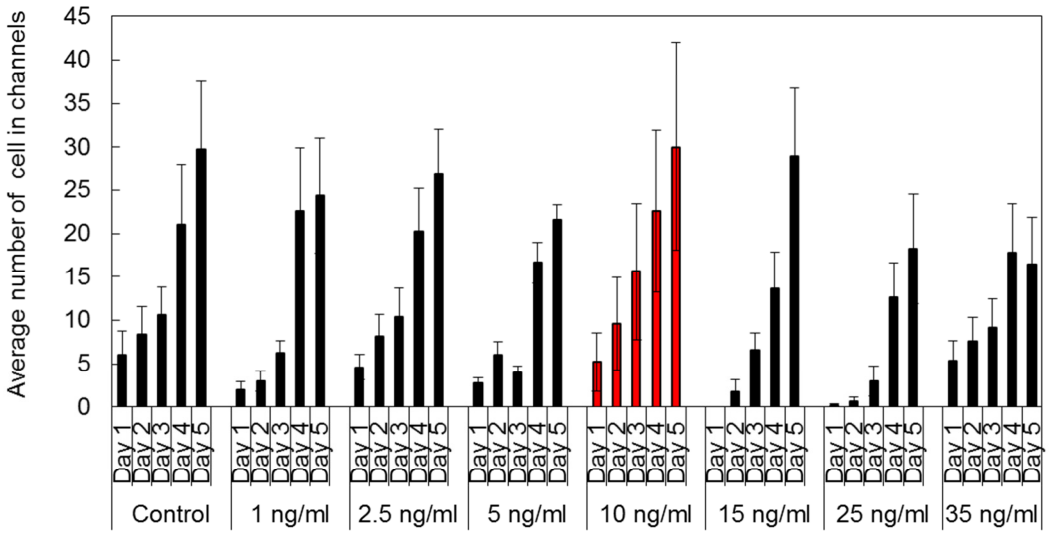

Figure A.2 Number of PC-3ML cells in channels in response to different concentrations of VEGF.

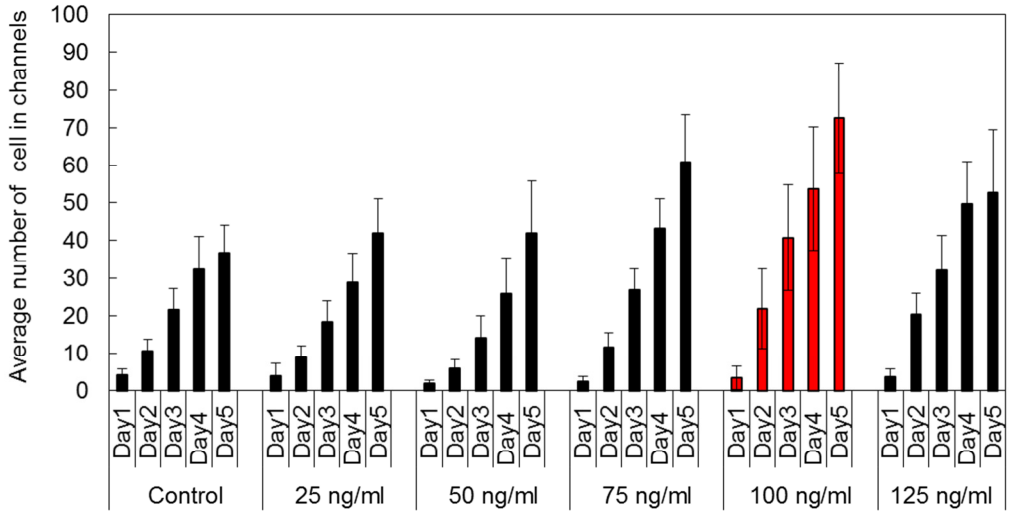

Figure A.3 Number of PC-3ML cells in channels in response to different concentrations of EGF.

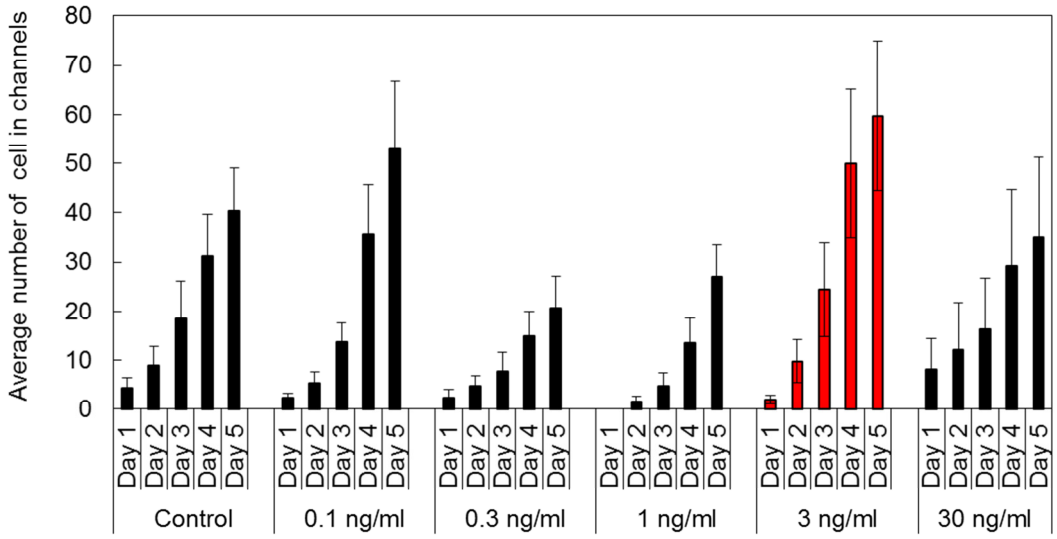

Figure A.4 Number of PC-3ML cells in channels in response to different concentrations of bFGF.

Experiment Parameters	
Cell Type	MDAMB 231
Cell seeding density	5000 cells per well
Media	RPMI 1640
Primed media	2% FBS + RPMI
Control	2% FBS_2%FBS
Experimental condition	2% FBS_2%FBS+ growth factor
N	5
Days of experiment	5 days
Growth factors	VEGF, EGF, bFGF and TGFβ
Concentrations	VEGF: 20, 40, 50, 60 and 100 ng/ml EGF: 1, 5, 10, 50 and 100 ng/ml FGF: 1, 10, 30, 50 and 70 ng/ml TGFβ: 0.01, 0.1, 1, 10 ng/ml

Table A.2 Experimental parameters used to test the migration of MDA-MB-231 cells to different concentrations of growth factors.

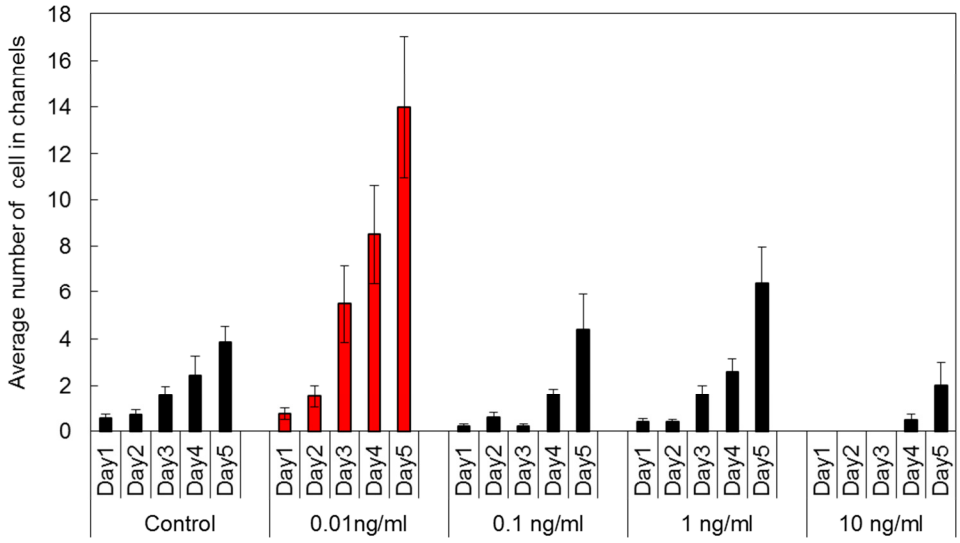

Figure A.5 Number of MDA-MB-231 cells in channels in response to different concentrations of TGFβ.

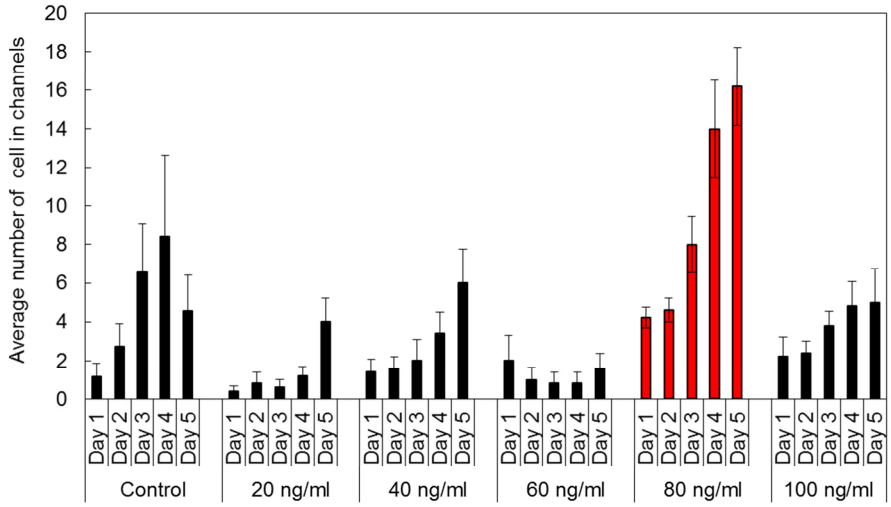

Figure A.6 Number of MDA-MB-231 cells in channels in response to different concentrations of VEGF.

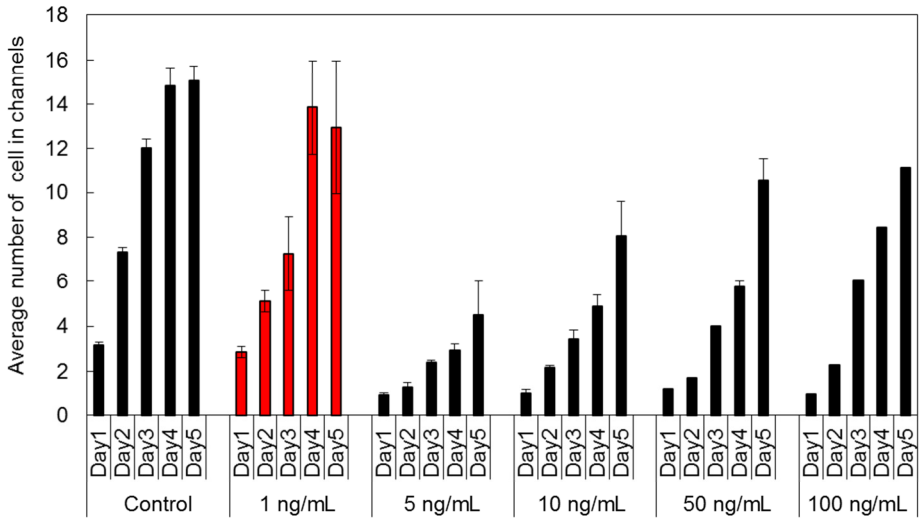

Figure A.7 Number of MDA-MB-231 cells in channels in response to different concentrations of EGF.

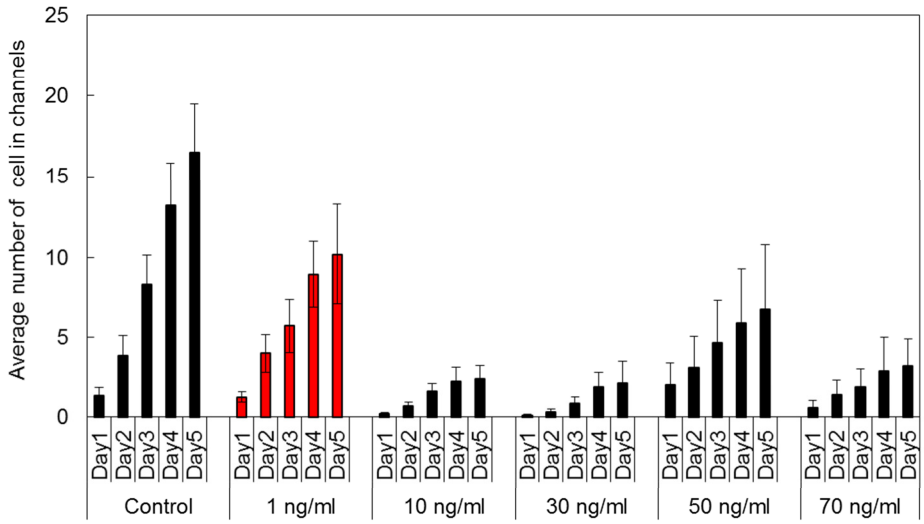

Figure A.8 Number of MDA-MB-231 cells in channels in response to different concentrations of bFGF.

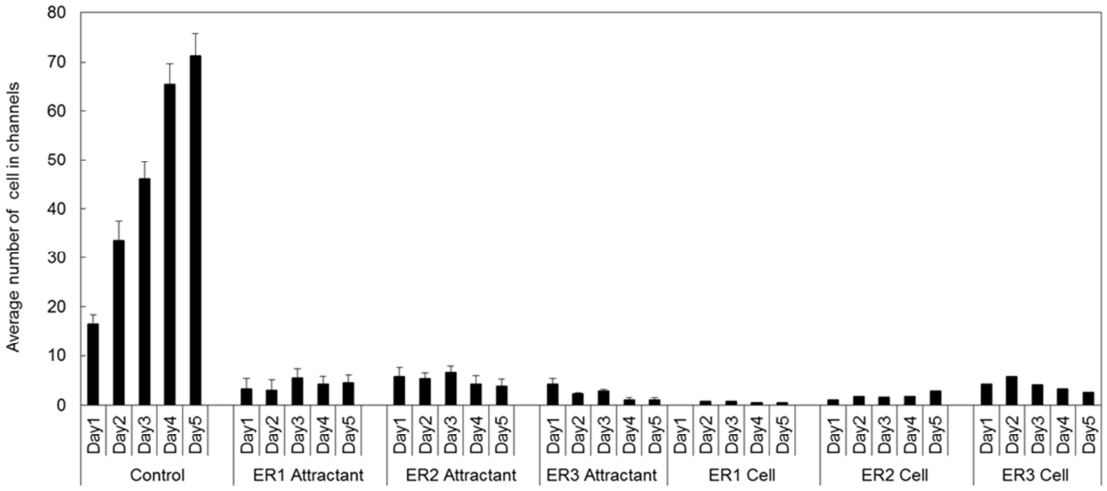

Figure A.9 Average number of migrating MDA-MB-231 cells in microchannels, when Epirubicin at three different concentrations was added to cells side and attractant side individually.

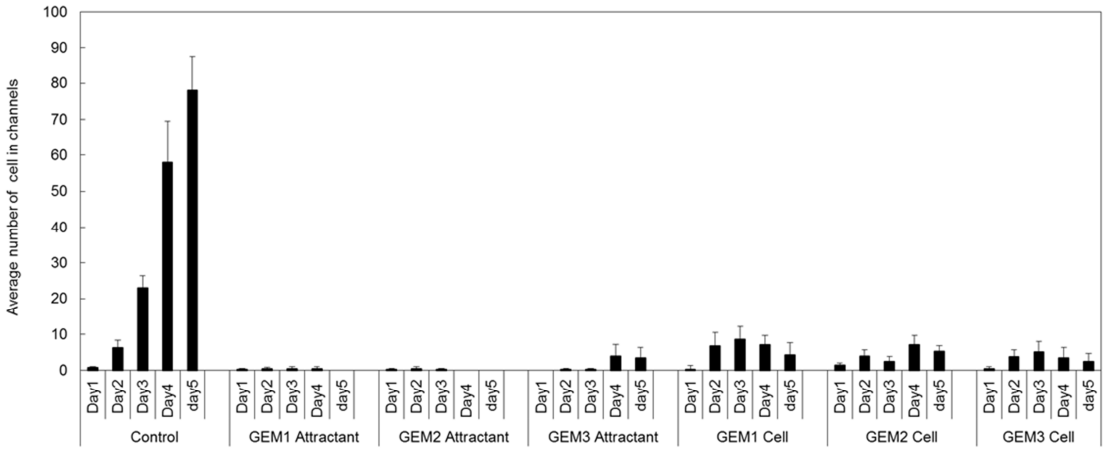

Figure A.10 Average number of migrating MDA-MB-231 cells in microchannels, when Gemzar at three different concentrations was added to cells side and attractant side individually.

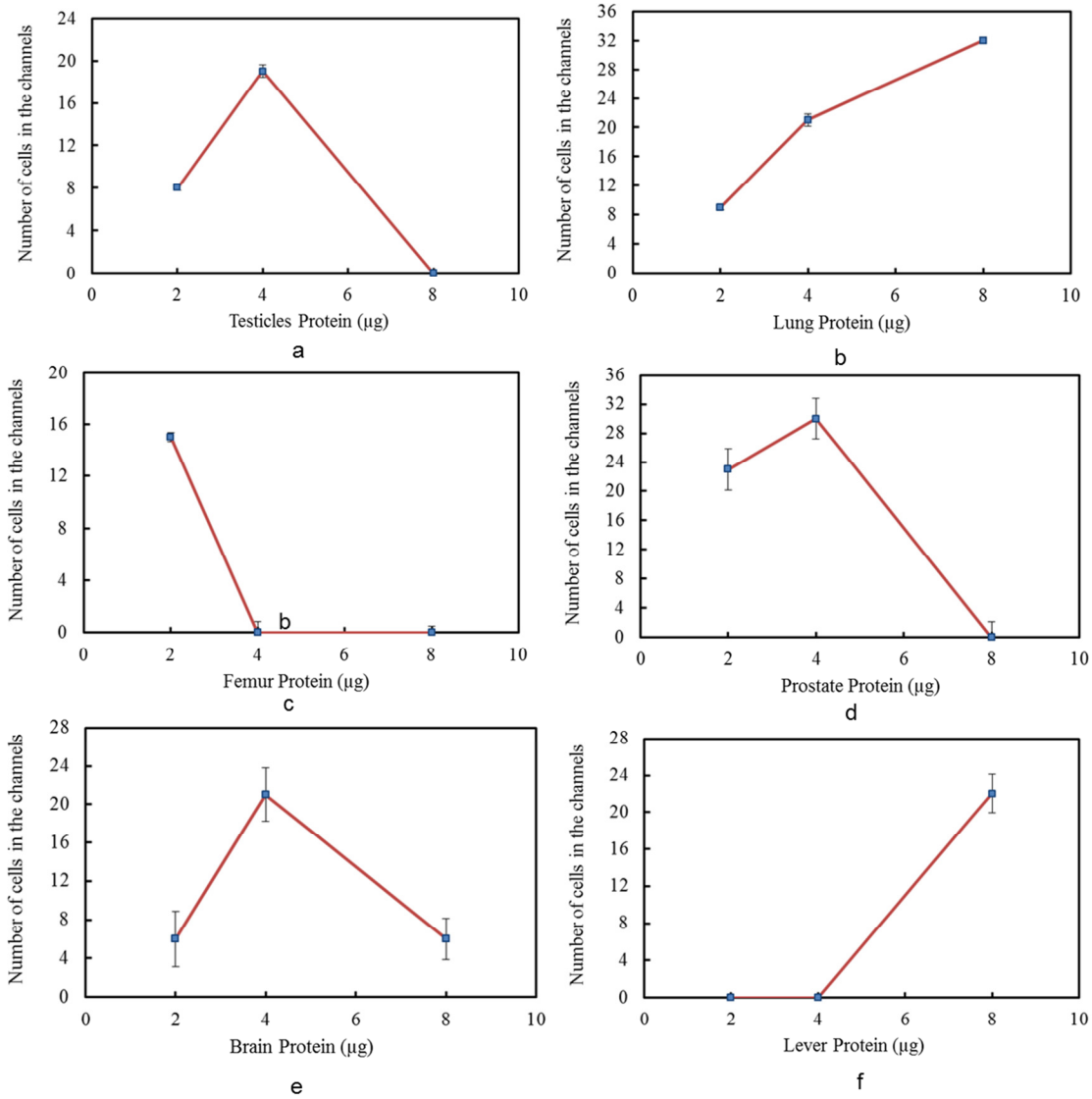

Figure A.11 PC-3ML cell migration response to testicles, lung, femur, prostate, brain and lever extracts at 2, 4 and 8 µg concentration.

.

REFERENCES

[1] Y.C. Lin, H.C. Ho, C.K. Tseng and S.Q. Hou, "A poly-methylmethacrylate electrophoresis microchip with sample preconcentrator," *J Micromech Microengineering*, vol. 11, pp. 189 2001.

[2] Y.C. Chan, M. Carles, N.J. Sucher, M. Wong and Y. Zohar, "Design and fabrication of an integrated microsystem for microcapillary electrophoresis," *J Micromech Microengineering*, vol. 13, pp. 914 2003.

[3] L. Lin, Y.T. Cheng and C.J. Chiu, "Comparative study of hot embossed micro structures fabricated by laboratory and commercial environments," *Microsystem technologies*, vol. 4, no. 3, pp. 113-116 1998.

[4] M. Heckele, W. Bacher and K. Müller, "Hot embossing-the molding technique for plastic microstructures," *Microsystem Technologies*, vol. 4, no. 3, pp. 122-124 1998.

[5] R.D. Loberg, C.J. Logothetis, E.T. Keller and K.J. Pienta, "Pathogenesis and treatment of prostate cancer bone metastases: Targeting the lethal phenotype," *Journal of clinical oncology*, vol. 23, no. 32, pp. 8232 2005.

[6] F. Saad, P. Perrotte, F. Benard, M. McCormack and P.I. Karakiewicz, "Bone health in men with prostate cancer: Diagnostic and therapeutic considerations," *Can.J.Urol.*, vol. 12 Suppl 2, pp. 9-15, Jun 2005.

[7] K.K. Yu and R.A. Hawkins, "The prostate: Diagnostic evaluation of metastatic disease," *Radiol.Clin.North Am.*, vol. 38, no. 1, pp. 139-157 2000.

[8] Vela, L. Gregory, E.M. Gardiner, J.A. Clements and D.L. Nicol, "Bone and prostate cancer cell interactions in metastatic prostate cancer," *BJU Int.*, vol. 99, no. 4, pp. 735-742 2007.

[9] F.W. Orr, H.H. Wang, R.M. Lafrenie, S. Scherbarth and D.M. Nance, "Interactions between cancer cells and the endothelium in metastasis," *J.Pathol.*, vol. 190, no. 3, pp. 310-329 2000.

[10] A.F. Chambers, A.C. Groom and I.C. MacDonald, "Dissemination and growth of cancer cells in metastatic sites," *Nature Reviews Cancer*, vol. 2, pp. 563-572 2002.

[11] M.J. Paszek, N. Zahir, K.R. Johnson, J.N. Lakins, G.I. Rozenberg, A. Gefen, C.A. Reinhart-King, S.S. Margulies, M. Dembo and D. Boettiger, "Tensional homeostasis and the malignant phenotype," *Cancer cell*, vol. 8, no. 3, pp. 241-254 2005.

[12] E. Sahai, "Illuminating the metastatic process," *Nature Reviews Cancer*, vol. 7, no. 10, pp. 737-749 2007.

[13] G.C. Cheng, P. Libby, A.J. Grodzinsky and R.T. Lee, "Induction of DNA synthesis by a single transient mechanical stimulus of human vascular smooth muscle cells: Role of fibroblast growth Factor–2," *Circulation*, vol. 93, no. 1, pp. 99 1996.

[14] P.R. Standley, T.J. Obards and C.L. Martina, "Cyclic stretch regulates autocrine IGF-I in vascular smooth muscle cells: Implications in vascular hyperplasia," *American Journal of Physiology-Endocrinology And Metabolism*, vol. 276, no. 4, pp. E697 1999.

[15] S. Boyden, "The chemotactic effect of mixtures of antibody and antigen on polymorphonuclear leucocytes," *J.Exp.Med.*, vol. 115, no. 3, pp. 453 1962.

[16] R.D. Nelson, P.G. Quie and R.L. Simmons, "Chemotaxis under agarose: A new and simple method for measuring chemotaxis and spontaneous migration of human polymorphonuclear leukocytes and monocytes," *The Journal of Immunology*, vol. 115, no. 6, pp. 1650 1975.

[17] S.H. Zigmond, "Ability of polymorphonuclear leukocytes to orient in gradients of chemotactic factors." *J.Cell Biol.*, vol. 75, no. 2, pp. 606 1977.

[18] D. Zicha, G.A. Dunn and A.F. Brown, "A new direct-viewing chemotaxis chamber," *J.Cell.Sci.*, vol. 99, no. 4, pp. 769 1991.

[19] G. Gerisch and H. Keller, "Chemotactic reorientation of granulocytes stimulated with micropipettes containing fMet-leu-phe," *J.Cell.Sci.*, vol. 52, no. 1, pp. 1 1981.

[20] J.W. Pollard and J.M. Walker, *Basic cell culture protocols*, Humana Pr Inc, 1997.

[21] O. Debeir, I. Camby, R. Kiss, P. Van Ham and C. Decaestecker, "A model-based approach for automated in vitro cell tracking and chemotaxis analyses," *Cytometry Part A*, vol. 60, no. 1, pp. 29-40 2004.

[22] N. Nitta, T. Tsuchiya, A. Yamauchi, T. Tamatani and S. Kanegasaki, "Quantitative analysis of eosinophil chemotaxis tracked using a novel optical device--TAXIScan," *J.Immunol.Methods*, vol. 320, no. 1-2, pp. 155-163 2007.

[23] R.B. Campenot, "Local control of neurite development by nerve growth factor," *Proceedings of the National Academy of Sciences*, vol. 74, no. 10, pp. 4516 1977.

[24] R.B. Campenot, "Development of sympathetic neurons in compartmentalized cultures:: I. local control of neurite growth by nerve growth factor," *Dev.Biol.*, vol. 93, no. 1, pp. 1-12 1982.

[25] D. Irimia, G. Charras, N. Agrawal, T. Mitchison and M. Toner, "Polar stimulation and constrained cell migration in microfluidic channels," *Lab Chip*, vol. 7, no. 12, pp. 1783-1790 2007.

[26] J. Diao, L. Young, S. Kim, E.A. Fogarty, S.M. Heilman, P. Zhou, M.L. Shuler, M. Wu and M.P. DeLisa, "A three-channel microfluidic device for generating static linear gradients and its application to the quantitative analysis of bacterial chemotaxis," *Lab Chip*, vol. 6, no. 3, pp. 381-388 2005.

[27] Shamloo, N. Ma, M. Poo, L.L. Sohn and S.C. Heilshorn, "Endothelial cell polarization and chemotaxis in a microfluidic device," *Lab Chip*, vol. 8, no. 8, pp. 1292-1299 2008.

[28] A.M. Taylor, S.W. Rhee, C.H. Tu, D.H. Cribbs, C.W. Cotman and N.L. Jeon, "Microfluidic multicompartment device for neuroscience research," *Langmuir*, vol. 19, no. 5, pp. 1551-1556 2003.

[29] P.J. Russell, S. Bennett and P. Stricker, "Growth factor involvement in progression of prostate cancer," *Clin.Chem.*, vol. 44, no. 4, pp. 705 1998.

[30] C. Festuccia, M. Bologna, G.L. Gravina, F. Guerra, A. Angelucci, I. Villanova, D. Millimaggi and A. Teti, "Osteoblast conditioned media contain TGF-β1 and modulate the migration of prostate tumor cells and their interactions with extracellular matrix components," *International journal of cancer*, vol. 81, no. 3, pp. 395-403 1999.

[31] E.R. Barrack, "TGFβ in prostate cancer: A growth inhibitor that can enhance tumorigenicity," *Prostate*, vol. 31, no. 1, pp. 61-70 1998.

[32] J. Folkman, "Angiogenesis and angiogenesis inhibition: An overview," *Regulation of angiogenesis*, vol. 79, pp. 1–8 1997.

[33] J. Folkman, "Antiangiogenic gene therapy," *Proceedings of the National Academy of Sciences*, vol. 95, no. 16, pp. 9064 1998.

[34] F.A. Ferrer, L.J. Miller, R.I. Andrawis, S.H. Kurtzman, P.C. Albertsen, V.P. Laudone and D.L. Kreutzer, "Angiogenesis and prostate cancer: In

vivo and in vitro expression of angiogenesis factors by prostate cancer cells," *Urology*, vol. 51, no. 1, pp. 161-167 1998.

[35] Y. Takahashi, Y. Kitadai, C.D. Bucana, K.R. Cleary and L.M. Ellis, "Expression of vascular endothelial growth factor and its receptor, KDR, correlates with vascularity, metastasis, and proliferation of human colon cancer," *Cancer Res.*, vol. 55, no. 18, pp. 3964 1995.

[36] R.A. Brekken, J.P. Overholser, V.A. Stastny, J. Waltenberger, J.D. Minna and P.E. Thorpe, "Selective inhibition of vascular endothelial growth factor (VEGF) receptor 2 (KDR/Flk-1) activity by a monoclonal anti-VEGF antibody blocks tumor growth in mice," *Cancer Res.*, vol. 60, no. 18, pp. 5117 2000.

[37] Mori, S. Arii, M. Furutani, M. Mizumoto, S. Uchida, H. Furuyama, Y. Kondo, M. Gorrin-Rivas, K. Furumoto and Y. Kaneda, "Soluble flt-1 gene therapy for peritoneal metastases using HVJ-cationic liposomes," *Gene Ther.*, vol. 7, no. 12, pp. 1027-1033 2000.

[38] M.N. Nakatsu, R.C.A. Sainson, S. Pérez-del-Pulgar, J.N. Aoto, M. Aitkenhead, K.L. Taylor, P.M. Carpenter and C.C.W. Hughes, "VEGF121 and VEGF165 regulate blood vessel diameter through vascular endothelial growth factor receptor 2 in an in vitro angiogenesis model," *Laboratory investigation*, vol. 83, no. 12, pp. 1873-1885 2003.

[39] R. Pérez, M. Pascual, A. Macías and A. Lage, "Epidermal growth factor receptors in human breast cancer," *Breast Cancer Res.Treat.*, vol. 4, no. 3, pp. 189-193 1984.

[40] G. Morris and J.G. Dodd, "Epidermal growth factor receptor mRNA levels in human prostatic tumors and cell lines," *J.Urol.*, vol. 143, no. 6, pp. 1272-1274 1990.

[41] P. Davies and C.L. Eaton, "Binding of epidermal growth factor by human normal, hypertrophic, and carcinomatous prostate," *Prostate*, vol. 14, no. 2, pp. 123-132 1989.

[42] J.E. Fowler Jr, J.L. Lau, L. Ghosh, S.E. Mills and A. Mounzer, "Epidermal growth factor and prostatic carcinoma: An immunohistochemical study," *J.Urol.*, vol. 139, no. 4, pp. 857-861, Apr 1988.

[43] D.F. Jarrard, B.F. Blitz, R.C. Smith, B.L. Patai and D.B. Rukstalis, "Effect of epidermal growth factor on prostate cancer cell line PC-3 growth and invasion," *Prostate*, vol. 24, no. 1, pp. 46-53 1994.

[44] J.W. Crabb, L. Armes, C.M. Johnson and W.L. McKeehan, "Characterization of multiple forms of prostatropin (prostate epithelial cell growth factor) from bovine brain," *Biochem.Biophys.Res.Commun.*, vol. 136, no. 3, pp. 1155-1161 1986.

[45] N. Nishi, Y. Matuo, T. Nakamoto and F. Wada, "Proliferation of epithelial cells derived from rat dorsolateral prostate in serum-free primary cell

culture and their response to androgen," *In Vitro Cellular & Developmental Biology-Plant*, vol. 24, no. 8, pp. 778-786 1988.

[46] M.T. Story, B. Livingston, L. Baeten, S.J. Swartz, S.C. Jacobs, F.P. Begun and R.K. Lawson, "Cultured human prostate-derived fibroblasts produce a factor that stimulates their growth with properties indistinguishable from basic fibroblast growth factor," *Prostate*, vol. 15, no. 4, pp. 355-365 1989.

[47] S.A. Shain and J.D. Koger, "Differences in responsiveness of clonally derived AXC/SSh rat prostate cancer cells to secreted or prototypic mitogens," *Cancer Res.*, vol. 49, no. 14, pp. 3898 1989.

[48] M.T. Hierowski, M.W. McDonald, L. Dunn and J.W. Sullivan, "The partial dependency of human prostatic growth factor on steroid hormones in stimulating thymidine incorporation into DNA," *J.Urol.*, vol. 138, no. 4, pp. 909-912, Oct 1987.

[49] P.E. Mansson, P. Adams, M. Kan and W.L. McKeehan, "Heparin-binding growth factor gene expression and receptor characteristics in normal rat prostate and two transplantable rat prostate tumors," *Cancer Res.*, vol. 49, no. 9, pp. 2485 1989.

[50] J.S. Horoszewicz, S.S. Leong, E. Kawinski, J.P. Karr, H. Rosenthal, T.M. Chu, E.A. Mirand and G.P. Murphy, "LNCaP model of human prostatic carcinoma," *Cancer Res.*, vol. 43, no. 4, pp. 1809 1983.

[51] K.R. Stone, D.D. Mickey, H. Wunderli, G.H. Mickey and D.F. Paulson, "Isolation of a human prostate carcinoma cell line (DU 145)," *International Journal of Cancer*, vol. 21, no. 3, pp. 274-281 1978.

[52] M.E. Kaighn, J.F. Lechner, K.S. Narayan and L.W. Jones, "Prostate carcinoma: Tissue culture cell lines," *Natl.Cancer Inst.Monogr.*, vol. (49), no. 49, pp. 17-21, Dec 1978.

[53] J.M. Kozlowski, R. McEwan, H. Keer, J. Sensibar, E. Sherwood, C. Lee, J. Grayhack, A. Albini and G. Martin, "Prostate cancer and the invasive phenotype: Application of new in vivo and in vitro approaches," *Tumor Progression, Metastasis*, pp. 189–231 1988.

[54] T. Nakamoto, C. Chang, A. Li and G.W. Chodak, "Basic fibroblast growth factor in human prostate cancer cells," *Cancer Res.*, vol. 52, no. 3, pp. 571 1992.

[55] C.A. Wilson, E.E. Cajulis, J.L. Green, T.M. Olsen, Y.A. Chung, M.A. Damore, J. Dering, F.J. Calzone and D.J. Slamon, "HER-2 overexpression differentially alters transforming growth factor-beta responses in luminal versus mesenchymal human breast cancer cells," *Breast Cancer Res.*, vol. 7, no. 6, pp. R1058-R1079 2005.

[56] M. Skobe, T. Hawighorst, D.G. Jackson, R. Prevo, L. Janes, P. Velasco, L. Riccardi, K. Alitalo, K. Claffey and M. Detmar, "Induction of tumor lymphangiogenesis by VEGF-C promotes breast cancer metastasis," *Nat.Med.*, vol. 7, no. 2, pp. 192-198 2001.

[57] J.T. Price, T. Tiganis, A. Agarwal, D. Djakiew and E.W. Thompson, "Epidermal growth factor promotes MDA-MB-231 breast cancer cell migration through a phosphatidylinositol 3′-kinase and phospholipase C-dependent mechanism," *Cancer Res.*, vol. 59, no. 21, pp. 5475-5478 1999.

[58] T.H. Lee, H.K. Avraham, S. Jiang and S. Avraham, "Vascular endothelial growth factor modulates the transendothelial migration of MDA-MB-231 breast cancer cells through regulation of brain microvascular endothelial cell permeability," *J.Biol.Chem.*, vol. 278, no. 7, pp. 5277-5284 2003.

[59] J. Chen, S. De, J. Brainard and T.V. Byzova, "Metastatic properties of prostate cancer cells are controlled by VEGF," *Cell communication and adhesion*, vol. 11, no. 1, pp. 1-11 2004.

[60] S. Magnetto, S. Boissier, P.D. Delmas and P. Clezardin, "Additive antitumor activities of taxoids in combination with the bisphosphonate ibandronate against invasion and adhesion of human breast carcinoma cells to bone," *International journal of cancer*, vol. 83, no. 2, pp. 263-269 1999.

[61] E. Germain, V. Chajès, S. Cognault, C. Lhuillery and P. Bougnoux, "Enhancement of doxorubicin cytotoxicity by polyunsaturated fatty acids in the human breast tumor cell line MBA-MB-231: Relationship to lipid peroxidation," *International journal of cancer*, vol. 75, no. 4, pp. 578-583 1998.

[62] D. Yamamoto, K. Tanaka, K. Nakai, T. Baden, K. Inoue, C. Yamamoto, H. Takemoto, K. Kamato, H. Hirata and S. Morikawa, "Synergistic effects induced by cycloprodigiosin hydrochloride and epirubicin on human breast cancer cells," *Breast Cancer Res.Treat.*, vol. 72, no. 1, pp. 1-10 2002.

[63] S. Ali, O. Aranha, Y. Li, G.R. Pettit, F.H. Sarkar and P.A. Philip, "Sensitization of human breast cancer cells to gemcitabine by the protein kinase C modulator bryostatin 1," *Cancer Chemother.Pharmacol.*, vol. 52, no. 3, pp. 235-246 2003.

[64] J.L. Holleran, C.J. Miller, N.L. Edgehouse, T.P. Pretlow and L.A. Culp, "Differential experimental micrometastasis to lung, liver, and bone with lacZ-tagged CWR22R prostate carcinoma cells," *Clinical and Experimental Metastasis*, vol. 19, no. 1, pp. 17-24 2002.

[65] T. Yoneda, A. Sasaki and G.R. Mundy, "Osteolytic bone metastasis in breast cancer," *Breast Cancer Res.Treat.*, vol. 32, no. 1, pp. 73-84 1994.

[66] A.F. Chambers, A.C. Groom and I.C. MacDonald, "Dissemination and growth of cancer cells in metastatic sites," *Nature Reviews Cancer*, vol. 2, pp. 563-572 2002.

[67] M.J. Paszek, N. Zahir, K.R. Johnson, J.N. Lakins, G.I. Rozenberg, A. Gefen, C.A. Reinhart-King, S.S. Margulies, M. Dembo and D. Boettiger, "Tensional homeostasis and the malignant phenotype," *Cancer cell*, vol. 8, no. 3, pp. 241-254 2005.

[68] E. Sahai, "Illuminating the metastatic process," *Nature Reviews Cancer*, vol. 7, no. 10, pp. 737-749 2007.

[69] S.J. Altschuler and L.F. Wu, "Cellular heterogeneity: Do differences make a difference?" *Cell*, vol. 141, no. 4, pp. 559-563 2010.

[70] M.R. Stratton, P.J. Campbell and P.A. Futreal, "The cancer genome," *Nature*, vol. 458, no. 7239, pp. 719-724 2009.

[71] J.E. Visvader and G.J. Lindeman, "Cancer stem cells in solid tumours: Accumulating evidence and unresolved questions," *Nat Rev Cancer*, vol. 8, no. 10, pp. 755-768 2008.

[72] M. Shackleton, E. Quintana, E.R. Fearon and S.J. Morrison, "Heterogeneity in cancer: Cancer stem cells versus clonal evolution," *Cell*, vol. 138, no. 5, pp. 822-829 2009.

[73] K. Yamauchi, M. Yang, K. Hayashi, P. Jiang, N. Yamamoto, H. Tsuchiya, K. Tomita, A.R. Moossa, M. Bouvet and R.M. Hoffman, "Induction of cancer metastasis by cyclophosphamide pretreatment of host mice: An opposite effect of chemotherapy," *Cancer Res.*, vol. 68, no. 2, pp. 516 2008.

[74] P. Friedl and K. Wolf, "Tumour-cell invasion and migration: Diversity and escape mechanisms," *Nature Reviews Cancer*, vol. 3, no. 5, pp. 362-374 2003.

[75] R.M.K.W. Lee, G.K. Owens, T. Scott-Burden, R.J. Head, M.J. Mulvany and E.L. Schiffrin, "Pathophysiology of smooth muscle in hypertension," *Can.J.Physiol.Pharmacol.*, vol. 73, no. 5, pp. 574-584 1995.

[76] Hughes, G. Clunn, J. Refson and C. Demoliou-Mason, "Platelet-derived growth factor (PDGF): Actions and mechanisms in vascular smooth muscle* 1," *General Pharmacology: The Vascular System*, vol. 27, no. 7, pp. 1079-1089 1996.

[77] T. Scott-Burden and P.M. Vanhoutte, "Regulation of smooth muscle cell growth by endothelium-derived factors." *Texas Heart Institute Journal*, vol. 21, no. 1, pp. 91 1994.

[78] B.S. Kim and D.J. Mooney, "Scaffolds for engineering smooth muscle under cyclic mechanical strain conditions," *J.Biomech.Eng.*, vol. 122, no. 3, pp. 210-215 2000.

[79] G.B. Chapman, W. Durante, J.D. Hellums and A.I. Schafer, "Physiological cyclic stretch causes cell cycle arrest in cultured vascular smooth muscle cells," *American Journal of Physiology-Heart and Circulatory Physiology*, vol. 278, no. 3, pp. H748 2000.

[80] K.G. Birukov, V.P. Shirinsky, O.V. Stepanova, V.A. Tkachuk, A.W.A. Hahn, T.J. Resink and V.N. Smirnov, "Stretch affects phenotype and proliferation of vascular smooth muscle cells," *Mol.Cell.Biochem.*, vol. 144, no. 2, pp. 131-139 1995.

[81] M. CATTARUZZA, C. DIMIGEN, H. EHRENREICH and M. HECKER, "Stretch-induced endothelin B receptor-mediated apoptosis in vascular smooth muscle cells," *The FASEB Journal*, vol. 14, no. 7, pp. 991 2000.

[82] H.E. Colley, G. Mishra, A.M. Scutt and S.L. McArthur, "Plasma polymer coatings to support mesenchymal stem cell adhesion, growth and differentiation on variable stiffness silicone elastomers," *Plasma Processes and Polymers*, vol. 6, no. 12, pp. 831-839 2009.

[83] M.A. Eddings, M.A. Johnson and B.K. Gale, "Determining the optimal PDMS–PDMS bonding technique for microfluidic devices," *J Micromech Microengineering*, vol. 18, pp. 067001 2008.

[84] C. Huggins, S.M.N. Rao, K. Nguyen and J.C. Chiao, "The analysis of surface treatment of PDMS on prostate cancer and smooth muscle cells," in *Proceedings of SPIE*, 2008, pp. 726914.

[85] J.P. Lynch and K.J. Loh, "A summary review of wireless sensors and sensor networks for structural health monitoring," *Shock Vib Dig*, vol. 38, no. 2, pp. 91-130 2006.

[86] M.N. Richard, J.F. Deniset, A.L. Kneesh, D. Blackwood and G.N. Pierce, "Mechanical stretching stimulates smooth muscle cell growth, nuclear protein import, and nuclear pore expression through mitogen-activated protein kinase activation," *J.Biol.Chem.*, vol. 282, no. 32, pp. 23081 2007.

[87] S. Kona, P. Chellamuthu, H. Xu, S.R. Hills and K.T. Nguyen, "Effects of cyclic strain and growth factors on vascular smooth muscle cell responses," *The Open Biomedical Engineering Journal*, vol. 3, pp. 28 2009.

[88] Beier, R. Düsing, H. Vetter and U. Schmitz, "Epidermal growth factor stimulates Rac1 and p21-activated kinase in vascular smooth muscle cells," *Atherosclerosis*, vol. 196, no. 1, pp. 92-97 2008.

[89] J.J. Hu, S. Baek and J. Humphrey, "Stress-strain behavior of the passive basilar artery in normotension and hypertension," *J.Biomech.*, vol. 40, no. 11, pp. 2559-2563 2007.

[90] H. Wang and J.A. Keiser, "Vascular endothelial growth factor upregulates the expression of matrix metalloproteinases in vascular smooth muscle cells: Role of flt-1," *Circ.Res.*, vol. 83, no. 8, pp. 832 1998.

[91] L. Goodman and R. Majack, "Vascular smooth muscle cells express distinct transforming growth factor-beta receptor phenotypes as a function of cell density in culture." *J.Biol.Chem.*, vol. 264, no. 9, pp. 5241 1989.

[92] B. Liu, M.J. Qu, K.R. Qin, H. Li, Z.K. Li, B.R. Shen and Z.L. Jiang, "Role of cyclic strain frequency in regulating the alignment of vascular smooth muscle cells in vitro," *Biophys.J.*, vol. 94, no. 4, pp. 1497-1507 2008.

[93] C. Iliescu, D.P. Poenar, M. Carp and F.C. Loe, "A microfluidic device for impedance spectroscopy analysis of biological samples," *Sensors Actuators B: Chem.*, vol. 123, no. 1, pp. 168-176 2007.

[94] Y. Cho, H.S. Kim, A.B. Frazier, Z.G. Chen, D.M. Shin and A. Han, "Whole-cell impedance analysis for highly and poorly metastatic cancer cells," *Microelectromechanical Systems, Journal of*, vol. 18, no. 4, pp. 808-817 2009.

BIOGRAPHICAL INFORMATION

Uday Tata was born in Parvathipuram, India. He received his Bachelor degree in Instrumentation Engineering from Osmania University, Hyderabad, India in 2006. He received his Master of Science in Electrical Engineering from The University of Texas at Arlington in August 2008 with the thesis “Study of Patch Antenna for Strain Measurement”. He received his PhD degree in Electrical Engineering from The University of Texas at Arlington in December 2012. His current research interests includes microfluidics for cancer cell migration, micro/nano fabrication, MEMS based microsensors for biomedical applications, optical fiber and wireless strain sensors for structural health monitoring. He has published several journal and conference papers. He has two US patent applications.